

**EVALUATION OF PHYTOCHEMICALS FROM  
*TINOSPORA CORDIFOLIA* AGAINST  
ONCOGENIC AND RESISTANCE-ASSOCIATED  
TARGETS IN LOW-GRADE SEROUS OVARIAN  
CARCINOMA**

**Thesis Submitted  
in Partial Fulfilment of the Requirements  
for the Degree of**

**MASTER OF TECHNOLOGY**

**in**

**Bioinformatics**

**by**

**Pratyaksha Singh  
(Roll No. 23/BIO/13)**

**Under the Supervision of  
Dr. NAVNEETA BHARADVAJA**



**Department of Biotechnology**

**DELHI TECHNOLOGICAL UNIVERSITY  
(Formerly Delhi College of Engineering)  
Shahbad Daultpur, Main Bawana Road, Delhi-110042. India  
May, 2025**

## **ACKNOWLEDGEMENT**

I would like to sincerely thank Dr. Navneeta Bharadvaja, my research supervisor, for her unwavering support, expert guidance, and encouragement throughout the duration of this work. Her deep knowledge, valuable suggestions, and timely feedback were instrumental in shaping the direction and quality of this thesis. I am truly grateful for the opportunity to work under her mentorship.

I would also like to express my appreciation to the Department of Biotechnology, Delhi Technological University, for providing the required facilities, resources, and a supportive academic environment that enabled the successful execution of this research.

Pratyaksha Singh  
(23/BIO/13)



# **DELHI TECHNOLOGICAL UNIVERSITY**

(Formerly Delhi College of Engineering)  
Shahbad Daulatpur, Main Bawana Road, Delhi-42

## **CANDIDATE'S DECLARATION**

I Pratyaksha Singh hereby certify that the work which is being presented in the thesis entitled Evaluation of Phytochemicals from *Tinospora cordifolia* Against Oncogenic and Resistance-Associated Targets in Low-Grade Serous Ovarian Carcinoma in partial fulfilment of the requirements for the award of the Degree of Master of Technology, submitted in the Department of Biotechnology, Delhi Technological University is an authentic record of my own work carried out during the period from January to May 2025 under the supervision of Dr. Navneeta Bharadvaja.

The matter presented in the thesis has not been submitted by me for the award of any other degree of this or any other Institute.

**Candidate's Signature**



# DELHI TECHNOLOGICAL UNIVERSITY

(Formerly Delhi College of Engineering)

Shahbad Daulatpur, Main Bawana Road, Delhi-42

## CERTIFICATE BY THE SUPERVISOR

Certified that **Pratyaksha Singh (23/BIO/13)** has carried out their search work presented in this thesis entitled “**Evaluation of Phytochemicals from *Tinospora cordifolia* Against Oncogenic and Resistance-Associated Targets in Low-Grade Serous Ovarian Carcinoma**” for the award of **Master of Technology** from Department of Biotechnology, Delhi Technological University, Delhi, under my supervision. The thesis embodies results of original work, and studies are carried out by the student herself and the contents of the thesis do not form the basis for the award of any other degree to the candidate or to anybody else from this or any other University/Institution.

Dr. Navneet Bharadvaja

Associate Professor

Department of Biotechnology

Delhi Technological University

Shahbad Daulatpur, Main Bawana Road,

Delhi-110042. India

Date:



# DELHI TECHNOLOGICAL UNIVERSITY

(Formerly Delhi College of Engineering)

Shahbad Daultpur, Main Bawana Road, Delhi-42

## PLAGIARISM VERIFICATION

Title of the Thesis EVALUATION OF PHYTOCHEMICALS FROM TINOSPORA CORDIFOLIA AGAINST ONCOGENIC AND RESISTANCE-ASSOCIATED TARGETS IN LOW-GRADE SEROUS OVARIAN CARCINOMA

Total Pages: 111

Name of the Scholar: Pratyaksha Singh

Supervisor

(1) Dr Navneeta Bharadvaja

(2) \_\_\_\_\_

(3) \_\_\_\_\_

Department

This is to report that the above thesis was scanned for similarity detection. Process and outcome are given below:

Software used:

\_\_\_\_\_

Similarity Index: \_\_\_\_\_, Total Word Count:

Date: \_\_\_\_\_

**Candidate's Signature**

**Signature of Supervisor**

## **ABSTRACT**

Low-grade serous ovarian carcinoma (LGSC) is not frequent but chemo-resistant subtype of epithelial ovarian cancer. Key features of this particular subtype are slow proliferation and poor response to conventional chemotherapy treatment. This study aims to identify plant-derived compounds that are capable of modulating key target involved in oncogenic and resistance pathways in LGSC. Here, the focus was on six molecular targets KRAS, BRAF, MEK1 are the oncogenic drivers of LGSC whereas as HES1, EGFR, PIK3CA are involved in drug-resistance.

Phytochemicals from *Tinospora cordifolia* (Giloy) which is a traditional medicinal plant belonging to the Menispermaceae family has been gaining significant attention recently due to its known anticancer properties. These phytochemicals were explored using a computational approach. Through literature mining a total of eighteen phytochemicals were shortlisted and seven with favourable ADME and drug-likeness profiles (DL score  $\geq 0.5$ ) were selected for further study. These shortlisted candidates were taken for molecular docking using AutoDock Vina using Pyrx, where Luteolin, Berberine, and Dehydrodiscretamine and Magnoflorine showed strong binding with key LGSC targets ( $>8.5$  kcal/mol).

All the promising ligand–protein complexes were then further analysed through molecular dynamics (MD) simulations using Desmond and Google Colab. Out of the tested protein-ligand complexes, good structural stability and a consistent binding throughout the course of simulation was observed in case of Luteolin-BRAF, Berberine-EGFR and Dehydrodiscretamine-BRAF complexes. The PI3KCA-Berberine complex however showed moderate stability. MM/GBSA binding energy analysis further supported their binding affinity and complex stability. Overall, Luteolin, Berberine, and Dehydrodiscretamine emerged as the strongest multitarget inhibitors among all the tested phytochemicals. These compounds have potential to disrupt oncogenic signalling and overcome chemoresistance in LGSC. These findings provide a computational framework and lay the foundation for future experimental validation and therapeutic development using *Tinospora cordifolia* phytochemicals.

**Keywords:** Low grade serous carcinoma, *Tinospora cordifolia*, BRAF, EGFR, Dehydrodiscretamine, Luteolin, Berberine, Magnoflorine.

## TABLE OF CONTENTS

Title	Page No
<b>Acknowledgment</b>	<b>II</b>
<b>Candidate's Declaration</b>	<b>III</b>
<b>Certificate</b>	<b>IV</b>
<b>Plagiarism Verification</b>	<b>V</b>
<b>Abstract</b>	<b>VI</b>
<b>Table of Contents</b>	<b>VII</b>
<b>List of Tables</b>	<b>IX</b>
<b>List of Figures</b>	<b>X</b>
<b>List of Abbreviations</b>	<b>XII</b>
<b>CHAPTER 1: INTRODUCTION</b>	<b>1-7</b>
1.1 Ovarian cancer overview .....	1
1.2 Phytochemical Potential of <i>T. cordifolia</i> : Hypothesis and Objectives.....	4
<b>CHAPTER 2: LITERATURE REVIEW</b>	<b>8-35</b>
2.1 Ovarian cancer overview .....	9
2.2 Biological basis for Clinical classification of Ovarian Cancer.....	13
2.2.1 Pathophysiology.....	13
2.2. Histopathology.....	14
2.3 Treatment of Ovarian Cancer.....	14
2.4 Drug resistance in Ovarian Cancer.....	20
2.4.1 Resistance mechanism to Platinum agents.....	20
2.4.2 Resistance mechanism towards Paclitaxel.....	21
2.4.3 Bevacizumab resistance mechanism.....	22
2.4.4 PARP inhibitors resistance mechanism.....	23
2.5 Role of phytochemicals in cancer therapy.....	25
2.5.1 Phytochemical classification.....	25
2.5.2 Phytochemicals biomedical importance.....	26
2.5.3 Limitations of Phytochemicals in Ovarian Cancer.....	26

2.5.4 <i>T. cordifolia</i> : A potential medicinal plant.....	28
2.5.5 <i>T. cordifolia</i> potential in cancer therapy.....	31
2.5.6 <i>T. cordifolia</i> phytochemical constituents.....	32
2.6 Research strategy.....	35
<b>CHAPTER 3: METHODOLOGY</b>	<b>36-59</b>
3.1 Selection of Phytochemicals.....	36
3.2 ADME & Druglikness analysis.....	37
3.3 Ligand Preparation.....	39
3.4 Target protein preparation.....	43
3.5 Molecular Docking.....	46
3.6 Molecular dynamic simulation.....	51
3.6.1 MD simulation on Google colab.....	51
3.6.2 MD simulation on Desmond Schrödinger.....	55
<b>CHAPTER 4: RESULT &amp; DISCUSSION</b>	<b>60-85</b>
4.1 ADME & Drug Likness analysis.....	60
4.2 Ligand Preparation.....	63
4.3 Protein preparation.....	65
4.4 Molecular docking.....	67
4.4.1 Phytochemical docking results.....	67
4.4.2 Control inhibitors docking result.....	72
4.5 Molecular dynamic simulation.....	73
4.5.1 Result of Dynamic Simulation Using Desmond Schrodinger .....	73
4.5.2 Result of Dynamic Simulation Using Google Colab.....	79
<b>CHAPTER 5: CONCLUSION &amp; FUTURE SCOPE</b>	<b>86-88</b>
<b>References</b>	<b>89-99</b>



## List of Tables

Table 1.1 Risk factor involved in Ovarian cancer.....	2
Table 2.1 EOC subtypes and their characteristics.....	12
Table 2.2 Tumor grading for NEOC.....	14
Table 2.3 Chemotherapy drugs for ovarian cancer.....	16
Table 2.4 Pharmacological actions of <i>T. cordifolia</i> .....	30
Table 2.5 Isolated Chemical constituents <i>T. cordifolia</i> .....	33
Table 2.6 <i>T. cordifolia</i> phytocomponents with anti-cancer relevance.....	34
Table 3.1 Candidate ligands from <i>T. cordifolia</i> .....	37
Table 3.2 SMILES notation of phytocompounds.....	38
Table 3.3 Control inhibitor/ligand of receptor proteins.....	42
Table 3.4 List of Target proteins involved in LGSC.....	43
Table 4.1 SwissADME Analysis of Anti-cancer Phytochemicals from <i>T. cordifolia</i> .....	61
Table 4.2 Molsoft Analysis of Anti-cancer Phytochemicals from <i>T. cordifolia</i> .....	62
Table 4.3 Best scoring Phytochemicals from SwissADME & Molsoft analysis.....	63
Table 4.4 Predicted binding pockets in target proteins.....	65
Table 4.5 Binding affinities of all Protein- ligand pairs.....	67
Table 4.6 Control inhibitor docking results.....	72
Table 4.7 MMPBSA/ GBSA binding free energy of EGRR-Luteolin.....	81
Table 4.8 MMPBSA/ GBSA binding free energy of BRAF-Luteolin.....	83
Table 4.9 MMPBSA/ GBSA binding free energy of BRAF-Magnoflorine.....	85

## List of Figures

Figure 1.1 Mechanisms of Resistance in Ovarian Cancer.....	4
Figure 1.2 Major classes of Phytochemicals.....	5
Figure 2.1 Relative Survival by Stage at Diagnosis.....	9
Figure 2.2 Classification of Ovarian Cancer.....	10
Figure 2.3 Histological subtypes of EOC.....	13
Figure 2.4 Structure of anti-OC agents used in chemotherapy.....	17
Figure 2.5 Structure of non-chemotherapeutic agents used in OC.....	19
Figure 2.6 Elevated DNA Damage & Repair Protein Expression in OC.....	21
Figure 2.7 Cancer stem cells in recurrence of OC.....	24
Figure 2.8 Phytochemicals classes.....	25
Figure 2.9 Schematic representation of phytochemical & health benefit.....	26
Figure 2.10 Morphology of <i>T. cordifolia</i> .....	29
Figure 2.11 Pharmacotherapeutic potential of <i>T. cordifolia</i> .....	29
Figure 2.12 Major constituent of <i>T. cordifolia</i> .....	32
Figure 2.13 Proposed methodology.....	35
Figure 3.1 SwissADME & Molsoft submission.....	39
Figure 3.2 Open Babel GUI file format conversion.....	40
Figure 3.3 Charge assignment & root detection in ligand.....	41
Figure 3.4 Torsion setting in ligand.....	42
Figure 3.5 Binding site prediction of protein target using CASTp 3.0 & PrankWeb.....	44
Figure 3.6 Protein structure cleaning on Discovery studio.....	45
Figure 3.7 Missing atom repair on ADL tools.....	45
Figure 3.8 Preference setting in Pyrx.....	47
Figure 3.9 Protein Grid boxes. (a) BRAF, (b) KRAS, (c) MEK1, (d) HES1, (e) EGFR, (f) PI3KCA.....	50
Figure 3.10 Google colab environment set up.....	52
Figure 3.11 Path determination to access input files.....	52
Figure 3.12 Topology file & Simulation box generation.....	53
Figure 3.13 Equilibration protocol parameters.....	54

Figure 3.14 Production run parameters.....	54
Figure 3.15 Concatenation of trajectory files.....	55
Figure 3.16 Docked protein- ligand visualization on Desmond Maestro.....	56
Figure 3.17 Protein preparation & refinement wizard.....	57
Figure 3.18 Solvation & Ions setting.....	58
Figure 3.19 MD simulation parameters setting.....	59
Figure 4.1 Radar plot of Phytochemicals.....	63
Figure 4.2 Ligand & control preparation in ADT tool.....	64
Figure 4.3 Heatmap of binding energies.....	68
Figure 4.4 Interaction map of BRAF-Luteolin.....	69
Figure 4.5 Interaction map of BRAF-Dehydrodiscretamine.....	69
Figure 4.6 Interaction map of EGFR-Luteolin.....	70
Figure 4.7 Interaction map of EGFR with Berberine .....	71
Figure 4.8 Interaction map of BRAF with Magnoflorine.....	71
Figure 4.9 Interaction map of PI3KCA with Berberine .....	72
Figure 4.10 MD simulation analysis of BRAF & Dehydrodiscretamine .....	75
Figure 4.11 MD simulation analysis of PIK3CA and Berberine.....	78
Figure 4.12 MD simulation analysis of EGFR with luteolin.....	80
Figure 4.13 MD simulation analysis of BRAF and Luteolin.....	83
Figure 4.14 MD simulation analysis of BRAF- Magnoflorine .....	85

## **List of Abbreviations**

ADME	Absorption, Distribution, Metabolism, Excretion
ADT	AutoDock Tool
AMBER	Assisted Model Building with Energy Refinement
BRAF	B-Raf Proto-Oncogene, Serine/ Threonine Kinase
CASTp	Computed Atlas of Surface Topography of Proteins
DCD	Dynamic Coordinate Data
EGFR	Epidermal Growth Factor Receptor
EOC	Epithelial Ovarian Cancer
GAFF2	General AMBER Force Field 2
GUI	Graphical User Interface
HES1	Hairy and Enhancer of Split Hololog-1
HGSC	High Growth Serous Carcinoma
KRAS	Kristen Rat Sarcoma Viral Oncogene Homolog
LGSC	Low Growth Serous Carcinoma
MD	Molecular Dynamics
MMFF94	Merck Molecular Force Field 94
MEK1	Mitogen Activated Protein Kinase 1
MMGBSA	Molecular Mechanics-Generalized Born Surface Area
MMPBSA	Molecular Mechanics- Poisson-Boltzmann Surface Area
NEOC	Non- Epithelial Ovarian Cancer
OC	Ovarian Cancer
OPLS3E	Optimized Potentials for Liquid Simulations 3e
PDB	Protein Data Bank
PDBQT	Protein Data Bank, Partial Charge & Atom Type
PI3KCA	Phosphatidylinositol-4,5-Bisphosphate 3-Kinase Catalytic Subunit Alpha
RMSD	Root Mean Square Deviation
RMSF	Root Mean Square Fluctuation
SDF	Structure Data File
TIP3P	Transferable Intermolecular Potential with 3 Point

# **CHAPTER 1**

## **INTRODUCTION**

### **1.1 OVARIAN CANCER OVERVIEW**

Ovarian cancer is a silent disease because its progression shows no symptoms in the early stages is the 7th most common cancer type. It has a five years survival rate of less than 50 %. It is one of the major reasons of death in women globally. Due to its asymptomatic nature in early stages, the disease tends to have delayed diagnosis in approximately 70% of cases till which it has already metastasized or reached stage III or IV (Stewart et al., 2019).

It is a collection of neoplasms. All the different subtypes of OC are treated as a one disease. However, efforts have been made to characterize these different subtypes. All these subtypes have distinct prognosis, molecular & clinicopathological features which shows that there is high tumour heterogeneity across various subtypes and within a single tumour(Kossai et al., 2018).

According to The Centre for Disease Control and Prevention (CDC), the highest incidence is observed among White women, with approximately 11.3 cases per 100,000 women, followed by Hispanic (9.8), Asian/Pacific Islander (9.0), African American (8.5), and American Indian/Alaskan Native (7.9) women (Stewart et al., 2019). The risk of formation of OC increases significantly with age, being extremely rare in women under 30, but rising sharply post 50 years old. Most diagnoses occur between the ages of 50 and 70 years (Varqa, 2014a). While incidence is highest in developed countries, mortality rates are disproportionately elevated in African populations which could be due to socioeconomic factors such as limited access to quality health-service, lack of awareness and poverty. The absence of effective screening programs in public health infrastructure further contributes to late-stage detection and poor clinical outcomes (Gaona-Luviano et al., 2020).

Several risk factors discovered that contribute to the formation of ovarian malignancies, encompassing reproductive, hormonal, lifestyle, medical, and genetic components. Among reproductive and hormonal factors, advanced age, early periods, delayed menopause, and nulliparity are associated with it. These conditions extend the duration of ovulatory cycles, thereby increasing exposure to hormonal fluctuations and oxidative stress in ovarian tissue.

In terms of lifestyle factors, obesity, perineal talc use, and smoking have been known in elevating ovarian cancer risk. Additionally, certain medical conditions, such as endometriosis and the use of replacement therapy of hormones (HRT), have been linked to the disease, likely due to the promotion of chronic inflammation, oxidative stress, and DNA damage.

Genetic predisposition plays a significant role in ovarian cancer etiology. A family history of breast or OC increases susceptibility. Notably, BRCA1/2 germline mutations are well-established risk factors. Other relevant mutations include those in DNA mismatch repair genes (as seen in Lynch syndrome), TP53 (Li-Fraumeni syndrome), STK11 (Peutz-Jeghers syndrome), as well as CHEK2, RAD51, BRIP1, and PALB2, all of which contribute to

compromised DNA repair mechanisms and heightened malignancy risk (Arora et al., 2024). Conversely, several protective factors have been recognized. Oral contraceptive use, particularly with long-term use, significantly reduces ovarian cancer risk by suppressing ovulation and thereby minimizing repeated epithelial trauma. Similarly, multiparity, breastfeeding, and other factors that reduce ovulatory frequency are associated with reduced risk. Surgical interventions, such as bilateral tubal ligation and salpingectomy, also offer protective effects by either preventing the ascent of carcinogens to the ovaries or removing the fallopian tubes (Flaum et al., 2020; Momenimovahed et al., 2019).

**Table 1.1-** Risk factor involved in Ovarian cancer

Factors	Protective	Predisposing	Controversial
<b>Demographic</b>			
Age		X	
<b>Reproductive</b>			
Menstrual-related factors		X	
Menarche & Menopause age			X
Parity	X		
Pregnancy characteristics			X
Higher age of childbirth		X	
<b>Gynaecologic</b>			
Pelvic inflammatory disease			X
Endometriosis		X	
<b>Hormonal</b>			
Contraceptive methods	X		
Hormone replacement therapy			X
Infertility treatments			X
<b>Genetic</b>			
Family history		X	
BRCA mutations		X	
Lynch syndrome	X		
<b>Lifestyle</b>			
Nutrition and diet			X
Alcohol caffeine and cigarettes			X
Obesity & physical activity			X
<b>Other</b>			
Lactation	X		
Lower socioeconomic status	X		

OC is both epithelial or non-epithelial in origin. The dominant type is Epithelial ovarian cancer (EOC) accounting for more than 95% cases and remaining 5% cases are non-epithelial in origin. On the basis of histology, subtypes of EOCs are; s endometrioid, mucinous serous & clear cell. Serous tumors are divided into High and Low- Grade Serous Carcinomas ie., (HGSCs and LGSCs). Out of all subtypes of EOCs, HGSC is seen more frequently and very

aggressive in nature (70-80%) while LGSC is relatively rare. Whereas the rest of the subtypes of EOCs including Endometrioid carcinoma, Mucinous carcinoma, Clear cell carcinoma has a relative frequency of approximately 10%, 3%, & 10% approximately. NEOC are namely germ cell, sex-cord stromal, germ cell and small cell OC. Out of all these, major types of OC include: epithelial (most common), germ cell, and sex-cord-stromal (*USCS Data Visualizations - CDC*, n.d.).

The current treatment paradigm for ovarian cancer involves a multimodal approach, typically combining cytoreductive (debulking) surgery and platinum-based chemotherapy, with the goal of reducing tumor burden and improving survival outcomes (Muggia, 2021). Neoadjuvant chemotherapy is done with help of drugs like carboplatin and paclitaxel, is often employed to shrink tumors prior to surgery. PARP inhibitors like olaparib and rucaparib have emerged as targeted therapies, particularly beneficial for patients with BRCA mutations, though high costs and selective efficacy limit their widespread use (Cook & Tinker, 2019; Parkes & Kennedy, 2016). Intraperitoneal (IP) chemotherapy offers localized drug delivery and improved outcomes in certain advanced-stage cases (Parkes & Kennedy, 2016). Additional strategies under investigation include the use of vitamin D analogs to enhance tumor suppression within the ovarian microenvironment (Guo & Rubinstein, 2018a).

While early rate of response to chemotherapy are often significant, a significant number of patients experience relapse, particularly in cases of HGSC, due to the development of chemo resistant disease. Recurrence remains common, with a median progression-free survival of approximately 18 months (Jayson et al., 2014a). Although targeted therapies offer some benefit, their use is constrained by high cost, toxicity, and inconsistent efficacy across patient populations. This ongoing challenge of drug resistance and tumor relapse highlights the immediate requirement for novel, safer, and highly effective curing strategies—particularly those obtained from natural places for example medicinal plants, which hold promise due to their multitargeted actions and lower toxicity profiles.

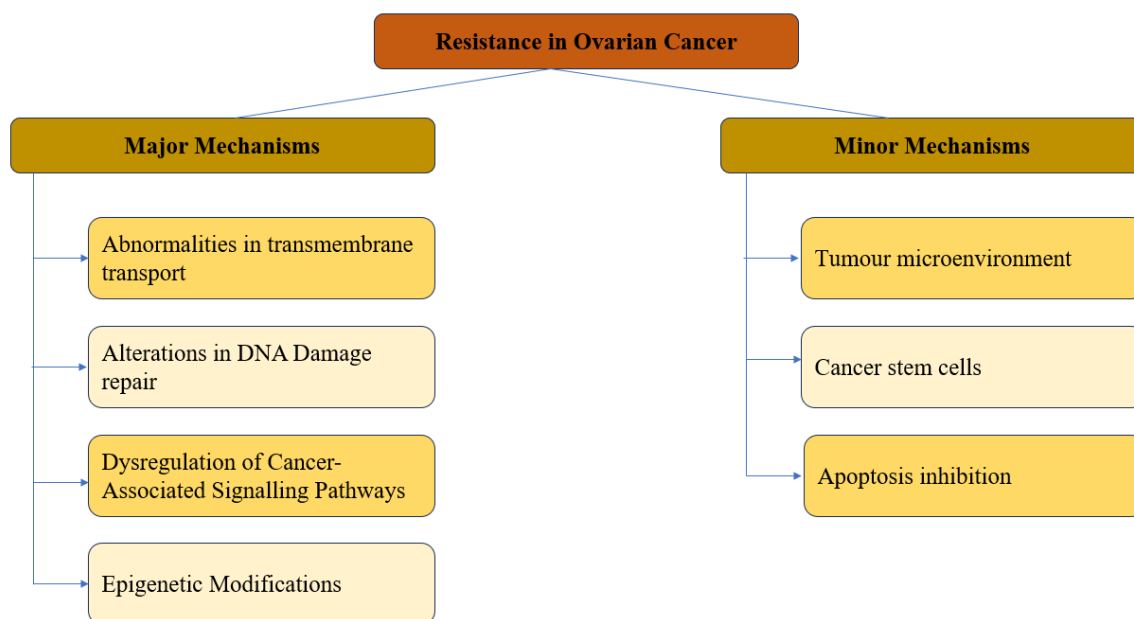
Drug resistance in OC is a complicated challenge. This happens when the tumor cells develop tolerance towards therapeutic agents. This results in reducing a drug's efficacy and its subsequent disease progression during the course of treatment. It can appear as **intrinsic (IR)** or **acquired resistance (IR)**.

IR refers to the inherent characteristics of a tumor that render it unresponsive or less responsive to therapeutic interventions from the outset. Several factors contribute to this form of resistance, including the overexpression of drug-metabolizing enzymes, which degrade therapeutic agents before they exert their effects; mutations in drug targets, which diminish drug binding and efficacy; and alterations in membrane transport mechanisms that impair drug uptake. Additionally, tumor microenvironmental factors such as hypoxia, poor vascularization, and dense extracellular matrix (ECM) components can create physical and biochemical barriers to drug delivery. Altered metabolic pathways within cancer cells also support survival under therapeutic stress, further contributing to resistance (Cornelison et al., 2017; Holohan et al., 2013).

Acquired resistance arises after initial exposure to chemotherapy or targeted therapy, as tumor cells undergo adaptive changes that allow them to survive continued treatment. Key

mechanisms include the overexpression of drug efflux transporters, particularly those of the ATP-binding cassette (ABC) family, which throws out the drugs out of cells, declining their concentrations in cell. Other adaptations involve the activation of survival signalling pathways that inhibit apoptosis and the inactivation or bypassing of DNA damage repair mechanisms, enabling cells to survive (Gatti & Zunino, 2005; Nikolaou et al., 2018) .

Both these resistance mechanisms operate through complex, often overlapping molecular pathways, collectively posing a significant challenge to effective and sustained cancer treatment outcomes.

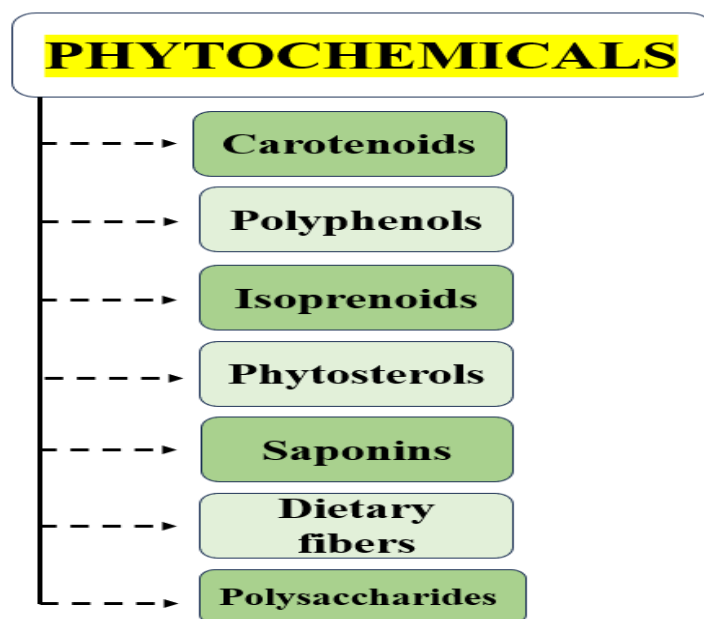


**Fig.1.1-** Mechanisms of Resistance in Ovarian Cancer

## 1.2 PHYTOCHEMICAL POTENTIAL OF *TINOSPORA CORDIFOLIA*: HYPOTHESIS AND OBJECTIVES

In light of the limitations posed by conventional therapies—including chemoresistance, toxicity, and limited efficacy— interest is increasing in exploring naturally derived compounds as complementary or alternative therapeutic agents in cancer treatment. These are bioactive compounds derived from a variety of plants like grains, vegetables and fruits, nuts, as well as herbs. Their main function is to provide plants with protection. These compounds possess a wide range of abilities like antioxidant activities and exhibit antimicrobial, antidiarrheal, anthelmintic, antiallergic, antispasmodic, and antiviral activities (Sharma et al., 2018). They are also involved in controlling transcription of genes, enhancing communication between gap junctions, improving immunity against cancer. Phytochemicals can lose their functional properties when used with non-compatible solvents & different temperatures (Choma & Nikolaichuk, 2022).





**Fig.1.2-** Major classes of phytochemicals

Phytochemicals are used widely due to their health benefits in the protecting from various diseases like cancer. A growing body of evidence from both population-based and laboratory studies supports the anticarcinogenic and antimutagenic potential of phytochemicals (Surh, 2003). Investigations utilizing various cell lines on cancer and animal models have demonstrated the efficacy of phytochemicals not only in cancer treatment but also in its prevention. These naturally occurring compounds, primarily derived from medicinal plants, have been shown to modulate multiple cellular and molecular pathways involved in tumorigenesis. Specifically, phytochemicals can suppress cell proliferation, induce programmed cell death (apoptosis), inhibit angiogenesis, and delay the processes of invasion and metastasis, DNA binding (Hadjzadeh et al., 2005). These multifaceted mechanisms highlight their therapeutic promise as complementary or alternative strategies in cancer management. The activities of different phytochemicals may differ, but a similar mechanism may be observed in the phytochemicals with similar structures.

Among the various medicinal plants explored for anticancer potential, *Tinospora cordifolia*, commonly known as Giloy, has garnered significant attention due to its diverse phytochemical profile and traditional use in Ayurveda. Revered as “Amrita,” or “the root of immortality,” Giloy has long been used for its immunomodulatory, anti-inflammatory, antipyretic, and rejuvenating properties

The genus *Tinospora*, belonging to the *Menispermaceae* family, includes around 34 species that are predominantly distributed across tropical and subtropical zones of Asia, Africa, and Australia (Udayan et al., 2009). In India, nine species of this genus have been reported to occur naturally across different states. Among them, Indian species of *Tinospora* are recognized for their longstanding use in traditional healing practices and are valued for a broad spectrum of pharmacological applications.

Among all, *Tinospora cordifolia* has garnered particular attention due to its wide usage in the Indian System of Medicine (ISM). This species possesses an array of bioactive products that are responsible for its effectiveness in curing various conditions, such as diabetes, cancer,

jaundice, fever, urinary disorders, helminthic infections, skin diseases, dysentery, and leprosy. Compared to other native species like *T. crispa*, *T. sinensis*, and *T. baenzigeri*, *T. cordifolia* is considered superior in therapeutic potential owing to its richer phytochemical composition (Chaudhary et al., 2024).

Despite its extensive use, the natural populations of *T. cordifolia* are diminishing at an alarming rate. This decline is primarily attributed to unsustainable harvesting and loss of habitat. Traditional propagation methods are insufficient to support both conservation efforts and the rising demand for this medicinal plant (Gururaj et al., 2007). To address this issue, advanced biotechnological techniques are being explored. Among them, in vitro micropropagation has emerged as a promising tool for rapid clonal multiplication of genetically stable and disease-free plantlets, ensuring a consistent yield of medicinally valuable secondary metabolites.

In addition to propagation, plant tissue culture techniques also enable large-scale production of phytochemicals under controlled conditions and provide a sustainable alternative to whole-plant harvesting. *T. cordifolia* adapts well to various environmental and soil conditions, though it flourishes best in warm, semi-arid climates with adequate humidity (Kattupalli et al., 2019).

Toxicological and safety profile of *Tinospora cordifolia* shows that *T. cordifolia* has high safety margin in both animal and human studies, with no significant adverse effects observed even at high doses. It does not impair liver, kidney, or neurological function and has even reduced drug-induced toxicity when used alongside standard treatments (Chaudhary et al., 2024).

Giloy contains a wide range of bioactive phytoconstituents, including alkaloids (berberine, tembetarine), glycosides, diterpenoid lactones (tinosporide, cordifolide), steroids, and polysaccharides. Many of these compounds displayed potential anti-inflammatory, antioxidant, and cell killing effects against cancer cell lines. Given this background, *Tinospora cordifolia* represents a promising natural source for the formation of new therapeutic agents. The present study is therefore aimed at exploring the potential of its phytochemicals in combating ovarian cancer progression and overcoming chemoresistance.

Given the limitations of conventional chemotherapy, including drug resistance, toxicity, and limited efficacy in ovarian cancer treatment, alternative therapeutic strategies are urgently needed. Phytochemicals derived from medicinal plants gave promising results in targeting various cancer-related pathways and reversing resistance towards drugs in several malignancies. Among these, *Tinospora cordifolia* (Giloy), known for its immunomodulatory, antioxidant, and anti-cancer properties, may offer a novel and less toxic approach to treating ovarian cancer.

This study hypothesizes that phytochemicals from *Tinospora cordifolia* possess the potential to interact with key molecular targets involved in OC progression and resistance, thereby offering a promising therapeutic alternative to conventional chemotherapy. With help of computational methods (molecular docking and molecular dynamics simulations), this research will evaluate the binding strength and stability of these phytochemicals with drug resistance proteins and cancer-related receptors, offering new insights into their therapeutic potential.

Objectives proposed for this study are

1. Evaluate the therapeutic potential of selected phytochemicals from *T. cordifolia* (Giloy) in combating ovarian cancer progression and overcoming drug resistance by assessing the stability and binding affinity of these compounds.
2. Identify key phytochemical compounds in *Tinospora cordifolia* with the highest potential for therapeutic use in ovarian cancer.
3. Explore the mechanisms through which *Tinospora cordifolia* phytochemicals may modulate drug resistance mechanisms in ovarian cancer.

## **CHAPTER 2**

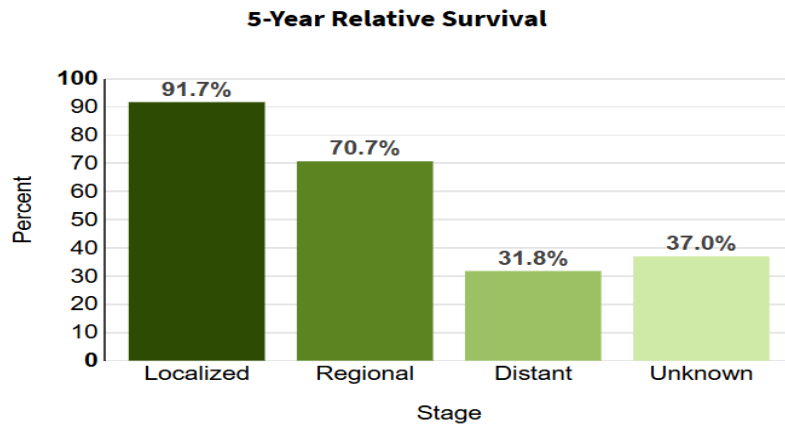
### **LITERATURE REVIEW**

OC is a leading female related disease with a high death rate on the global scale. Ovaries are essential reproductive structures in a female, situated on both sides of uterus. These paired structures are not only essential for production of the female gamete called oocyte but in producing female reproductive hormones i.e., estrogen and progesterone. When the malignant cells in the ovaries undergo an uncontrolled mitotic division, it results in development of ovarian cancer. Therefore, it can be defined as a malignant neoplasm of the ovaries. The many subtypes of OC vary from each other in terms of their prognosis, molecular and pathological features that defines them but all these subtypes are treated as a single entity.

This disease is known to be a silent killer because of its asymptomatic nature of progression when it is in the initial phase, making an early detection of disease challenging. As a result, a majority of OC (70%) cases remains undetected for a longer time till then the disease already reaches to stage III or IV (Shaik et al., 2020). In the late stages the disease already spreads to the pelvis and stomach. A consequence of that is reduction in survival rates at advanced stages to just 47%.

It represents a significant public health worry, with an estimated 20,890 new cases and 12,730 deaths expected in the United States in 2025 alone. Although it contributes 1.0% of new cases, it contributes to 2.1% of cancer-related deaths among women, reflecting its high mortality rate. According to SEER data, the 5-year survival rate for OC stands at 51.6%, highlighting the requirement for better detection and treatment plans.

The survival rate of OC is heavily influenced by the stage at which it is diagnosed. If it has localized (limited to the initial site), the 5-year survival is a promising 91.7%. However, only 20.3% of OC are diagnosed at the localized stage. As it progresses to a regional or distant stage, the survival rate significantly declines. Early detection remains a key factor in improving survival outcomes, making the local stage diagnosis crucial for improving long-term prognosis (Ovarian Cancer — Cancer Stat Facts, 2025).



**Fig.2.1-** 5-Year Relative Survival by Stage at Diagnosis: Ovarian Cancer (Source: Surveillance, Epidemiology, and End Results Program, 2025)

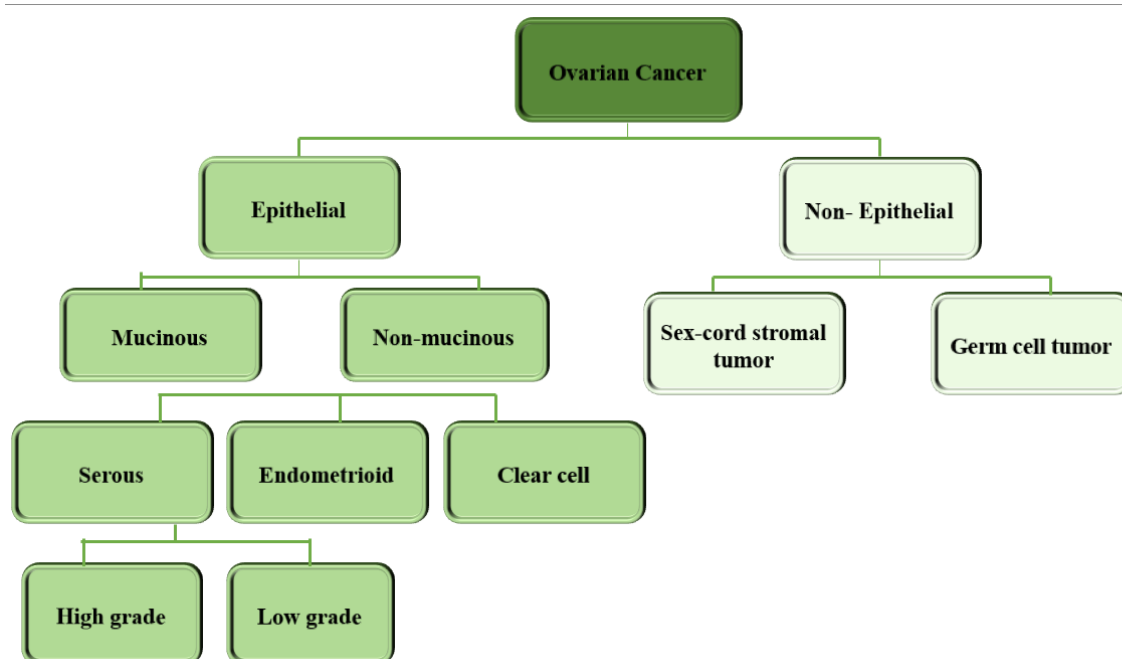
In its early stages, OC has symptoms that are not clear such as pelvic or abdominal pain, bloating, a sensation of abdominal heaviness, early satiety, back pain, and abnormal vaginal bleeding or discharge—particularly between menstrual cycles or after menopause. Patients may also experience changes in bowel/urinary habits. In some cases, it demonstrates metastatic behaviour, spreading to adjacent places like bladder or colon. Although the disease is uncommon in young women under the age of 30 but the risk increases with rising age and most of women are diagnosed between ages 50 to 70 (Stewart et al., 2019).

Even though awareness regarding OC is increasing by the day, rates of success for curing the disease and the survival statistics has not shown much change which could be attributed to mainly failure in early diagnosis. This can have fewer reasons like absence of a clear screening method and the fact that the symptoms are often vague and can be confused with other benign cancerous conditions (Kossai et al., 2018).

## 2.1 OVARIAN CANCER CLASSIFICATION

OC is a group of different tumors that come from various tissues within or near the ovaries. Although traditionally believed to originate in the ovary itself, recent studies show that some of the highly aggressive forms, like HGSC, may actually begin in the fallopian tubes at the fimbrial end. Tumors can also arise from nearby tissues such as the peritoneum or endometrium (in cases linked with endometriosis), making the classification complex.

OC has two types, epithelial & non-epithelial types based on the kind of cell they arise from. EOC is predominant or most common form of OC while Non-Epithelial Ovarian Cancer (NEOC) accounts of approximately 5-10% of overall cases. So EOC can develop from the surface that lines the ovaries whereas the NEOC usually originates from cells producing hormones, structural cells or embryonic germ cells.



**Fig.2.2-** Classification of ovarian cancer

Further subtypes of EOC are namely serous, endometrioid, mucinous and clear cell carcinoma (Shaik et al., 2020). Serous carcinoma further has two types namely, HGSC and LGSC. Out of which, HGSC is the highly aggressive and fatal compared to LGSC. Prevalence of rest of types of EOC are highest for endometrioid followed by mucinous cancer and least for clear cell carcinoma (CCC). It was thought that CCC is linked to endometriosis which is considered the most probable precursor lesion (Tang et al., 2018). However, this association is still under investigation. Likewise, endometrioid carcinoma is also known to be associated with endometriosis (Lalwani et al., 2011). Mucinous carcinoma is usually diagnosed at early stages of disease (Xu et al., 2016).

EOCs can either originate from the ovaries, fallopian tubes or from other sites located in the pelvic region. It is divided into two types on basis of lethality scale of tumors formed. Type I tumors in EOC are considerably less lethal than type II tumor because they are detected early so usually don't have fatal outcomes. It primarily occurs due to inflammation in the pelvic region, endometriosis or continuous ovulation cycles. Type II tumor are much more dangerous and usually have a fatal outcome because they get diagnosed late. These tumors arise mainly due to mutations in genes like BRCA and p53. There site of origin is fallopian tubes mainly and can migrate from there to other sites.

Serous carcinoma, a subtype of EOC has further been classified into HGSC and LGSC. When comparing their prognosis, LGSCs which originate from ovaries score better than HGSCs. Patients with LGSc are diagnosed at young ages but women diagnosed with HGSCs are known to have a fatal prognosis because women get diagnosed with later stages of disease (Bergamini et al., 2016).

HGSCc arise from tubes but can spread to peritoneum or the ovaries and it affects women in post-menopausal stage. Such patients have a 10- year mortality rate of 70%. HGSC cells are usually irregular and fast-growing and they form papillary structures or solid masses. They also show abnormalities in their nuclei and rapid division. In terms of markers, HGSC have

presence of CK7, PAX8, and WT1, but no CK20. These cells also show abnormal p53 protein due to mutations and around 22% have BRCA1 or BRCA2 mutations (Soslow et al., 2012). Despite being a complex, only a few genes get mutated in HGSCs. Another defect seen in the cells are a faulty DNA repair (homologous recombination) and higher genetic alterations, including many regions of DNA gains and losses. Within HGSCs different subtypes are also available with different molecular features and showing different behaviour. Tumor - microenvironment also varies within these subtypes and immune cells inside the tumor, especially CD3+ and CD8+ T cells, are linked to better survival (Zhang et al., 2003).

However, LGSCs cells look similar to HGSC cells under microscope but they divide comparatively slowly. In terms of markers, these cells stain positively for WT1 and CK7 along with receptor for estrogen hormone, and estrogen receptor (ER), but it does not show abnormal p53 expression. It is genetically stable and majority of cases show mutations in genes like KRAS or BRAF, but these mutations do not occur together in the same tumor (Jones et al., 2012).

Endometrioid carcinoma (EC) as the name suggests arises from endometriosis and it has an early and favourable prognosis which is due to the fact that this subtype shows sensitivity towards chemotherapy making its treatment successful (Varqa, 2014b). Coming to its morphology, it appears as unilateral solid mass so present in only one of the ovaries. They are similar to glandular cells present in endometrium but can show squamous differentiation. EC usually show staining for CK7 and PAX8, and hormone receptors (estrogen and progesterone) only. On the molecular front EC frequently harbours mutations in the somatic cell in CTNNB1, PIK3CA, protein phosphatase 2, regulatory subunit 1, alpha, ARID1A and PTEN genes. Endometriosis can act as a precursor lesion for EC because it is usually found associated with endometriosis and both show shared mutation in PTEN and ARID1A genes (Wiegand et al., 2010a).

Clear cell carcinomas (CCC), a rare subtype occurring in younger women usually show a good prognosis if detected early (Varqa, 2014b). If not then it shows outcome similar to what is observed in serous and endometrioid types because during later stages the tumor cells become resistant towards chemotherapy -based options and other complication that arises mainly due to formation of blood clots and paraneoplastic hypercalcemia (Rendi et al., 2024). They appear as large masses, unilateral (McCluggage, 2008). Certain complication attached to it are thromboembolism and hypercalcemia. Also, compared to serous subtype the rate of lymph node metastasis is high here. CCC cells are composed of clear, glycogen-rich cells arranged in various patterns, including solid, papillary, and tubulocystic. Distinguishing CCC from other subtypes (like EC or HGSC) can be difficult, especially in mixed tumors. It has presence of napsin A marker only and no WT1, p53, and ER. It also shows mutations in the ARID1A and PI3KCA genes (Wiegand et al., 2010b).

Mucinous Carcinoma (MC) are often times diagnosed at stage 1. Metastasis of GI tract can be linked to MC. (Varqa, 2014c). It shows positive prognosis if surgically removed but if MC recurs or spreads then outcomes get worse. These are solid- large, unilateral, and multicystic in appearance and rich in mucus. Their growth pattern is either expansive or infiltrative (Rodríguez & Prat, 2002). The former is less aggressive and shows clustered glands which are well formed but the latter has the capacity to spread beyond the ovary. Therefore, it follows destructive tissue invasion. MCs are typically positive for CK7 and CK20 but shows variability

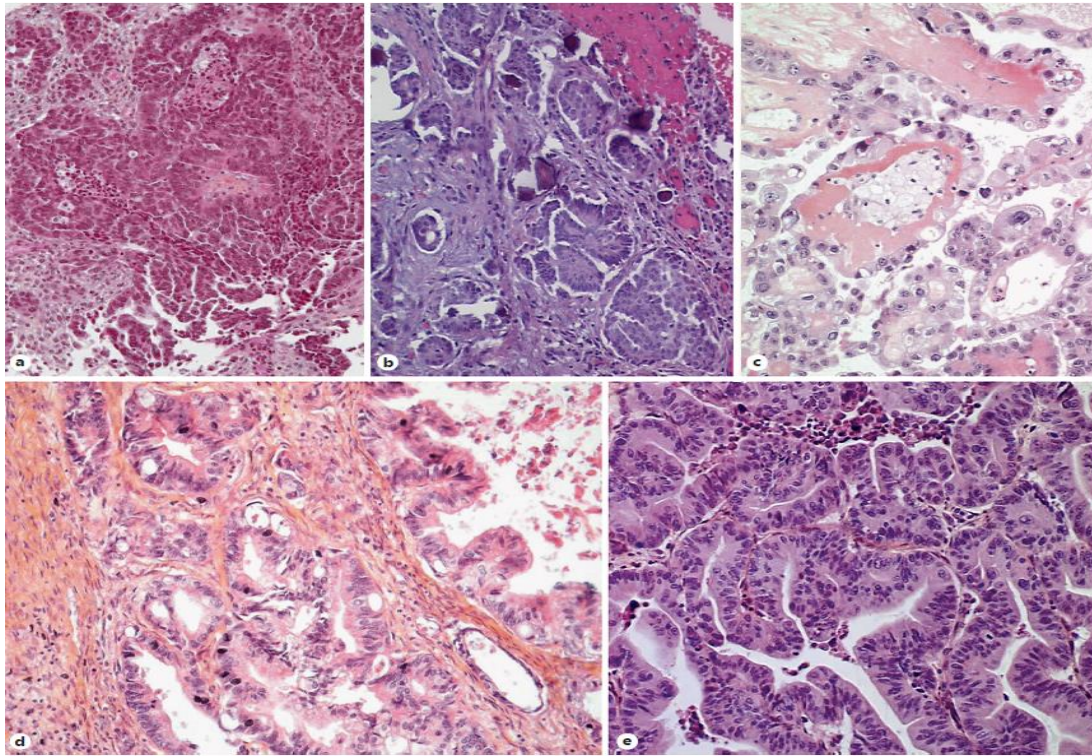
in expression for PAX8(Chailyan et al., 2011). MCs commonly carry KRAS mutations (seen in about 75% of cases), often shared across different tumor stages from benign to malignant — suggesting a stepwise evolution.

**Table 2.1-** EOC subtypes and their characteristics

SEOC			
Features	HGSC		LGSC
Cases	70		3
Diagnosis age	61		43
Tumor Marker	Cancer antigen -125		Cancer antigen-125
Genetic risk factor	BRCA 1 & BRCA 2		Serous borderline tumor
Stage during presentation	Late stage		Late stage
Response to chemotherapy	Sensitive		Resistant
Gene mutations	P53; BRCA 1/2; HR defects		BRAF; KRAS; NRAS; ERBB2; PIK3CA
Common immune cells	WT1 and CK7 present; P53 present; PAX8present; elevated Ki67		Presence of WT1, CK7, Pax8+ P53 is normal and lower Ki67
NSEOC			
Characteristics	CCC	EC	MC
Cases	12	11	3
Diagnosis age	55	56	53
Tumor Marker	Cancer antigen-125	Cancer antigen-125	Carcinoembryonic antigen; Cancer antigen19-9
Genetic risk factor	HNPCC	BRCA/HNPC	Not known
Stage at time of presentation	Early	Early	Early
Response to chemotherapy	Resistant and radiosensitive	Sensitive	Resistant
Gene mutations	PIK3CA; ARD1A; PTEN; MSI	CTNNB1; ARID1A; PTEN; MSI; PIK3CA; PPP2R1A	KRAS; HER2; CDKN2A
Common immune profile	Napsin A+; HNF β+; WT1-; ER	CK7+; Pax8+; ER+; Pax8+; vimentin+ WT1-; P53 is normal	CK20+; Cdx2+; CK7+; ER-; WT1-; PAX8 variable

NEOC are less significant when compared to EOC. Tumors in the germ cell are not frequent (3% of total OC cases). These are found to occurs in young women (age 10-30 years). Histologically speaking they are similar to germ cell tumors seen in men’s testes. Sex cord ovarian cancer tumors are the least common type of OC. They are often benign and they are detected early too. It is more commonly seen in women of African American decent (Gershenson, 2024) .





**Fig.2.3-** Histological slides of EOC subtypes. HE-saffron. **a** HGSC.  $\times 10$ . **b** LGSC.  $\times 20$ . **c** CCC.  $\times 10$ . **d** MC.  $\times 20$ . **e** EC.  $\times 20$ .

## 2.2 BIOLOGICAL BASIS FOR CLINICAL CLASSIFICATION OF OC

A comprehensive understanding of this disease requires insight into both its biological underpinnings and clinical progression. This section explores the pathophysiological mechanisms that drive tumor development and behaviour, along with the histopathological characteristics that distinguish its subtypes.

### 2.2.1 PATHOPHYSIOLOGY

Uncovering the pathogenesis of OC is difficult because of its property of heterogeneity among various histological subtypes of OC. However, certain theories are proposed such as; Incessant Ovulation Theory suggests that OC starts from surface lining the ovary called as ovarian surface epithelium. In every ovulation cycle, this surface epithelium bears damages which it repairs itself. This repeated damage and repair acquired through many ovulatory cycles throughout a women's life may cause DNA mutations in epithelial cells. Some damaged cells may spread into the inner tissues of ovary called a stroma and creates certain pockets known as **cortical inclusion cysts** which get constantly exposed to hormones that stimulate their growth, which might lead to cancer (Erickson et al., 2013). Theory is backed by various studies showing more ovulation cycles over the lifetime and fewer pregnancies without any use of birth control is associated with a higher predisposition to OC.

However, certain limitations of this theory are its inadequacy in explaining the pathogenesis of different subtypes of OC. Surface epithelium is not similar histologically to subtypes of EOC (mucinous and non-mucinous). Also, it doesn't explain how women suffering with polycystic

ovary syndrome have a higher risk of developing OC despite experiencing lesser ovulation cycles (Kurman & Shih, 2010).

Theory on fallopian Tube (FT) tells that according to newer research many ovarian cancers may actually start in the FT, not ovary itself as believed earlier, especially in women with BRCA1/2 mutations. Examination of fallopian tubes removed from women as part of preventive surgery showed abnormal cells called TICs (tubal intraepithelial carcinoma) are often found in the fimbriae, the part of the tube closest to the ovary (Visvanathan et al., 2010).

These TICs look like HGSC, and they often have TP53 mutations, just like ovarian tumors. This suggests cancer might begin in the FT and then move towards ovary.

Two-Pathways Theory divides OC into two types, namely type 1 and type 2 OC. Type I OC are slow-growing, less aggressive and it contains LGSCs, MC, EC and CCC transitional types. In these the precursor lesion often develops within the ovary and grow slowly and are genetically stable. They undergo morphological changes and once it crosses intermediate stage it becomes OC. Therefore, its progression follows the traditional path where the inclusion cysts will receive stimulations for growth from its surrounding for transformation into cancerous cell. Most common mutations here are in KRAS and BRAF genes (Budiana et al., 2019).

Whereas in second type, the precursor lesions usually arise on the outer surface of ovary, often in the FT, and genetically not very stable. These are fast-growing, aggressive. It includes, HGSCs, undifferentiated, and carcinosarcomas. These usually arise outside the ovary, often in the FT, and are not stable genetically. Common mutations in the genes include tumor protein53, Human epidermal growth factor 2/neu, and BRCA1/2. Other than genetic mutations stress in form of inflammatory cytokines and reactive oxygen species (ROS) trigger epithelial cells of the tubal region to undergo uncontrolled division leading to neoplasms (Koshiyama et al., 2014).

## 2.2.2 HISTOPATHOLOGY

OC is diagnosed histologically. Tumor is graded in case of non-serous ovarian cancers (which includes CCC, endometrioid carcinoma and mucinous carcinoma) on basis of histologic architecture whereas the serous carcinomas are graded biologically (Lin et al., 2021).

**Table 2.2-** Tumor grading for Non-serous Ovarian cancer

Grading	Interpretation
GX	Grade can't be determined
G1	Differentiated
G2	Moderate level of differentiation
G3	Low level of differentiation

## 2.3 TREATMENT OF OC

Treatment basically depends on the stage disease is at along with how the patient is performing to said treatment. As primary treatment is responsible for determining chances of OC getting cured which indirectly depends on biology of the tumor and the stage it is at. If treated when tumor is in early stages cure rate increases to 90% but due to poor diagnosis of this disease at later stages, the treatment strategy often fails to cure the disease.

## **Surgical Treatment**

Surgery is an essential treatment option. The goal is to remove all visible tumors, but if the cancer has spread too extensively—like to the small intestine, stomach, or pancreas—complete surgery may not be possible. In early-stage cases, doctors usually perform an exploratory laparotomy in which a vertical cut is made from the chest bone to the pubic area in order to look at the abdominal cavity and collect fluid samples for testing. The surgery also involves removing both ovaries and FT, the uterus, from the pelvic and para-aortic areas, the fatty tissue layer, and taking samples from the peritoneum for biopsy. The collected tissues are then examined to determine the type of cancer, grade, and FIGO stage, which basically guides planning future treatment.

If more than 1 cm of tumor remains after surgery, the procedure is considered less effective. This is especially important for low-grade serous cancers, which respond poorly to chemotherapy, making surgery more critical. Lymph node removal doesn't improve survival if the nodes appear normal, and it may increase risks like infections and complications. Older patients (especially over 75) often have worse outcomes because their surgeries are less complete and they tolerate chemotherapy poorly. Their treatment should be based on overall health, not just age (Bardram et al., 1995).

In case of advanced-stage ovarian cancer, treatment can start from surgery called as primary debulking or with a few cycles of chemotherapy followed by surgery called as interval debulking. Debulking surgery is important when remaining tumor nodules are < 1 cm in diameter, as this is associated with improved outcomes.

Interval Debulking Surgery (IDS), done after three chemo cycles, is debated. It may reduce complications, surgery time, blood loss, and hospital stay. However, studies supporting IDS have flaws, including fewer complete tumor removals and short surgeries. Still, IDS can be useful for frail patients or those who can't safely undergo extensive surgery at diagnosis (e.g., due to blood clots). In cases where the cancer recurs or relapses more surgeries like secondary or even tertiary cytoreduction may be considered, which depends on the patient's condition and response to prior treatments given (Vergote et al., 2010).

## **Neoadjuvant Therapy and Chemotherapeutic Agents**

In advanced OC cases, neoadjuvant therapy is often used prior to surgery to reduce tumor size and improve the effectiveness of surgical removal. As NCCN instructions, IV combinations such as taxane/ carboplatin or liposomal doxorubicin/carboplatin are recommended for both neoadjuvant and adjuvant treatment. The standard and widely used chemotherapy for ovarian cancer continues to be a combination of carboplatin and paclitaxel, with carboplatin remaining the preferred agent for adjuvant therapy over the past 15 years (Van Der Burg et al., 2014a).

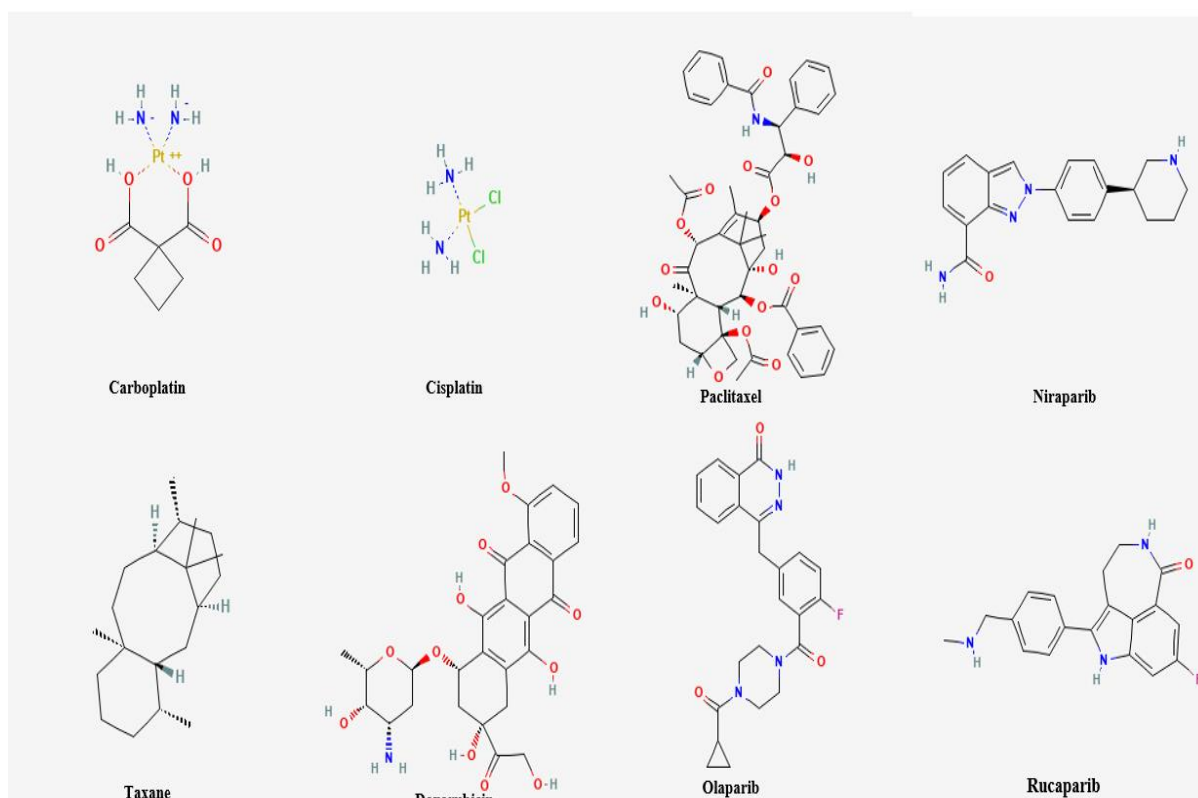
A significant recent development in ovarian cancer treatment is the introduction of poly (ADP-ribose) polymerase (PARP) inhibitors like olaparib and rucaparib (Van Der Burg et al., 2014b). These work by blocking the PARP protein used by cancer cells to repair the DNA damage done by chemotherapy. In cancers with faulty repair mechanisms of DNA, such as those with mutations in BRCA or homologous recombination deficiency (HRD), inhibiting PARP leads to the collection of DNA damage causing death of cancer. These inhibitors have shown

significant progression-free survival (PFS) benefits in ovarian cancer patients who respond to first-line platinum-based chemotherapy (Kuroki & Guntupalli, 2020). Inhibiting this repair process prevents tumor cells from surviving and proliferating. Although PARP inhibitors show great promise, they are costly, and ongoing studies are aimed at identifying the most suitable patients and tumor types for their effective use.

**Table 2.3-** Commonly used chemotherapy agents for ovarian cancer (Stewart et al., 2019)

Medication	Administration Route	Applicable Stage	Treatment Duration
Paclitaxel & Carboplatin	Intravenous	Stage I	21 days
Paclitaxel & Carboplatin	Intravenous	Stage I	7 days
Docetaxel & Carboplatin	Intravenous	Stage I	21 days
Paclitaxel & Cisplatin	Intravenous/ Intraperitoneal	Stage II, III, IV	21 days
Paclitaxel & Carboplatin	Intravenous/ Intraperitoneal	Stage II, III, IV	21 days
Dose-dense Paclitaxel & Carboplatin	Intravenous	Stage II, III, IV	21 days
Paclitaxel & Carboplatin	Intravenous	Stage II, III, IV	7 days
Docetaxel & Carboplatin	Intravenous	Stage II, III, IV	21 days
Carboplatin & Liposomal Doxorubicin	Intravenous	Stage II, III, IV	28 days
Bevacizumab with Paclitaxel & Carboplatin	Intravenous	Stage II, III, IV	21 days

Data from the National Comprehensive Cancer Network. Ovarian cancer: including fallopian tube cancer and primary peritoneal cancer.



**Fig 2.4-** Structure of anti-OC agents used in chemotherapy & as inhibitors (National Center for Biotechnology Information (NCBI). (2025). *PubChem Compound Summary*. Retrieved May 12, 2025, from <https://pubchem.ncbi.nlm.nih.gov>)

### Intraperitoneal Chemotherapy

OC patients in late stages of epithelial/ peritoneal cancers who have undergone debulking surgery, post which if they have low-volume residual disease are chosen as candidates for intraperitoneal therapy. This treatment has proven to be effective in enhancing the survival chances. In this method a small cut is created in abdomen wall, followed by threading a catheter via the subcutaneous tissue, and then positioning in peritoneal cavity. The catheter facilitates the chemotherapy drugs to be infused directly into the cavity, thereby enhancing localized treatment (Kimyon Comert et al., 2018).

### Hyperthermic Intraperitoneal Chemotherapy

According to the guidelines IC is not considered as a standard treatment of OC and should only be done in clinical trials. There are two types: one is done after surgery using a catheter, and the other, called HIPEC (Hyperthermic Intraperitoneal Chemotherapy), is done during surgery. In HIPEC, heated chemotherapy like cisplatin (temperature around 40°C) is circulated in the abdomen for about an hour after all visible tumors have been removed (Friedrich et al., 2021). The heat helps the drugs work better and reach cancer cells more effectively which means it enhances cytotoxic effect of the drug, its penetration power and ability to cross link with DNA. One major study has shown that adding HIPEC improves survival by about 14 months without causing more serious side effects. However, questions remain about the best drug



combinations, duration, and possible complications. Because of this, HIPEC should only be used in hospitals with experience and as part of clinical research (Friedrich et al., 2021).

### **Vitamin D % Molecular Hydrogen**

Patients having lower levels of vitamin D are more chances of developing OC. Taking vitamin D supplements may reduce cancer-related deaths by about 13%.

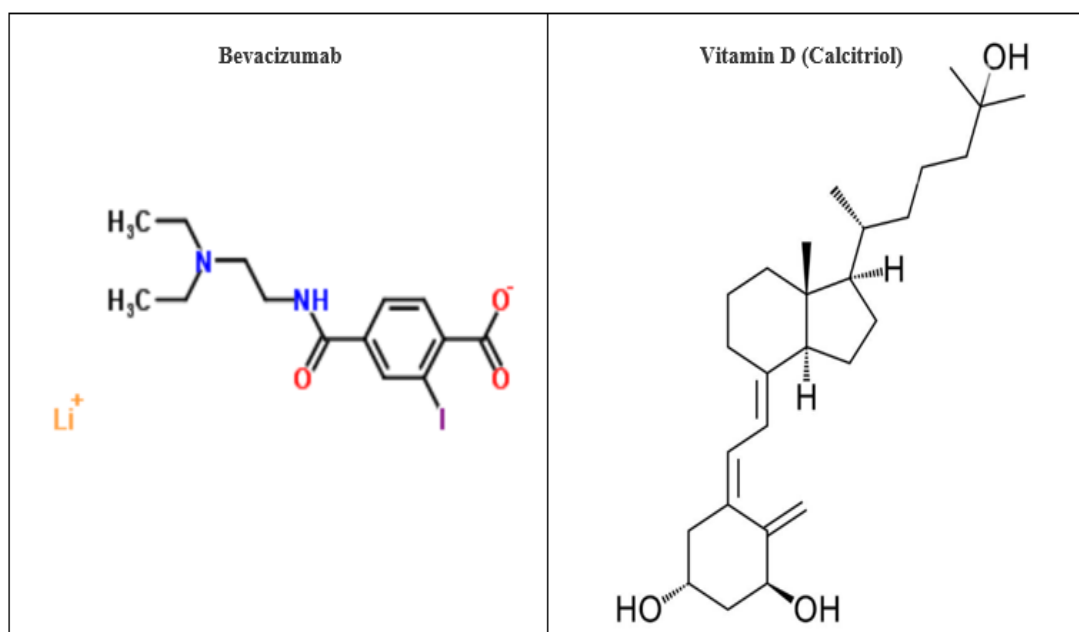
So as advancement towards OC treatment, combination of active vitamin D form has been proven to be effective. The fatty tissue layer surrounding the ovaries known as omentum makes such an environment which makes treating OC difficult. This is because in the environment there are cells like adipocytes, immune cells, microvascular cells, and fibroblasts all of which basically facilitates the cancer to grow (Guo & Rubinstein, 2018b). In this regard when vitamin D is given along with chemotherapeutic agents, it enhances elimination of cancer cells in the omentum surrounding ovary.

However, vitamin D itself isn't active in itself — it must first be converted in the body. Sunlight helps produce a form of vitamin D in the skin known as previtamin D, which is then changed in the kidneys/liver to its active state, called **calcitriol**. This active form can also be produced in certain tissues, including cancer cells. Calcitriol slows down ovarian cancer cell proliferation and trigger cell death. It does this by stopping cells from progressing through the cell cycle, particularly by acting on proteins like **P21 and P27**, which help block the cell at a key checkpoint (Deeb et al., 2007).

Besides vitamin D, molecular hydrogen has also shown anti-cancer effects. In a study using mice with ovarian cancer, breathing in hydrogen gas for six weeks significantly reduced tumor size. Lab tests confirmed that hydrogen treatment also slowed cancer cell growth and movement. Hydrogen was especially effective at stopping cancer cells from spreading and forming new colonies (Shang et al., 2018). So, high concentrations of hydrogen gas could help in fighting ovarian cancer.

### **Bevacizumab antibody**

Bevacizumab is a monoclonal antibody which is created recombinantly that targets and neutralizes VEGF A, stopping it from binding thereby triggering on VEGF receptor. This new treatment can increase survival in combination paclitaxel/carboplatin. It is currently part of ongoing trials, in order to evaluate its effectiveness in frontline ovarian cancer treatment (Sambasivan, 2022).



**Fig 2.5-** Structure of non-chemotherapeutic agents used in ovarian cancer management (ChemSrc. (2025). *Chemical Structure Database*. Retrieved May 12, 2025, from <https://www.chemsrc.com/en/>)

### Short -term and long -term effects

Taking out FT and the ovaries which are the sites of origin of OC is a major step towards treating it. After treatment the time a patient survives without the disease worsening is about 18 months. But if disease is diagnosed at later stages, there is a higher risk of recurrence of it. If the disease reoccurs, the earliest sign to look out for is increase in the CA125 marker (Jayson et al., 2014b). In that case majority of patients are taken for second line of chemotherapy and only a smaller proportion of individuals are considered for surgery. As OC also targets the urogenital tracts, short-term and long-term effects may involve symptoms such as abdominal enlargement, feeling bloated, bleeding or blockage in the urinary tract, disturbed bowel movement, weight gain/loss, loosing appetite etc and abdominal pain due to the size of the tumor or metastasis (Slatnik & Duff, 2015).

### Genetic testing

A significant proportion of epithelial ovarian cancers are associated with mutations in genes involved in homologous recombination repair (HRR), such as BRCA1, BRCA2, RAD51C/D, BRIP1, PALB2, and BARD1 (Wilson et al., 2017). According to guidelines provided by bodies like SGO, ASCO, and NCCN, all the patients that are newly diagnosed with OC are required to go for genetic testing as well. If the testing shows mutation of mentioned genes, then family members of such patients should also be tested. BRCA1/2 gene testing specifically for non-mucinous ovarian cancers is also recommended, as it can predict responsiveness of the patient towards PARP inhibitors (N. Colombo et al., 2019). However, despite being useful genetic testing remains underutilized.

## **2.4 DRUG RESISTANCE IN OC**

For past two decades. The treatment prescribed for treating OC is chemotherapy using platinum either cisplatin/ carboplatin or together with paclitaxel. Majority of the patients affected by it show positive response towards this treatment strategy however, around 80% of them develop a resistance towards platinum which is detrimental factor for treatment efficacy and patient's survival(Ortiz et al., 2022) . Therefore, drug resistance is a challenge in treating OC as it determines the drug efficacy, disease progression and recurrence. Resistance towards therapeutics agents in tumors can manifest in form of either IR or AR. IR is due to certain factors that are already associated with the tumor. For example, if the enzyme responsible for metabolizing the drug gets overexpressed it will result in its degradation, or if the drug target gets mutated then its therapeutic action will be affected, if transport mechanism responsible for drug uptake gets modified, or because of the tumor microenvironment (ECM interaction and poor vascularization), changes in cellular metabolism etc (Cornelison et al., 2017; Holohan et al., 2013). While AR happens when tumor adapts itself to the treatment that is given. For example, in response to drug given, the drug efflux proteins start overexpressing, signalling pathways involved in tumor survival getting activated, inhibition of DNA repair mechanisms etc (Gatti & Zunino, 2005; Nikolaou et al., 2018).

### **2.4.1 MECHANISMS OF RESISTANCE TO PLATINUM AGENTS**

Platinum agents like carboplatin or cisplatin mainly works by forming cross links with DNA in cancer cells. This basically damages the DNA because it can no longer undergo replication/transcription ultimately leading to cell death. Mechanism adopted by cancer cells to evade from the agents is either by stopping agents from reaching DNA via help of efflux transporters or by activating DNA repair pathways.

#### **Cisplatin transporters for Influx/ efflux**

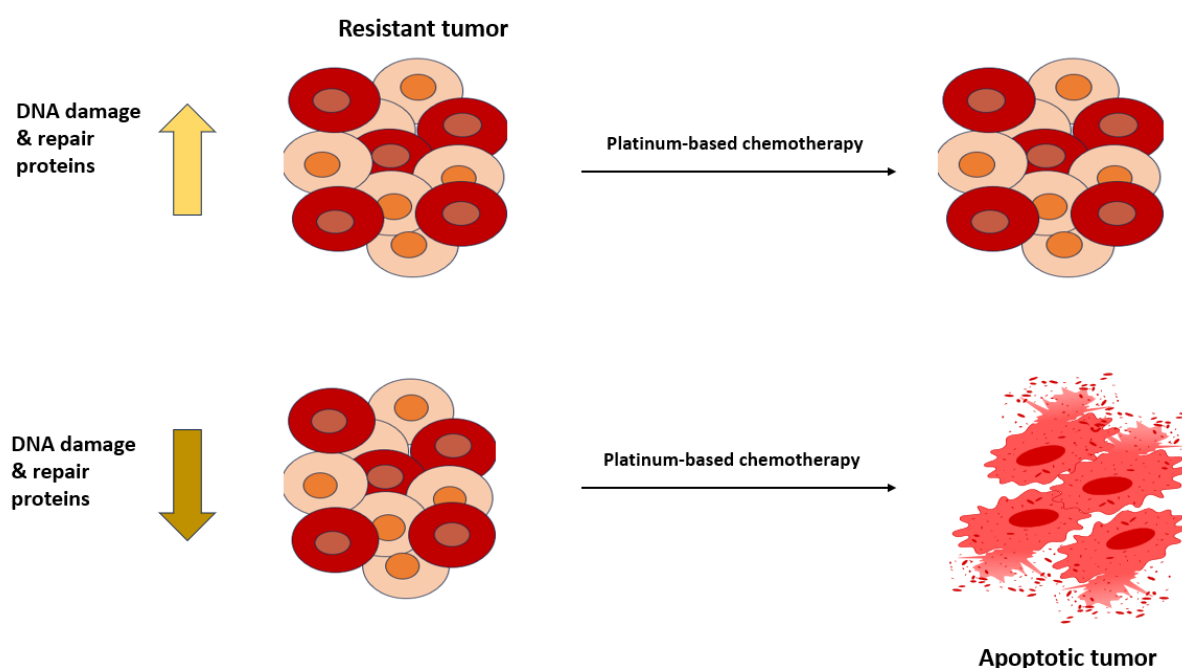
Major reason behind platinum mediated resistance in EOC involves the dysregulation of drug transporters that mediate cisplatin influx and efflux. Copper transporter 1 (CTR1) facilitates cisplatin entry into cells, and its expression is typically higher in cisplatin-sensitive ovarian cancer cells (Ortiz et al., 2022). However, exposure to cisplatin induces a rapid downregulation of CTR1, thereby reducing drug accumulation and contributing to resistance. This downregulation can be inhibited by proteasome inhibitors like bortezomib. On the other hand, ATP7B, a copper-exporting ATPase, functions as an efflux transporter, removing cisplatin from cells and promoting resistance. Silencing ATP7B has been shown to restore cisplatin sensitivity, and its high expression is associated with poor prognosis in patients (Mangala et al., 2009).

#### **DNA repair mechanism**

After intracellular uptake of platinum-based drugs through CTR1, these agents move to the nucleus where they form cross links with tumor cell DNA, the cross-links can be intra-strand and interstrand thereby forming DNA lesion. These lesions are then recognized and repaired by various DNA repair mechanisms leading to platinum resistance. Lesions in single-strand of DNA are repaired via the nucleotide excision repair (NER) pathway(P. E. Colombo et al., 2014). Endonucleases like ERCC1-XPF and XPG together remove the damaged DNA. Whereas in case of double-strand breaks or lesions, repair is facilitated through help of either homologous recombination (HR) or non-homologous end joining (NHEJ) (Du et al., 2016).



Additionally, resistance can arise due to dysfunction in the mismatch repair (MMR). Its role is to recognize and corrects errors in DNA replication. Epigenetic silencing of MLH1 promoter hypermethylation, impairs MMR function, further aggravating resistance(Arnold et al., 2003).



**Fig 2.6-** Elevated DNA Damage & Repair Protein Expression in OC

### **Other additional mechanism**

Other than the classical pathways recent research has identified additional mechanisms involved in platinum resistance in OC which are enhanced de-ubiquitination of proteins targeted for proteasomal degradation, thereby stabilizing proteins involved in cell survival(Shen et al., 2020). Exposure to cisplatin has been found to increase autophagy thereby promoting drug resistance by helping cells to survive when stressed. Furthermore, resistant cancer cells have been shown to shift their metabolic dependency toward mitochondrial oxidative phosphorylation, to improve energy efficiency and supporting survival in presence of chemotherapeutic agents. Metabolic reprogramming and angiogenesis are well known cancer hallmarks, are found to be contributors to chemoresistance. For example, upregulation of the serine/threonine kinase Aurora-A in cisplatin-resistant ovarian cancer has been found to enhance glycolysis and suppress senescence by activation of SOX8 transcription factor(Sun et al., 2020). Similarly, fibrillin-1 (FBN1) is also found to be overexpressed in resistant tissues and organoids. It is involved in phosphorylation of VEGFR2 and nuclear translocation of STAT2 ultimately increasing glycolysis, angiogenesis. FBN1 inhibition with anti-angiogenic therapy is found to resensitize cells to cisplatin(Z. Wang et al., 2022).

### **2.4.2 MECHANISMS OF RESISTANCE TOWARDS PACLITAXEL**

Paclitaxel basically causes tubulin polymerization by binding to its beta subunit in absence of GTP which is important for microtubule polymerization. This association prevents tubulin from depolymerizing decreasing the length of microtubules which are needed at time of cell division resulting in cancer cell's death.

### **P-glycoprotein efflux**

Paclitaxel is a target for P-gp transporter a type of ABC transporter and overexpression of P-gp can significantly reduce intracellular drug accumulation, thereby leading to treatment failure (Vahedi et al., 2017).

### **Composition of Tubulin isotype**

No response to paclitaxel in OC is partly attributed to increased expression of the  $\beta$ III-tubulin isoform, which forms fewer stable microtubules. This reduced stability counteracts paclitaxel's mechanism of microtubule stabilization, allowing resistant cells to continue dividing. Up to a four-fold increase in  $\beta$ III-tubulin has been observed in resistant tumors, highlighting its role as a potential biomarker and target in drug resistance (Maloney et al., 2020).

### **PI3KT/AKT pathway**

It plays a crucial role in mediating paclitaxel resistance and metastasis in ovarian cancer. Hyperactivation of this pathway, often caused by loss of PTEN gene, activating changes in PI3K gene, or increased AKT activity, increases cell proliferation and survival. These alterations help the tumor cells to protect against paclitaxel mediated anti-mitotic effects, contributing to therapy failure (Maloney et al., 2020).

### **Glutathione S-transferase 1**

In OC, resistance to paclitaxel is done through the elevated activity of glutathione mediated detoxification pathway. Downregulation of PRMT6 in resistant cells leads to elevated levels of glucose-6-phosphate dehydrogenase (G6PD), which elevates levels of GSTP1 (Feng et al., 2020).

### **B-cell lymphoma 2 family**

Bcl-2 protein family contribute to apoptotic regulation. Protein like BAD and BAX influences cell death, while Mc1-1 along with Bcl-2 and Bcl-XL inhibit it. Paclitaxel basically mimics the nuclear orphan receptor Nurr77, binding to loop present on the N terminal of gene Bcl-2 and induce a change in the conformation in it followed by phosphorylation which converts the protein into a pro-apoptotic one triggering apoptosis. In case of resistance cancer cells upregulate proteins anti-apoptotic protein in the Bcl-2 family suppressing expression of apoptotic factors impairing paclitaxel mediated cell death (Ferlini et al., 2009; Huang et al., 1999; Whitaker & Placzek, 2019).

### **Cross resistance towards Paclitaxel and cisplatin**

Cells fights against combination of cisplatin- and paclitaxel-mediated cell killing by upregulating cell survival pathways like TNF/NF $\kappa$ B (Patel et al., 2021).

## **2.4.3 BEVACIZUMAB RESISTANCE MECHANISM**

Bevacizumab is a human based monoclonal antibody (TgG1). As a part of maintenance therapy, it is used to work on VGEF used by cancerous for promoting formation of blood vessels so that tumor cells can use it to derive nutrition for survival. The antibody binds to the growth factor and prevents it from forming vessels and starving cells to death.

### **Decreased antibody uptake**

In solid tumors like ovarian cancer, new blood vessels often form abnormally. This makes it harder for chemotherapy drugs to reach the tumor properly. A study using mice with ovarian tumors showed that treatment with bevacizumab (a drug that blocks blood vessel growth) reduced the amount of drug that reached the tumor. This happened because there were more pericytes (cells that support blood vessels), which made the vessels more stable and harder for drugs to pass through. Also, cancer cells can escape this treatment by using other pathways to grow blood vessels. One such way is through the PI3K/Akt pathway, which increases another blood vessel growth factor called FGF2, helping the tumor grow even without VEGF (Arjaans et al., 2013; Franco et al., 2011; Pinto et al., 2016).

### **Ephrin type-B receptor 4**

This receptor participates in blood vessel formation. It is reported high levels of EphB4 in bevacizumab-resistant OC models. Bevacizumab along with EphB4 inhibitor (NVP-BHG712) as treatment can reverse resistance suppressing tumor growth suggesting that EphB4 can have a role in imparting resistance to OC cells (Erber et al., 2006).

## **2.4.4 PARP INHIBITORS RESISTANCE MECHANISM**

Olaparib and niraparib inhibitors of PARP, they either capture the PARP enzymes at the DNA damage site or prevent them from carrying out their catalytic activity which prevents NAD<sup>+</sup> from binding. NAD<sup>+</sup> binding is required for PARP enzyme-mediated modification of protein which is called as PARylation. A result of this is collection of unrepaired ss breaks which enhances creation of more ds DNA breaks enhancing hence cancer cell killing.

### **DNA Repair**

Olaparib inhibitor is useful in case of OC cells having mutation in genes like BRCA or in homologous recombination (HR). In that case it stops ss-DNA repair causing cell death. Resistance happens by restoring the repair mechanisms. One key pathway is upregulating the microhomology-mediated end joining (MMEJ) pathway which is mediated by BRD4.(Vescarelli et al., 2020) It triggers ALDH1A1 enzyme responsible in resistance and ROS removal. Upregulating the expression of EHMT1/2 also causes resistance due to histone modification (H3K9me2) & recruiting repair machinery. Or by activating the Wnt/ $\beta$ -catenin signaling pathway as it promotes both HR and non-homologous end joining (NHEJ) facilitating cancer cells survival (Watson et al., 2019; Yamamoto et al., 2019).

### **Cell cycle**

In HGSOC, loss of p53 makes cells rely on the G2/M checkpoint for DNA repair, mediated by Chk1, ATM, and ATR. Chk1 helps translocate BRCA2 and RAD51 for DNA repair. Inhibiting Chk1 with prexasertib disrupts HR, sensitizing cells to PARPi and enhancing DNA damage (Kastan & Bartek, 2004; MacQueen, 2015; Nair et al., 2020). Targeting these pathways promotes cell death by forcing cells into mitosis with unrepaired DNA.

### **Efflux transporter**

Ovarian cancer resistance to olaparib can involve efflux transporters like P-gp (encoded by ABCB1) and neuropilin-1 (NRP1). P-gp is linked to resistance to paclitaxel and PARPi due to

increased expression and copy number, leading to the efflux of both drugs. NRP1 is overexpressed in resistant cells and contributes to tumorigenesis and evasion of cell contact (Vaidyanathan et al., 2016).

### Autophagy of OC cells

Autophagy is involved as resistance mechanism in OC cells treated with stopping agents like niraparib and olaparib. It helps the cells to live in stress condition by providing energy and giving the hypoxic microenvironment needed for cancer cells to protect from cell death (Mirza et al., 2016; Santiago-O’Farrill et al., 2020).

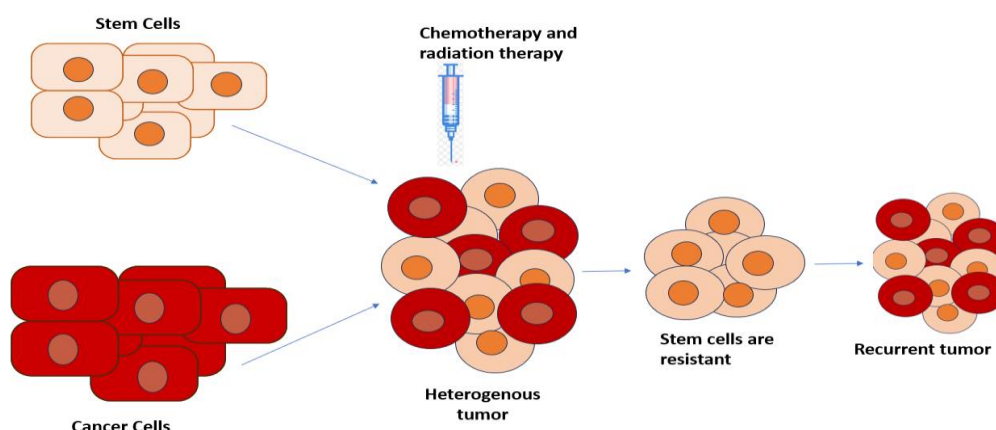
Some other minor mechanisms of drug resistance in OC are;

### Tumor microenvironment

TME also contributes to drug resistance. It has plenty of roles like supporting tumor growth, immune cell evasion, and decreasing therapeutic potential. Important constituents of TME are stromal cells, immune cells, ECM and abnormal blood vessels. All of which interact with cancer cells to increase their survival. Hypoxia in TME activates hypoxia-inducible factors (HIFs) as well as enhances drug movement out of cell via P-glycoprotein (P-gp), here the vasculature acts as a barrier and hinders drug delivery (Alatise et al., 2022). Therefore, the ECM entirely form a barrier against drug penetration. Suppression of immune response is facilitated by immune cells which includes as TAMS, myeloid based suppressing cells (MDSCs), Tregs. They basically secrete pro-tumor cytokines.

### Cancer stem cells

These can renew themselves and to initiate tumors. TME also supports their survival (due to ECM interaction, GF and cytokines). The cells usually stay in dormant or quiescent state thereby escaping from action of therapies that usually target rapidly dividing cells. They also possess enhanced DNA repair mechanisms, activate survival signalling (Wnt/ $\beta$ -catenin/ Hetch hog and Notch and higher levels of P-glycoprotein (P-gp) expression). In this way CSCs causes tumors to relapse and metastasize. (N. Ahmed et al., 2014; Motohara & Katabuchi, 2019)



**Fig 2.7-** Cancer stem cells in recurrence of OC

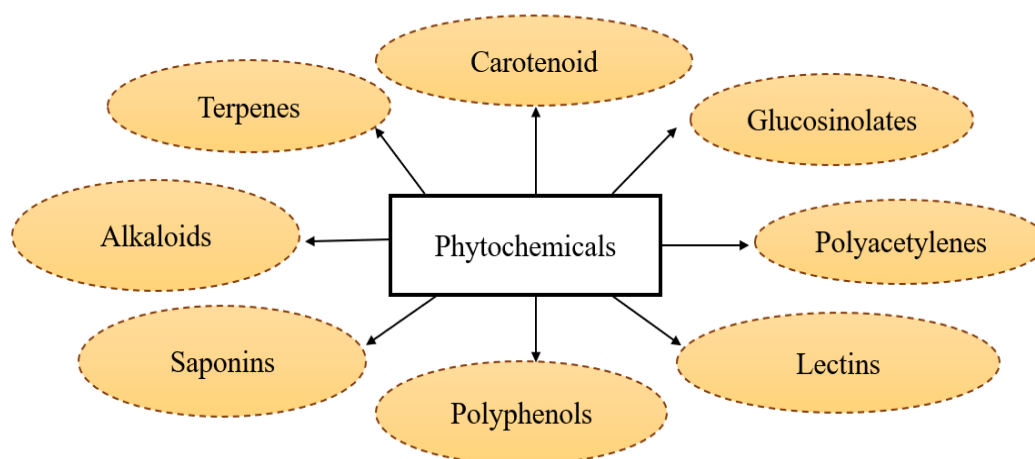
## 2.5 ROLE OF PHYTOCHEMICALS IN THERAPY

Phytochemicals are naturally present chemical compounds found in plants. There is high. These chemical compounds possess variety of bioactive properties. These can be found in a variety of plant sources including but not limited to fruits, whole cereals, vegetables, nuts and botanicals (Eze et al., 2023). Till now thousands of phytochemicals have been identified. These phytonutrients have garnered a lot of attention today in the clinical setting as part of potential therapeutic agents this due to minimal levels of toxicity and negligible side effects and reduced interactions with drug compared to the traditional treatment strategies available for a variety of diseases. It can be used as an alternative optional to the conventional treatment options available as serves to reduce the overall healthcare cost (Gupta & Prakash, 2014).

General protective functions that these phytonutrients impart are antiviral, antimicrobial, antiallergic, antidiarrheal, antioxidant and anthelmintic (Ahmad et al., 2020; Kumar et al., 2011; Sharma et al., 2023). Other than being useful to consumer it also a variety of biological function in the plant host such as protection against predator, competitors, pathogen and in plant growth.

### 2.5.1 PHYTOCHEMICALS CLASSIFICATION

Bioactive compounds are known to interact with components present in living tissue in order to exert their biological activity. These bioactive phytochemicals are broadly classified into lipids, phenolic compounds, alkaloids, terpenoids, carbohydrates and nitrogen containing compounds on basis of chemical properties & structure (Campos-Vega & Dave Oomah, 2013). These major classes can have subclasses on basis of origin and biosynthetic pathway. However, because of extensive variability present in their structure and functions, these compounds don't have a universally accepted classification system as of now (Koche et al., 2022). Still, as they have significant physiological health effects they are considered a subject of extensive research.



**Fig 2.8-** Phytochemicals classes

## 2.5.2 PHYTOCHEMICALS BIOMEDICAL IMPORTANCE

Phytochemicals are diverse bioactive compounds present in plants that contribute to their colour, flavour, and defence mechanisms. Numerous studies have reported their wide-ranging biological activities.

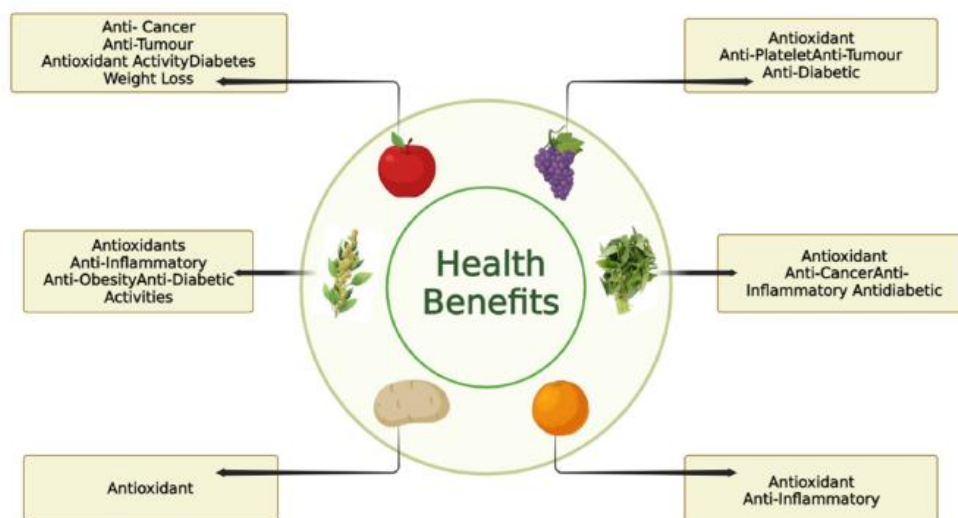


Fig 2.9- Schematic representation of phytochemical & health benefit (Pawase et al., 2024)

## 2.5.3 PHYTOCHEMICALS IN OVARIAN CANCER & LIMITATIONS

Phytochemicals exert multiple anti-cancer effects against ovarian carcinoma through diverse molecular mechanisms. Ovarian cancer, particularly epithelial ovarian cancer (EOC), remains one of the most lethal gynaecological malignancies due to its high mortality rate and the development of resistance to conventional therapies (Rais et al., 2017a). Tumor progression is the supportive environment around a tumor, which is shaped by host-derived cells like fibroblasts, endothelial cells and inflammation causing cells. These are called by cytokines released by EOC cells. Phytochemicals like apigenin, curcumin, baicalein, genistein, quercetin and oridonin have shown significant potential in modulating this microenvironment by deactivating NF- $\kappa$ B (transcription factor) involved in inflammation. They achieve this either by preventing the nuclear translocation of NF- $\kappa$ B or by directly suppressing its activity, thereby reducing pro-inflammatory signals that contribute to tumor progression (S. Ahmed et al., 2008; Gulcubuk et al., 2006a, 2006b; Seo et al., 2010).

A therapeutic difficulty in treating advanced EOC is the emergence of drug resistance, often due to mutations or deletions in the TP53 gene, which impair DNA repair and apoptosis. NF- $\kappa$ B and p53 are not agonistic, with activated NF- $\kappa$ B causes suppression of p53 tumor suppressor functions. Several phytochemicals mentioned above have demonstrated the ability to upregulate wild-type p53, thus reactivating apoptotic pathways. Moreover, these compounds can overcome resistance to TRAIL (TNF-related apoptosis-inducing ligand)-induced apoptosis (Rais et al., 2017b). Compounds such as baicalein, curcumin, luteolin, procyanidins, quercetin, resveratrol, sulphoraphane, wogonin, and hispidulin have been shown to sensitize

TRAIL-resistant ovarian cancer cells and induce apoptosis effectively (Lee et al., 2009; Rushworth & Micheau, 2009).

In addition to modulating apoptosis and inflammation, phytochemicals also exhibit anti-angiogenic properties. Aggressive type-2 EOC cells have higher VEGF level expression and enhanced vasculogenesis. Phytochemicals such as apigenin, quercetin, genistein, and kaempferol inhibit VEGF production in OC cell lines like OVCAR-3. Wogonin along with kaempferol also reduce VEGF expression across different cancer cell models. By targeting VEGF pathways, these natural compounds limit tumor blood supply, thereby inhibiting tumor growth and metastasis (Bast et al., 2009). Collectively, the multi-targeted actions of phytochemicals highlight their potential as complementary agents in the treatment of ovarian cancer, particularly in overcoming chemoresistance and halting tumor progression (Park et al., 2007).

Shortcoming: While these phytochemicals show promise in targeting HGSC, the most prevalent and aggressive subtype of EOC, their efficacy against Low-Grade Serous Carcinoma (LGSC) remains underexplored. LGSC has distinct features, such as the presence of KRAS and BRAF mutations, and tends to be less responsive to chemotherapy.

The current studies evaluating the anticancer potential of phytochemicals such as luteolin, ellagic acid, and pomegranate extracts have shown promising results in inhibiting OC cell increase and movement migration by downregulating MMP-2 and MMP-9, with no apparent toxicity in animal models. However, these findings are primarily based on non-serous ovarian cancer cell lines such as ES-2 (clear cell carcinoma), A2780 (endometrioid carcinoma), and SKOV3 (non-serous, p53 wild-type), which do not accurately represent the molecular or clinical profile of Low-Grade Serous Carcinoma (LGSC) (Singer et al., 2003). As a result, while the data indicate strong anti-cancer activity, the relevance of these phytochemicals in the context of LGSC remains unexplored. This highlights a significant gap in the current research and emphasizes the need for further studies specifically targeting LGSC models, which are characterized by distinct features such as MAPK pathway mutations and a low proliferative index (Wong et al., 2021).

$\beta$ -Sitosterol (SIT), a plant-derived phytosterol, has been identified via network pharmacology useful for OC therapy. Mechanistically, SIT selectively binds to ASS1, which is more expressed in ovarian tumors, and enhances Keap1-mediated ubiquitination and degradation of Nrf2. This suppresses Nrf2's downstream antioxidant targets HO-1 and NQO1, leading to a buildup of reactive oxygen species (ROS), upregulation of the tumor suppressor PTEN, and inhibition of AKT phosphorylation (H. Wang et al., 2023). The resulting disruption of AKT signalling impairs cell cycle progression, survival resulting in ovarian cancer cell death. These findings not only underscore the potential of SIT as a redox-modulating anticancer candidate but also reveal a novel role for ASS1 in regulating redox homeostasis. Importantly, this study focuses on aggressive, high-ASS1-expressing ovarian tumor models and does not address Low-Grade Serous Carcinoma (LGSC), highlighting a clear need for future investigation phytochemicals in LGSC-specific systems (H. Wang et al., 2024).

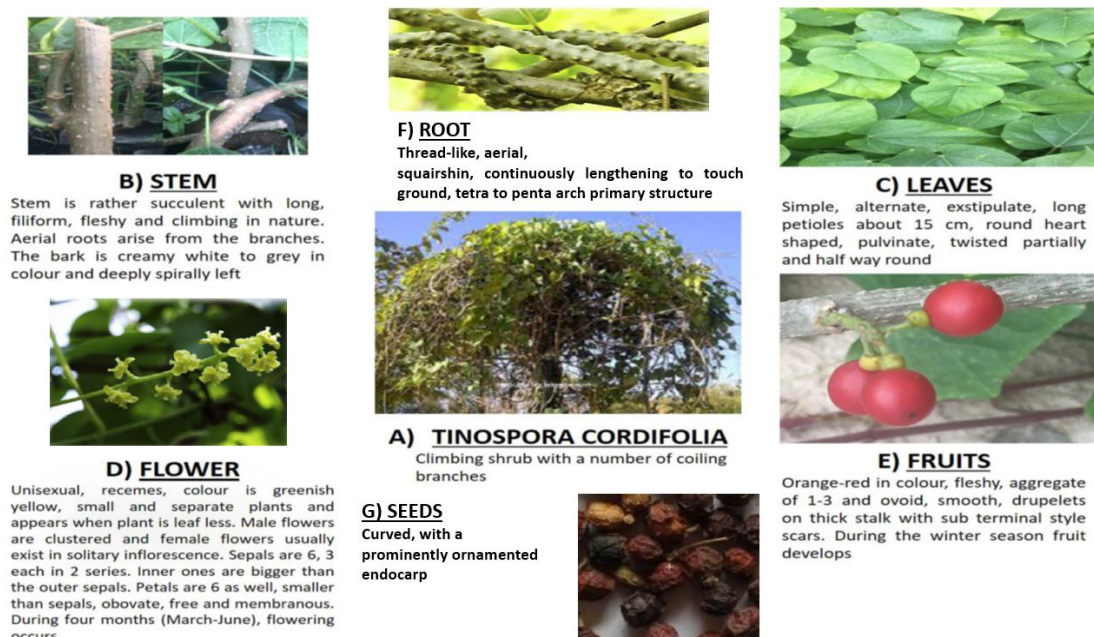
## 2.5.4 *TINOSPORA CORDIFOLIA*: A POTENTIAL MEDICINAL PLANT

*Tinospora* is an important medicinal plant used in traditional medicine. It has the ability to cure many ailments like diabetes, leprosy, cardiovascular diseases, autoimmune diseases like rheumatoid arthritis etc. It is widely known as panacea owing to its therapeutic potential that ranges from its clinical usage to its phytochemistry and pharmacological studies. Within the *Tinospora* genus, three important medicinal species exists namely *Tinospora cordifolia*, *Tinospora crispa*, and *Tinospora sinensis* (also called as *T. malabarica*). All three of them belong to Menispermaceae family under the group Angiosperms (Saha & Ghosh, 2012). Even though their regional prevalence differs, all three species show similarity in their visual and phytochemical profile, especially with respect to their plant parts. They are used in Africa, Asia & Australia due to their therapeutic usage. Studies show that *Tinospora* species has been used clinically to treat problems like UTIs, diabetes, fever, skin inflammation etc because of their rich phytochemical profile including of alkaloids, flavonoids, aliphatic compounds, glycosides, diterpenoids, lactones, tannins, vitamins, lignans, steroids, coumarins, triterpenes & nucleosides (Chaudhary et al., 2024).

Geographically, *Tinospora* species are found across tropical India in regions up to 1,200 meters above sea and also in China, Sri Lanka, Pakistan, Myanmar. These plants are deciduous and perennial and require warm climates to thrive and can be grown in a many types of soils condition like clay loam, sandy, medium-black and also red soils. Therefore, soils that are drained properly having adequate amount of moisture and rich in organic content are ideal for their optimal growth (Arunachalam et al., 2022).

Out of the three species of *Tinospora*, *Tinospora cordifolia* (Giloy/ Heart-leaved Moonseed) is a medicinal plant with multifaceted properties is of utmost importance in therapeutics and is considered sacred in traditional Indian medicine. It is a climbing shrub and has many coiling branches. This plant is divided into multiple parts like lamina, seeds, stem, aerial roots, flowers, leaves and fruits. Structure of their aerial roots distinguishes them from other species, as they a tetra or penta arch vascular structure. A thick outer wall & an inner **parenchymatous zone** forms the root cortex. An ovate shaped lamina which is 10-20cm in length and 15 cm in breadth. The leaf base is distinctly deeply cordate, while the surface is membranous, covered with fine hairs (pubescent), and it shows a whitish tomentose texture. A very well defined reticulate venation pattern can also be seen clearly on the underside. The seeds of this plant are curved in shape & embryo conforms to this curvature. Endocarp shows a distinct ornamentation. This is used as an essential taxonomic feature helpful for species identification. The unisexual flowers of *T. cordifolia* grows in auxiliary position and they emerge from 2-9cm long leaflet branches. Typically, they are yellow-greenish in colour. Female flowers grows solitarily but the male flowers grow typically in clusters. Fruits produced by these plants have only one seed which develops in winter while flowering occurs in summers (KLANGJAREONCHAI et al., 2015).

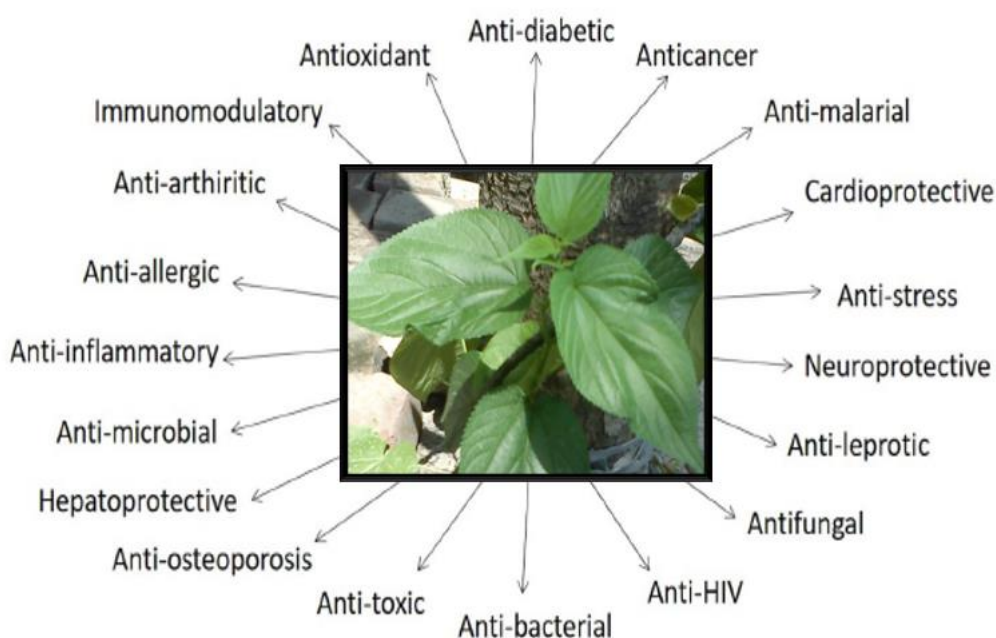




**Fig 2.10-** Morphology of *T. cordifolia*

### Pharmacological activities of *T. cordifolia*

In recent years, *T. cordifolia* has gained attention for its therapeutic effects—such as anti-diabetic, antioxidant, and anticancer etc. These effects are linked to its bioactive compounds like alkaloids, glycosides, and steroids, mostly studied through crude extracts and isolated constituents.



**Fig 2.11-** Therapeutic potential of *T. cordifolia*.

**Table 2.4-** Pharmacological actions of *T. cordifolia*

Property	Study	Mechanism
<b>Anti-diabetic Activity</b>	Alkaloid-rich fraction from the stem (palmatine, jatrorrhizine, magnoflorine)	Insulin-mimicking and insulin-releasing effects in-vitro and in-vivo
	<i>T. cordifolia</i> extract on diabetic model	Decreases high glucose levels, showing anti-hyperglycaemic activity (KLANGJAREONCHAI et al., 2015)
<b>Immunomodulatory Activity</b>	<i>T. cordifolia</i> extract in arthritic inflammation	Suppresses pro-inflammatory cytokines (IL-1 $\beta$ , TNF- $\alpha$ , IL-6, IL-17) and reduces bone/cartilage damage (Ranjith et al., 2008)
	<i>T. cordifolia</i> extract in RAW cells	Inhibits COX-2, TNF- $\alpha$ , IL-6, IL-1 $\beta$ , and iNOS without affecting COX-1 expression
	Methanolic extract of <i>T. cordifolia</i>	Inhibits LOX/COX activity, TNF- $\alpha$ , IL-1 $\beta$ production, and demonstrates moderate NO scavenging activity (Persson et al., 2000)
<b>Hepatoprotective activity</b>	Ethanollic extracts has potential against liver damage in rats due to carbon tetrachloride	The extracts normalized liver function and reduced liver damage markers (SGPT, SGOT, ALT, AST, bilirubin). (Dabur & Mittal, 2016)
<b>Cardioprotective activity</b>	Root extract (200 mg/kg) showed cardio protection cardiotoxicity in STZ diabetic rats	Scavenged free radicals, protected Mg <sup>2+</sup> dependent Ca <sup>2+</sup> -ATPase enzyme. (Rao et al., 2005)
	Methanolic extract attenuated isoprenaline-induced myocardial infarction in Wister rat	Strengthened the myocardial membrane and mitigated infarction-induced damage. (Puranik et al., 2025)

### Safety and toxicological profile *T. cordifolia*

Limited clinical trials available on this plant species suggest 300 mg of standardized aqueous stem extract if taken thrice daily for up to 6 months is effective in treating conditions like HIV & allergic rhinitis but consistent dosing guidelines as of now are still lacking. Generally, it is considered safe at Ayurvedic doses with few reported side effects like nausea, anorexia and vomiting. No toxicity has been reported in healthy volunteers (they were given 500 mg/day for 21 days), rabbits (up to 1.6 g/kg), or rats (1,000 mg/kg). (Alajmi et al., 2018) However, concern exists due to a study which reported 40% mortality in mice when they were given higher doses

at 500 mg/kg. *T. cordifolia* also showed no genotoxic or mutagenic effects in standard tests but hydroalcoholic extracts were capable of inducing micronuclei in bone marrow cells. *T. crispa* which is related species and medicinally interchangeable to *T. cordifolia* can cause hepatotoxicity in one case. According to a particular study using this plant extract is not recommended in patients suffering with prostate cancer patients due to observed cell proliferation in in vitro study until more data is available. Therefore, *T. cordifolia* when taken in moderate therapeutic doses is generally safer but still it requires further clinical validation with respect to long-term use (Alajmi et al., 2018).

### **2.5.5 TINOSPORA CORDIFOLIA POTENTIAL IN CANCER THERAPY**

From the emerging studies, the anticancer activity of this plant has been shown to be connected to its potential to stop the cell cycle in various stages. It has been shown that extract from this plant can cause cell arrests in the G0/G1; G2/M phases by reducing the expression of protein like cyclin D1 which is a G1/S phase-specific protein and the anti-apoptotic protein like Bcl-xL (Vaghasia et al., 2025). This leads to stopping of proliferation of cancer cell and triggers apoptotic cell killing. The plant extract can also elevate the activity of lactate dehydrogenase (LDH) enzyme, reduce the cell viability and increase activity of glutathione S-transferase (GST). This suggests that *T. cordifolia* has potential role in cytotoxicity and detoxification of cancer cells. Therefore, this plant has antiproliferative and apoptosis-inducing capabilities (Vaghasia et al., 2025).

*T. cordifolia* has shown potential cytotoxic activity against variety of cancer cell lines. The aqueous extract extracted from the plant shows potential against cell lines on colon cancer like Colo-205 and cell lines of lung cancer (A-549 /NCI-H322). Additionally, a methanolic extract has activity against (MDA-MB-231) breast cancer cell line. This broad-spectrum activities of *T. cordifolia* shows it can be used a potential candidate to treat ovarian cancer and resistance (Mishra & Kaur, 2013).

In-vivo studies performed on this plant has shown its ability to reduce the tumor mass and improve overall survival. Plant extract obtained from *T. cordifolia* has shown anti-angiogenic effects by stopping production of blood vessels needed for tumors to grow. It is also shown to increase level of pro-inflammatory cytokines like IL-1 $\beta$ , IL-6, TNF- $\alpha$  (Deepa et al., 2019).

Phytoconstituents isolated from the plant such as 20  $\beta$ -hydroxyecdysterone, Cordioside, and Columbin has potential to reduce tumor mass in mice affected with Ehrlich ascites carcinoma (a type of mouse-specific mammary adenocarcinoma) (Patil et al., 2021).

It also showed chemo preventive and radioprotective properties in male Swiss albino mice by reducing testicular damage which is inflicted by sublethal gamma radiation. Diterpenoids obtained from this medicinal plant shows chemo preventive functions in diethylnitrosamine (DEN)-induced hepatocellular carcinoma (HCC). The compound was capable of enhancing activities of liver in order to stop the tumor from growing (Arpita R. Pawar, 2024).

*T. cordifolia* contains terpenoids and alkaloids like Tinocordiside/ Magnoflorine/ Palmatine and Cordifolioside A that have important anticancer activity and hence can be used as an adjunct therapy in order to decrease toxicity associated with conventional chemotherapy thereby, enhance efficacy of treatment.

## 2.5.6 PHYTOCHEMICAL CONSTITUENTS IN *T. CORDIFOLIA*

*Tinospora cordifolia* a renowned medicinal plant is member of Menispermaceae family. It is widely recognized in traditional Indian systems of medicine including Ayurveda, Siddha, and Unani. The plant is being highly recognized for its adaptogenic, immunomodulatory, and antioxidant properties due to phytochemicals present in its roots, stems, leaves, and other parts of this plant. Recent studies have highlighted *T. cordifolia* as a potential source of treatment especially in field of cancer therapeutics (Singh & Chaudhuri, 2017).

### Classes of Phytochemicals in *T. cordifolia*

Phytochemical investigations done on this plant *T. cordifolia* has revealed the presence of several classes of secondary metabolites/ phytonutrients, each contributing to its broad pharmacological profile (Saha & Ghosh, 2012). These classes include;

**Alkaloids-** It comprises isoquinoline and protoberberine-type alkaloids which have many activities, including antimicrobial, antioxidant, and anticancer effects.

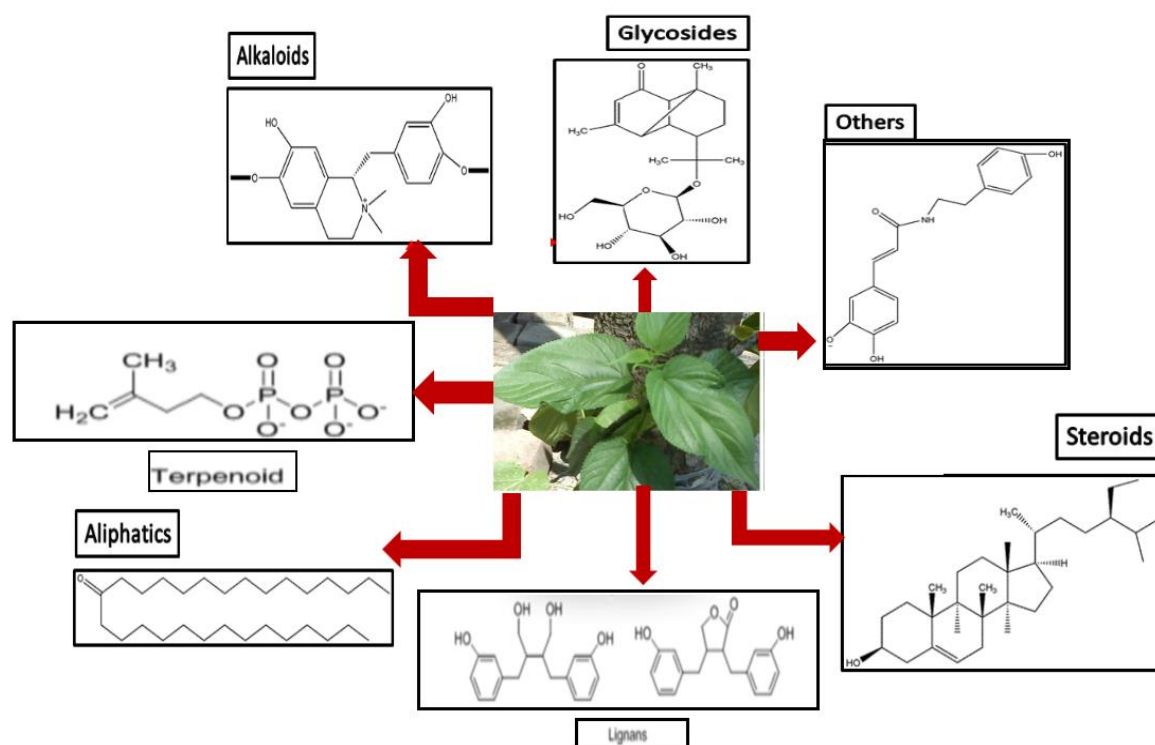
**Terpenoids-** often associated with immunomodulatory and cytoprotective properties.

**Steroids-** They have roles in anti-inflammatory and hormone-mimicking activities.

**Glycosides-** These molecules often serve as potent immunomodulators and enzyme inhibitors

**Phenolics and Flavonoids-** Phenolic derivatives such as flavonoids and lignans exhibit strong antioxidant and free-radical scavenging properties.

**Aliphatic Compounds and Essential Oils-** Long-chain alcohols along with various fatty acids and hydrocarbons, contribute to the plant's anti-inflammatory and anti-tumor actions.



**Fig 2.12** - Major constituent of *Tinospora cordifolia*

**Table 2.5-** Isolated Chemical constituents *T. cordifolia* (Chaudhary et al., 2024)

Class (Active component)	Isolated compounds
Alkaloids	Berberine Palmatine Magnoflorine Tembetarine Isocolumbin Choline
Steroids	$\beta$ -Sitosterol Ecdysterone Giloinsterol Makisterone A
Terpenoids (Diterpenoid lactones & sesquiterpenoids)	Tinocordside Syringin Columbin Jateorine Tinosporon Clerodane derivatives
Glycosides	Tinocordifolin Cordifolioside A/C Amritiside A Tinocordiside
Aliphatic compounds	Octacosanol Heptacosanol
Miscellaneous	Jatrorrhizine Gilloin

**Anti-Cancer Phytochemicals in *T. cordifolia***

Several phytochemicals in *T. cordifolia* have shown promising anticancer activities, making them ideal candidates for the current study.

**Table 2.6- *T. cordifolia* phytochemicals with anti-cancer relevance**

Phytochemical	Class	Mechanism/Activity
<b>Berberine</b>	Alkaloid	Inhibits topoisomerase II, suppresses tumor proliferation
<b>Columbin</b>	Diterpenoid	Chemopreventive against colon cancer
<b>Palmatine</b>	Alkaloid	Enhances antioxidant defense, reduces tumor size
<b>Octacosanol</b>	Aliphatic Alcohol	Inhibits MMPs and angiogenesis; anti-metastatic
<b>ECD (Epoxy Clerodane Diterpene)</b>	Diterpenoid	Modulates p53 and Cdkn2A expression in cancer cells
<b>Cordifolioside A</b>	Glycoside	Cytoprotective, immunomodulatory
<b>Tinosporide</b>	Diterpenoid	Cardio- and chemo-protective properties
<b>Piperine</b>	Alkaloid (piperidine-type)	Modulates GSK-3 $\beta$ /AKT/PI3K, enhances bioavailability of other drugs,
<b>Tetrahydropalmatine</b>	Isoquinoline alkaloid	CNS and anticancer activity; may affect signaling in neuro-oncology
<b>Magnoflorine</b>	Benzylisoquinoline alkaloid	Anti-inflammatory, apoptosis modulation
<b>Isocolumbin</b>	Diterpenoid	Known for cytotoxicity against cancer cells in in vitro studies
<b>Tinosporin</b>	Diterpenoid	Reported as anticancer and anti-inflammatory
<b>Jatrorrhizine</b>	Protoberberine alkaloid	Antimicrobial and potential anti-proliferative agent
<b>Dehydrodiscretamine</b>	Alkaloid	High AKT1 binding energy; possible anticancer interaction
<b>Sitagliptin</b>	Synthetic gliptin	Synthetic drug with reported anti-inflammatory and DPP4 inhibition
<b>Amritoside</b>	Glycoside (diterpenoid-based)	involved in aging and cancer pathways

Given their pharmacologically validated anticancer properties, the above-mentioned phytochemicals from *T. cordifolia* serve as suitable ligand candidates for in silico molecular docking and molecular dynamics study against ovarian cancer-related protein targets. Their structural diversity and bioactivity offer a strong foundation for computational screening.

## 2.6 RESEARCH STRATEGY

To address the therapeutic challenges associated with LGSC progression and chemoresistance, a computational approach was designed to evaluate selected *Tinospora cordifolia* phytochemicals against LGSC-specific molecular targets. The methodology adopted here is represented by the flow chart in below figure.

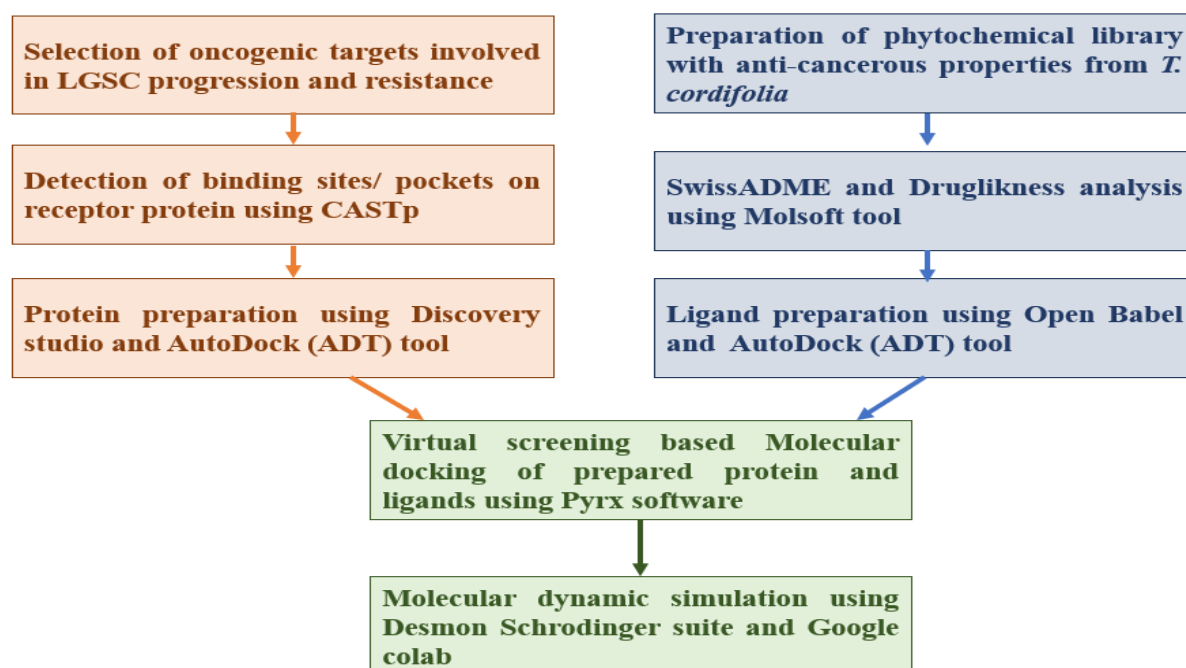


Fig 2.13 – Proposed methodology



## **CHAPTER 3**

### **METHODOLOGY**

#### **3.1 SELECTION OF PHYTOCHEMICALS**

*Tinospora cordifolia*, also known as the heart- leaved moonseed is a vine. It has been recognized for its broad therapeutic potential including antioxidant, removing inflammation, microbial killing, and antitumor properties. In the recent years, this plant has been getting significant attention due to its anti-carcinogenic constituents or phytocomponents. According to the ongoing studies these compounds has been proved to be effective as therapeutic agents against different cancer like hepato-carcinoma, lymphoma, and bone cancer cell lines, oral cancer, colon cancer etc(Singh & Chaudhuri, 2017).

For the current study, several phytochemicals from *Tinospora cordifolia* has been chosen as the potential candidates. These phytochemicals were selected on the basis of their proven pharmacological actions and relevance to anticancer or chemo modulatory mechanisms. against different type of cancers(Tiwari et al., 2018).

A comprehensive literature review and database mining approach was employed to identify candidate compounds with documented or predicted therapeutic effects. These compounds were given priority because of their structural diversity ranging from alkaloids to flavonoids, their availability in public chemical databases such as PubChem, and prior evidence of bioactivity in cancer-related pathways.

These phytochemicals were subsequently subjected to ADME analysis, drug likeliness and molecular property prediction first in order to determine whether the candidate compound is likely to be absorbed, spread in the body, metabolized, and removed out efficiently in body and so these predictions help in identifying all the drug-like molecules that have a favourable pharmacokinetic property. This evaluation which is done priority helps to focus only on the most promising candidates for further computational studies.

Table 3.1 shows the phytochemicals that were chosen as ligands for the current study from *T. cordifolia* to test against targets from Low-grade serous cancer and associated drug-resistance.



**Table 3.1-** Candidate ligands from *T. cordifolia*

Sr No.	Phytochemical	Class
1.	<b>Berberine</b>	Alkaloid
2.	<b>Columbin</b>	Diterpenoid
3.	<b>Palmatine</b>	Alkaloid
4.	<b>Octacosanol</b>	Aliphatic Alcohol
5.	<b>Epoxy Clerodane Diterpene</b>	Diterpenoid
6.	<b>Cordifolioside A</b>	Glycoside
7.	<b>Tinosporide</b>	Diterpenoid
8.	<b>Piperine</b>	Alkaloid
9.	<b>Tetrahydropalmatine</b>	Isoquinoline alkaloid
10.	<b>Magnoflorine</b>	Benzylisoquinoline alkaloid
11.	<b>Isocolumbin</b>	Diterpenoid
12.	<b>Tinosporin</b>	Diterpenoid
13.	<b>Jatrorrhizine</b>	Protoberberine alkaloid
14.	<b>Dehydrodiscretamine</b>	Alkaloid
15.	<b>Sitagliptin</b>	Synthetic gliptin
16.	<b>Amritoside</b>	Glycoside
17.	<b>Beta-sisterol</b>	Phytosterol
18.	<b>Luteolin</b>	Flavonoid

### 3.2 ADME AND DRUG-LIKENESS ANALYSIS

For estimating the pharmacokinetic features of the 16 phytochemicals selected from *T. cordifolia* these were subjected to in silico ADME analysis and Drug-likeness prediction on Molsoft server. The main purpose of carrying out this analysis is to first rule out all the ligands having unfavourable pharmacokinetic properties and toxicological properties. The Molsoft server helps to identify and eliminate the compounds not viable to developed as oral drugs. The compounds that pass these servers are more likely to be bioavailable, safe, and effective and likely to function well in vivo making them better drug candidates.

Before subjecting the compounds to these evaluations. The SMILES format of all the 16 compounds were procured from PubChem and then fed into these two online tools. ADME analysis was carried out using SwissADME which can be accessed through the link (<http://www.swissadme.ch/>) and Molsoft server can be accessed via (<https://molsoft.com/mprop/>). Just by pasting the SMILES format of each compound one at a

time on these tools and hitting calculate properties display different properties of the submitted compound. Some of the key parameters on the basis of which the compounds are selected are;

- Gastrointestinal (GI) absorption
- Lipophilicity (LogP)
- Bioavailability score
- Bioavailability radar
- Drug-likeness score (DL score)
- Lipinski's Rule of 5
- Rule of Veber
- Ghose filter, Egan rule, Muegge rule
- PAINS
- Synthetic accessibility

**Table 3.2-** SMILES notation of phytocompounds

Phytochemical	SMILES format	Phytochemical	SMILES format
Berberine	COC1=C(C2=C[N+]3=C(C=C2C=C1) C4=CC5=C(C=C4CC3)OC(O)OC	Isocolumbin	C[C@@]12CC[C@H]3C(=O)O [C@H][C](C@13)[C@H]1[C@H]4C=C [C@]2(C(=O)O4)O)C)C5=COC=C5
Columbin	C[C@@]12CC[C@H]3C(=O)O[C@H] (C[C@]3([C@H]1[C@H]4C=C[C@H]2 (C(=O)O4)O)C)C5=COC=C5	Tinosporin	COC(=O)C1(O)C2OC2CC2C3(CC (c4ccoc4)C(=O)C3(O)CCC21C
Palmatine	COC1=C(C2=C[N+]3=C(C=C2C=C1) C4=CC(=C(C=C4CC3)OC)OC)OC	Jatrorrhizine	COC1=C(C2=C[N+]3=C(C=C2C=C1) C4=CC(=C(C=C4CC3)O)OC)OC
Octacosanol	CCCCCCCCCCCCCCCCCCCCCCCCCCCO	Dehydrodiscretamine	COC1=CC2=C3C=C4C=CC(=C4C=[NH+] 3CCC 2=CC1=O)OC)O
Cordifolioside A	COC1=CC(=CC(=C1O[C@H]2[C@@H] ([C@H])([C@H])([C@H](O2)CO)O)O [C@H]3[C@H]([C@H](CO3)(CO)O)O)OC)/C= C/CO	Sitagliptin	C1CN2C(=NN=C2C(F)(F)CN1C (=O)C[C@H](CC3=CC(=C(C=C3F)F)N
Tinosporide	CC12CC(c3ccoc3)OC(=O)C1CCC1 (C)C2C2OC(=O)C1(O)C1OC21	Amritoside	C1=C2C3=C(C(=C1O)O)OC(=O)C4=CC (=C(C(=C43)OC2=O)O)OC5C(C(C(C(O5) COC6C(C(C(C(O6)CO)O)O)O)O)O C[C@H]12O[C@H]1CC [C@H]1[C@@]3(C[C@H] (OC3=O)C3=COC=C3)[C@H](C)OCC(=O)[C@] 21C
Piperine	O=C(N1CCCCC1)\C=C\C=C\c2ccc3OCOc3c2	ECD (Epoxy Clerodane Diterpene)	
Tetrahydropalmatine	COC1=C(C2=C(CC3C4=CC (=C(C=C4CCN3C2)OC)OC)C=C1)OC	Beta-sitosterol	CC[C@H](CC[C@H](C)[C@H]1CC [C@H]2[C@@]1(CC[C@H]3 [C@H]2CC=C4[C@@]3(CC[C@H](C4)O)C)C( Cl)C

The image shows the SwissADME & Molsoft submission page with several annotations in blue boxes:

- SwissDrug Design toolbar**: Points to the top navigation bar.
- For information**: A text box stating: "We have changed the look and feel of our tool. However, we have **NOT** changed the underlying technologies and parameters. Consequently, this updated Web tool provides exactly the same results as the previous version."
- Molecular sketcher: to draw, edit, import and molecular structures from file**: Points to the Marvin JS sketcher interface.
- Transfer sketched structure to SMILES list**: Points to the arrow button between the sketcher and the SMILES list.
- Enter a list of SMILES here:**: Points to the text input area for SMILES.
- SMILES list pasted one molecule in one line and name separated by space**: Points to the input area.
- Run calculations**: Points to the "Run!" button.
- Paste the SMILES, MOL, InChi file of the compound here**: Points to the input area for pasting files.
- Structure of the drawn here**: Points to the chemical structure drawing area.

The chemical structure shown is a complex molecule with a carboxylic acid group, a pyrrole ring, and a p-tolyl group.

**Fig 3.1-** SwissADME & Molsoft submission page

### 3.3 LIGAND PREPARATION

Following ADME-analysis and drug likeliness scoring, the phytochemical compounds that generated the best pharmacokinetic profiles and DL scores, were then chosen as ligands and taken for detailed structural preparation before molecular docking.

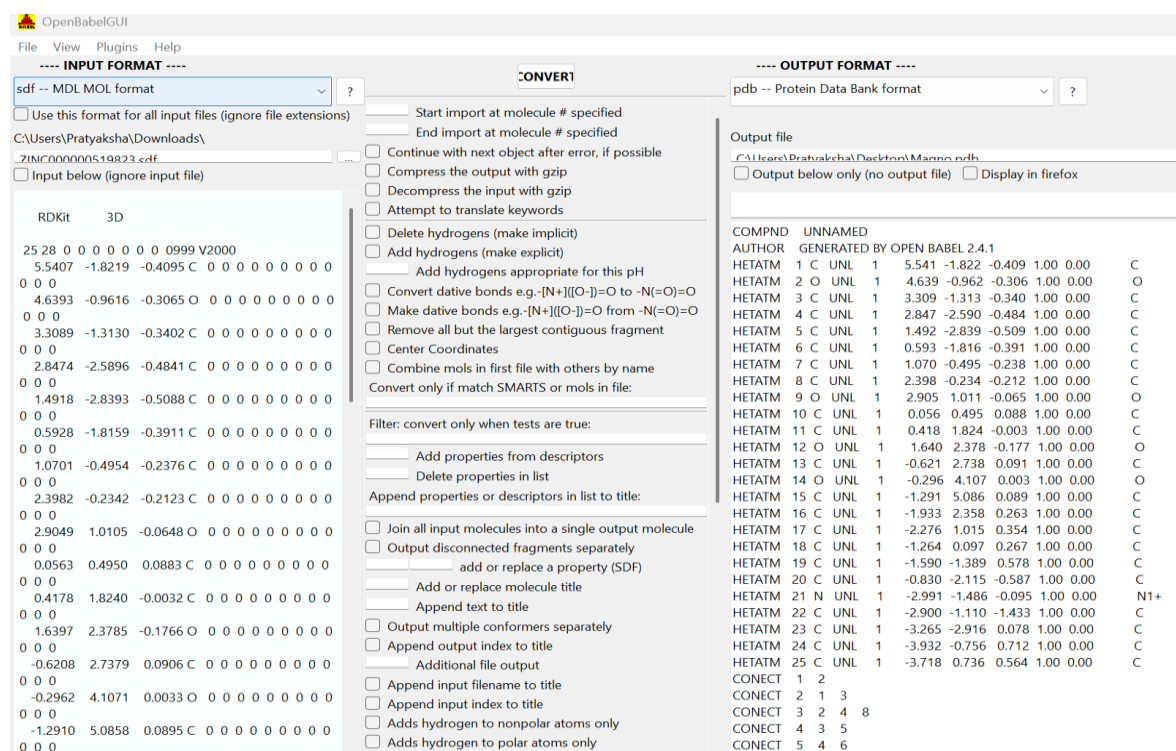
#### 1. Retrieval of 3D structures

First, the 3D structure of all ligands selected were retrieved from databases such as Pubchem and ZINC15 databases. These can be accessed via the links <https://pubchem.ncbi.nlm.nih.gov/>

and <https://zinc15.docking.org/>. The structures were downloaded in the SDF file format. Retrieval of the ligand structure, can be through either through unique CID identifiers/ZINC ID, by their SMILES or InChI format or just by simply writing their name.

## 2. Conversion to PDB file format

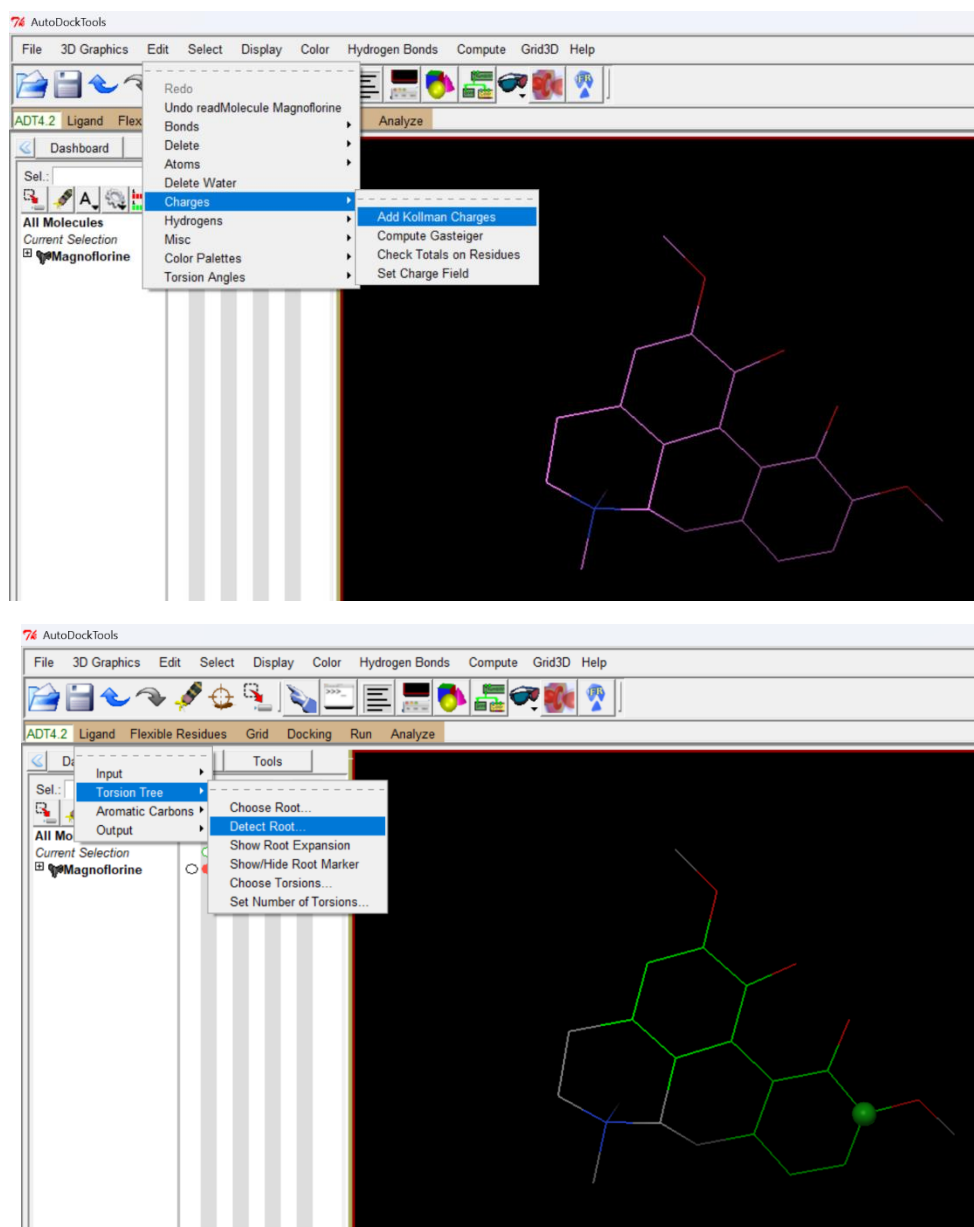
To convert the 3D SDF file of ligand into 3D PDB file, their SDF file was loaded on the Open Babel which is an open-source chemical toolbox. As it supports more than 110 file formats including SMILES, SDF, PDB, MOL2, and PDBQT. It is widely used for interconversion of chemical file formats and preparing molecular structures. It can be accessed through command-line interface, GUI, or Python scripting making it accessible and efficient for both single-file and batch processing tasks. Here in the input format, SDF file format was chosen and output format was chosen as PDB and the file were interconverted after choosing a specific location.



**Fig 3.2-** Open Babel GUI file format conversion

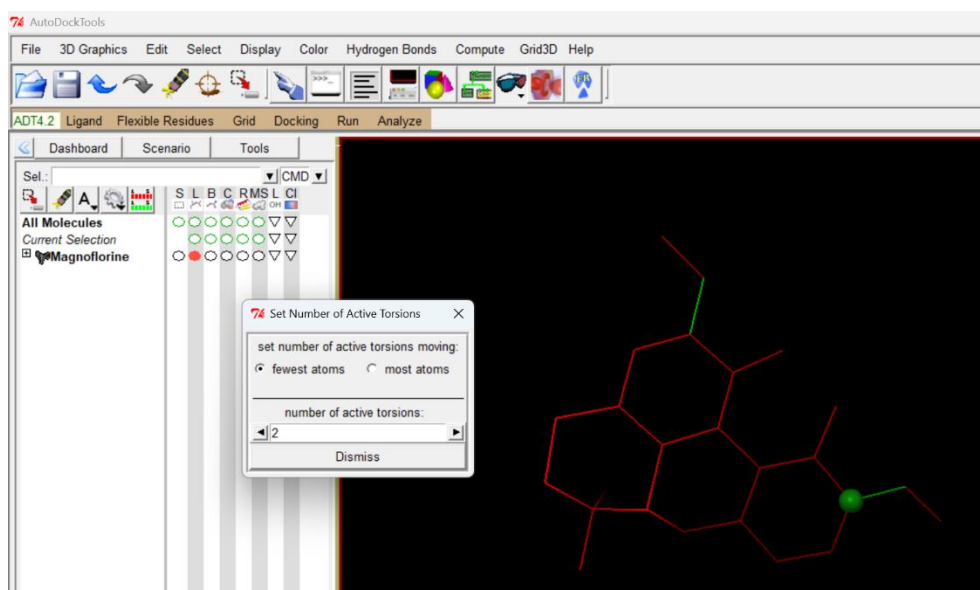
### 3. Docking File Preparation

Once the ligands were converted to PDB format on Open Babel, the ligands were individually loaded on the AutoDock Tools (version 1.5.7). ADT is an interface which is graphical used for preparing molecular structures for docking with AutoDock and AutoDock Vina. It allows users to prepare both ligands and receptors by adding charges, defining rotatable bonds, and converting files into the PDBQT format required for docking. ADT also enables the setup of docking grids, visualization of molecular interactions, and analysis of docking results. Ligand.pdb file was first loaded on ADT tool, then the ligand was checked first for Kollman charges and then by going to Ligand -> choose -> Macromolecule \_-> select the ligand and select molecule for AutoDock4 will lead to addition of Gasteiger charges to the ligand, merging of hydrogen atoms which are not polar, detection and determination of rotatable bonds.



**Fig 3.3-** Charge assignment and root detection in ligand

Next, go to ligand -> torsion tree -> detect root -> and the set no of torsions. Maximum no of torsions that can be set are 32 depending on the rotatable bonds. At last, go to ligand -> output and save the file in system in PDBQT file format.



**Fig 3.4-** Torsion setting in ligand

In addition to the selected phytochemical ligands, known small-molecule inhibitors or natural ligands co-crystallized with each target protein were prepared in an identical manner to serve as reference controls. Their 3D structures were downloaded from the database Protein Data Bank entry or from PubChem (using the same CID or ligand identifier), converted to PDB file with Open Babel. Each control inhibitor molecule was converted to PDBQT format in the ADT tool by assigning Gasteiger charges and defining rotatable bonds—so that both phytochemical and reference ligands could be directly and consistently compared in subsequent docking studies.

**Table 3.3-** Control inhibitor/ligand of receptor proteins

Receptor Protein	Know inhibitor/ligand	PDB ID
BRAF	Vemurafenib	032
KRAS	Sotorasib	MOV
EGFR	Eai045	57N
MEK1	Fenebrutinib	77D
PI3KCA	Alpelisib	PBU
HES1	No known ligand	

### 3.4 TARGET PROTEIN PREPARATION

#### 1. Selection of Target Proteins

On the basis of an in-depth review of available literature and database mining, the key molecular driver proteins of LGSC progression and those involved in LGSC drug resistance were identified as targets as part of this study.

**Table 3.4-** List of Target proteins involved in LGSC

Target Protein	PDB ID
KRAS	6OIM
BRAF	3OG7
MEK1	3SLS
EGFR	5D41
PI3KCA	4OVV
HES1	7C4O

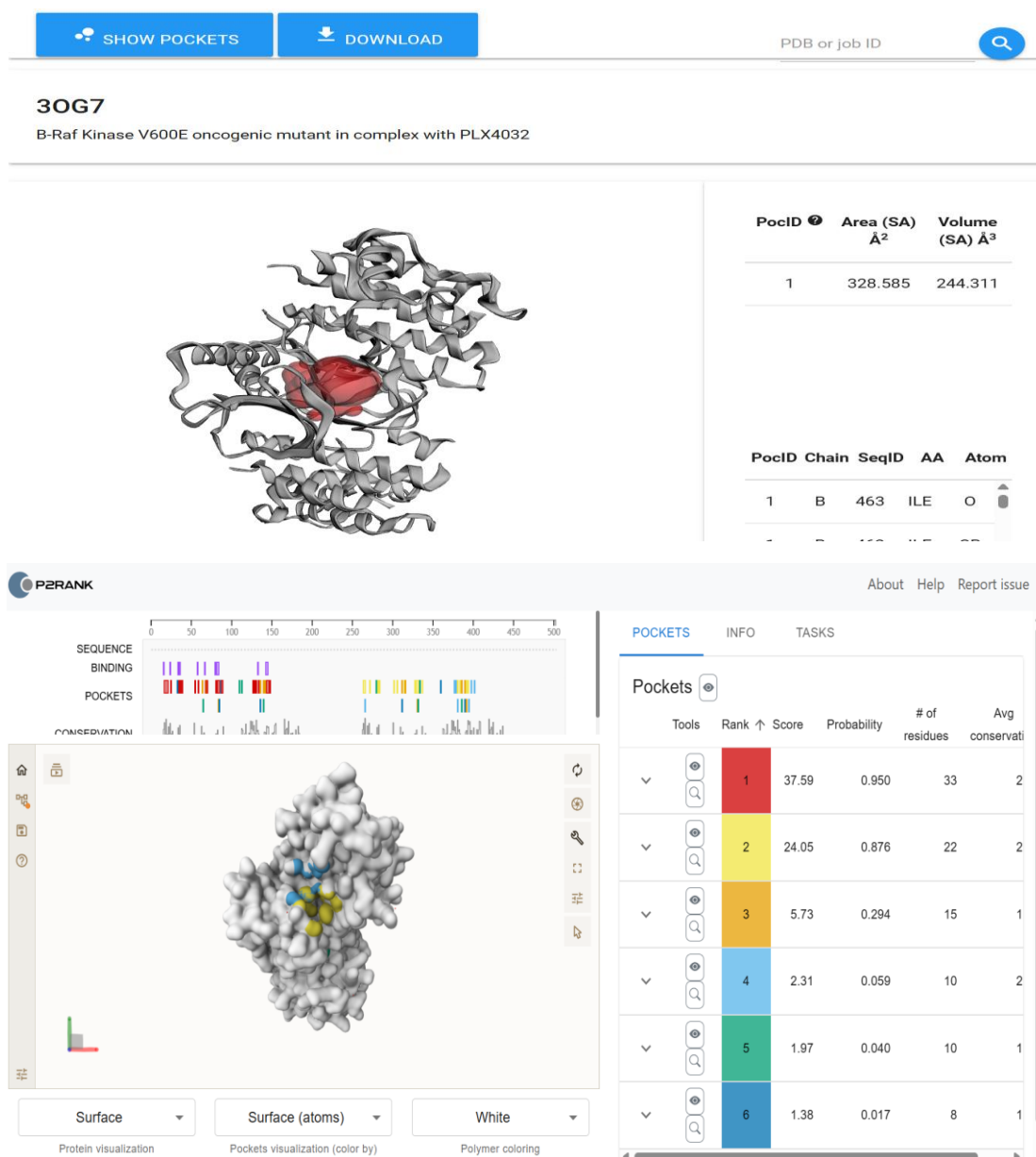
#### 2. Ligand binding site prediction

In order to determine the active site where the ligands are going to bind in protein structure needs to be determined first before protein files are prepared for molecular docking. This is done here using the Computed Atlas of Surface Topography of Proteins (CASTp 3.0) web server tool. It is basically used to identify, locate, and measure active sites, binding pockets, and cavities on a protein's surface. It does so by analysing the 3D structure of a protein and then it gives a detailed information regarding the volume, area, and residues that line each pocket or channel in the protein's structure. Therefore, it helps in predicting potential ligand-binding sites and is helpful in guiding docking studies.

Protein is searched here by its PDB ID and it calculates the binding site/pocket location on the periphery or surface of our protein target and the amino acid atoms present in the binding location/pocket.

The results generated on CASTp were confirmed or validated using the results generated on PrankWeb. It is basically an online tool used for predicting ligand-binding sites on protein structures. It employs the deep learning algorithms, specifically based on machine learning models like P2Rank, to identify potential binding pockets with high accuracy.

You upload the PDB format of the target protein and predicts different pockets. These are ranked by their probability scores, along with the key amino acid residues involved. For every predicted pocket it also gives centre coordinates (X, Y, Z) of the pocket.



**Fig 3.5-** Binding site prediction of protein target using CASTp 3.0 & PrankWeb

### 3. Retrieval of Crystal Structures

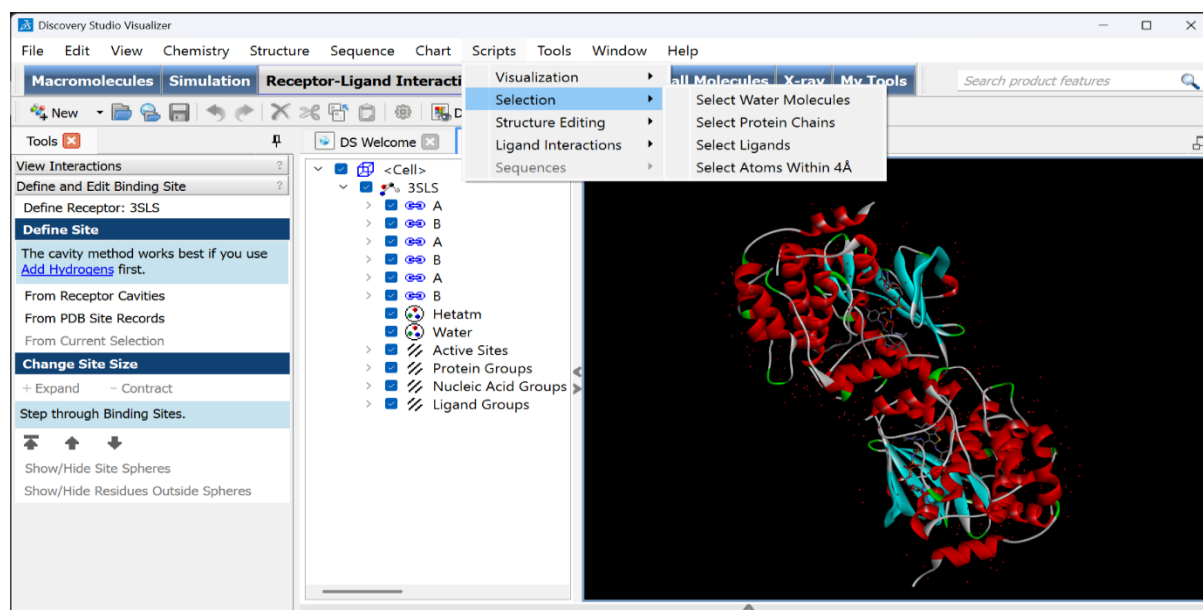
For each of the target protein, their three- dimensional coordinate stricture were taken from the RCSB Protein Data Bank (<https://www.rcsb.org/>) in PDB format.

### 4. Structure Cleaning and Preparation

After downloading the .pdf file of proteins, it is opened in Biovia Discovery studio which is a comprehensive software suite which is used for advanced molecular modelling and dynamic simulation, protein-ligand interaction analysis structural bioinformatics. It is used widely to visualize molecular structures, predict drug properties, and optimize compounds for better binding and efficacy. Once the protein file loads on the software one can visualize the protein here. The hierarchy of the protein helps to see the different chains, heteroatoms, water molecules and natural ligands co-crystallized with the protein structure. By going to Scripts ->

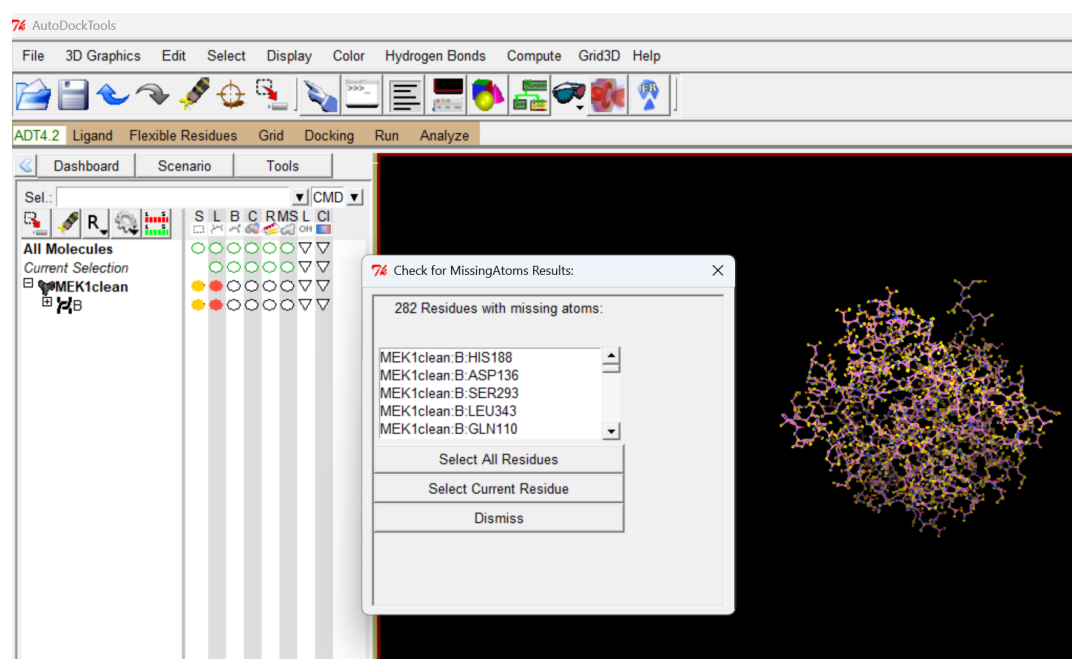


selection -> select the water molecules and ligands followed by delete. Once the protein structure is cleaned it is saved in PDB format.



**Fig 3.6-** Protein structure cleaning on Discovery studio

Next, using the AutoDock Tools (ADT) 1.5.7 which has an interface that is user friendly used to prepare the structures of protein for molecular docking. The PDF file of each cleaned protein from the previous step are individually loaded onto the ADT tool. Here, since the Protein's binding site and chain it lies in is already known from previous steps, the extra chain in the structure are deleted by selecting it. Next is to check the missing atoms in the protein by going to Edit -> Misc. Next is to repair the missing atoms by again going to Edit -> Misc and repair. Select all residues with missing atoms. Once it is done pop shows up. Select save as 2 sets.



**Fig 3.7-** Missing atom repair on ADL tools

Next is to add polar hydrogen atoms (Edit -> Add hydrogens) followed by addition of Kollman charges and then check total residues once to ensure charges are spread to all atoms. If not then select spread charge deficit over all atoms in residue to spread charge evenly. Next go to Grid -> choose -> macromolecule -> choose the protein and save it as PDBQT file format. Hence, the protein is now ready for docking.

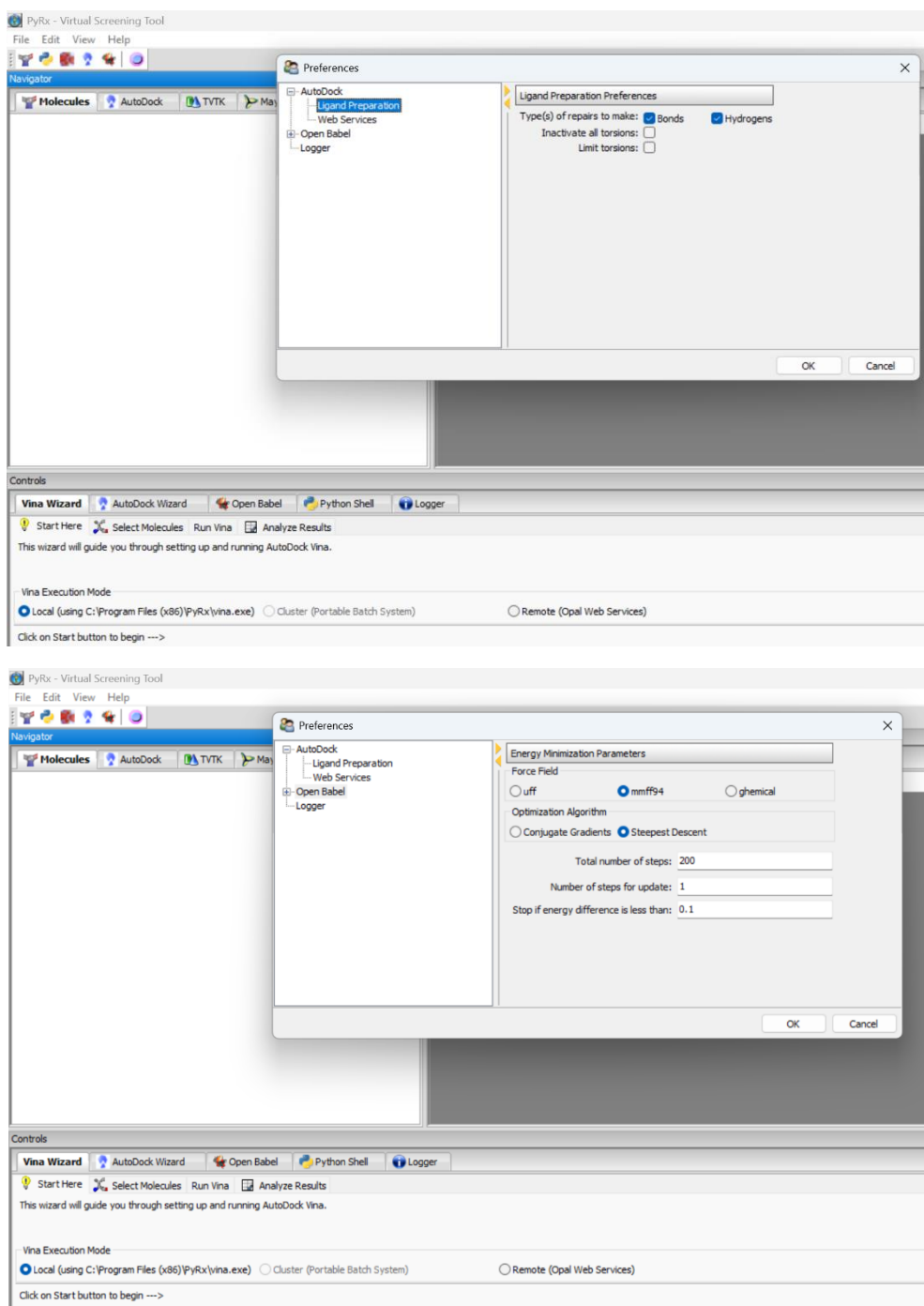
### 3.5 MOLECULAR DOCKING

It is an important in silico technique which is used to study the interaction between two molecules like receptor and ligand. Receptor can be a protein or enzyme and the ligand can be a drug or small molecule like phytochemical. Docking helps to predict the best-fit orientation and binding affinity of the ligand with its receptor when it binds to either the active site or allosteric site of the receptor. Docking software uses scoring functions to estimate binding energy ( $\Delta G$ ). Lower binding energy indicates a more in strength and more favourable interaction or association between ligand and protein. The Binding energy of the docked complex of protein ligand is usually expressed in kcal/mol. In case of natural product-based drug discovery, phytochemicals (bioactive plant compounds) are docked to disease-related proteins to identify their potential therapeutic roles. Mainly tools are used in docking studies. One such tool is the Pyrx software.

#### 1. Software installation

Pyrx is an open-source platform and it is used for virtual screening tool. It uses the graphical user interface that integrates AutoDock and AutoDock Vina both for molecular docking. In virtual screening multiple ligands or phytochemicals can be screened against a particular protein target at once efficiently. In this study as well, the seven phytochemicals were docked against the protein targets of Low-grade serous cancer to determine how efficiently these compounds are binding to the protein's active site to determine their therapeutic potential.

The Pyrx software can be installed from the website <https://pyrx.sourceforge.io/> and installed on your system. Once it is set up, the preferences are set in the Pyrx window in edit tab regarding the AutoDock workspace, Ligand preparation preferences including the types of repairs to make, setting the number of torsions etc.



**Fig 3.8-** Preference setting in Pyrx

In the Energy minimization parameters, force field was chosen as MMFF94 (Merck Molecular Force Field 1994) is a widely used force field designed to model the geometry and energy of small organic molecules. It calculates molecular energy based on parameters like stretching of bond, bending of angle, torsions and van der Waals interactions, and electrostatics. It is used in the docking setup for ligand energy minimization to optimize the 3D structure before docking which ensures that the ligand adopts a low-energy and relevant conformation in order to increase docking accuracy.

As for optimization algorithm steepest descent method was selected. This algorithm is used to minimize energy. It does so by moving atoms in the direction of the minus gradient of the

potential energy (i.e., the direction of steepest energy decrease), step by step, until a local energy minimum is reached. This helps in basically removing any steric clashes, repair the geometry and prepare the ligand and protein in a low energy conformation suitable for docking.

## 2. Performing virtual screening

To perform virtual screening of ligands against protein target first select Vina wizard in bottom region. Click on the start button and then load the all the ligands that were prepared on ADT tool. The file format is PDBQT. Once the ligand is loaded. By choosing Macromolecule, load the PDBQT format of the protein that was prepared on ADT tool. In the 3D window the protein along with the ligands or phytochemicals can be visualized. From the navigator window select the proteins and all seven ligands and click on the forward button. On the next page click on Run vina. The grid box will appear around the protein. The grid box dimensions need to be set here now. The dimension of the X, Y, Z coordinates depend on the active site/ binding pocket predicted in the protein by CASTp in the earlier steps. Grid box dimension can be set either by selecting the residues that are part of the active site or by directly moving the grid box on protein ensuring that the X, Y, Z coordinates are matching to that mentioned in the results by CASTp/PrankWeb.

## 3. Docking parameters

Exhaustiveness controls how thoroughly the conformational space is searched. Higher values ensure more accurate results however it also means longer computation time. The default in AutoDock Vina is set at 8, but 10–16 is often used for more reliable results. Here in this study the exhaustiveness is set at 9.

Number of output modes (poses) were set at 9 and the energy range was kept as 3 kcal/mol

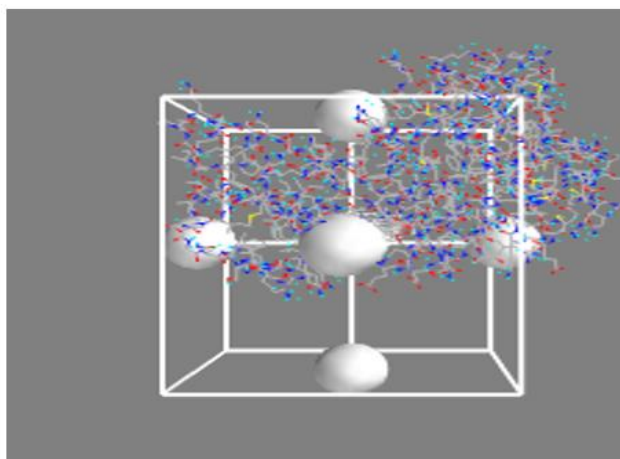
Grid box defines the search space where the ligand will try to bind to the protein. These values are often derived from binding pocket prediction tools like PrankWeb or CASTp.

Centre (X, Y, Z): Coordinates of the predicted active/binding site.

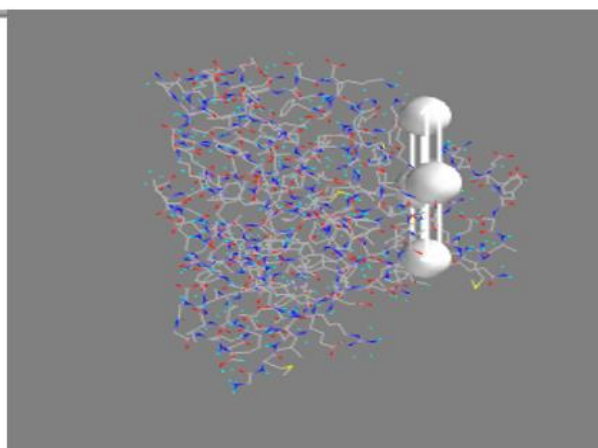
Dimensions (Size X, Y, Z): Size of the box around the binding site. It must be large enough to allow the ligand to survey every possible binding mode.

The grid box set for all the 7 phytochemicals are-

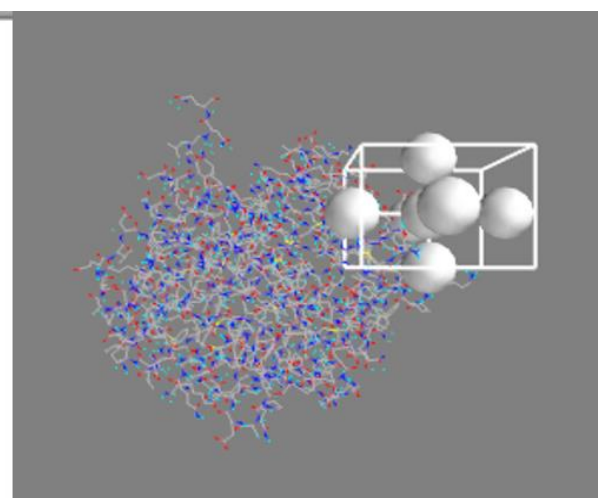
```
receptor = BRAF.pdbqt
exhaustiveness = 9
center_x = -1.86508691394
center_y = -2.87845999687
center_z = -20.1035359257
size_x = 41.9201738279
size_y = 49.4339199937
size_z = 73.8244718514
```



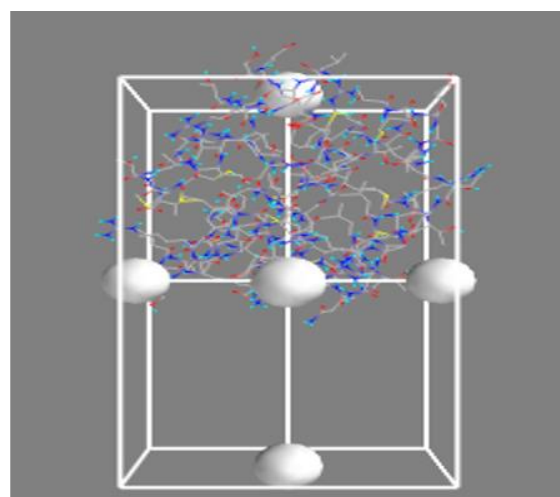
```
receptor = KRAS.pdbqt  
exhaustiveness = 9  
center_x = -5.20827249084  
center_y = 3.52421953266  
center_z = 7.192  
size_x = 1.13425501832  
size_y = 18.8293609347  
size_z = 25.0
```



```
receptor = MEK1.pdbqt  
exhaustiveness = 8  
center_x = -23.0725944039  
center_y = 48.3450223436  
center_z = -30.2694344818  
size_x = 21.1381888078  
size_y = 16.0752227929  
size_z = 45.9134689635
```



```
receptor = HES1.pdbqt  
exhaustiveness = 9  
center_x = 32.9994363507  
center_y = -6.43998490951  
center_z = 0.992442369886  
size_x = 24.9977272986  
size_y = 46.027569819  
size_z = 28.0865152602
```

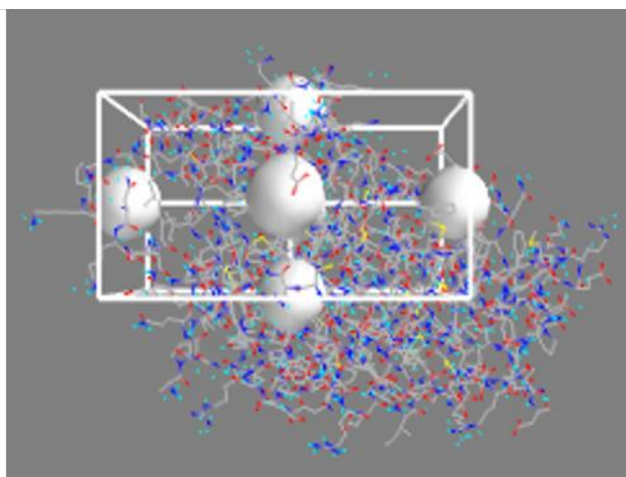




```

receptor = EGFR.pdbqt
exhaustiveness = 9
center_x = -27.836994797
center_y = 34.4527479099
center_z = 14.4979986089
size_x = 36.5296104061
size_y = 19.3730179159
size_z = 46.5345280069

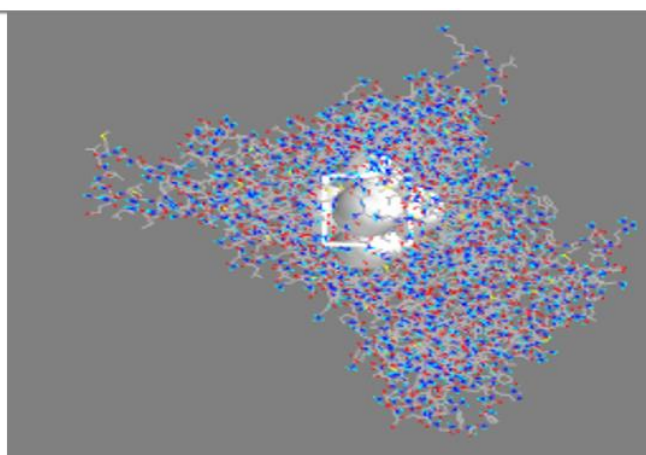
```



```

receptor = PI3Kalphaclean.pdbqt
exhaustiveness = 9
center_x = 63.1578958178
center_y = 67.2249757354
center_z = 95.9993572163
size_x = 31.1896083645
size_y = 15.4530485292
size_z = 16.6534855674

```



**Fig 3.9-** Protein Grid boxes. (a) BRAF, (b) KRAS, (c) MEK1, (d) HES1, (e) EGFR, (f) PI3KCA

Once the grid box and rest docking parameters are set. Click on forward and the docking starts.

The same process was followed for natural ligands/ inhibitors of target protein that are being used as control here. These control inhibitors are redocked with their receptor protein/ enzyme as redocking is an essential validation step in studies using molecular docking used to check the reliability of the docking protocol. It involves removing the native or co-crystallized ligand from the protein's active site and then docking it back using the same parameters intended for novel ligands. The primary aim is to evaluate whether the docking tool and setup (such as the grid box, force field, and scoring function) can accurately reproduce the ligand's original binding pose observed in the crystal structure.

#### 4. Output analysis

Since the exhaustiveness was kept 9 for each ligand protein complex 9 results were generated and the binding energies and poses were recorded for all ligand–protein combinations. The top-scoring poses based on the on the lowest binding energy ( $\Delta G$  in kcal/mol) were selected and then these were visualized and analysed using PyMOL (v2.5) for 3D structure orientation followed by Discovery Studio Visualizer in order to understand the 2D interaction happening between the ligand-protein pair. This feature helps to map different types of interaction not including but not limited to h- bonds, stacking of  $\pi$ – $\pi$ , and hydrophobic interactions. It was

kept in consideration that all ligands were docked under identical conditions which ensure uniform comparison of docking scores and interaction profiles across the different targets.

Here the control inhibitor ligands are also visualized and their RMSD value is also calculated. If the RMSD comes for the re-docked and original pose is  $\leq 3.0$  Å, the method is considered valid and reliable and it confirm that subsequent docking results done with our ligands under study (new or unknown compounds like phytochemicals), are trustworthy and meaningful.

### **3.6 MOLECULAR DYNAMIC SIMULATION**

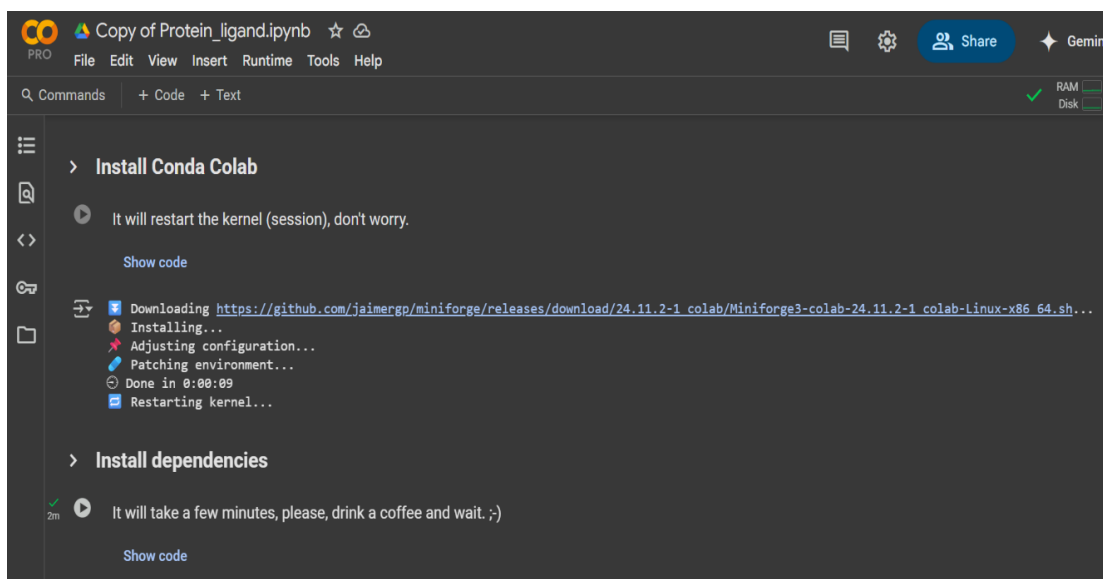
Molecular dynamics (MD) simulation is carried out to inspect the structural stability, flexibility, and interaction behaviour of the top-performing phytochemical–target complexes generated during molecular docking over time in a simulated physiological environment. This procedure helps in validating the dynamic behaviour of ligand binding under near-biological conditions. Therefore, it is used to complements the results produced in molecular docking.

Here the MD simulation is done using both Desmond Schrödinger and Make It Rain" Google Colab notebook. It is a browser-based platform. It operates on virtual machines (VMs) that execute Jupyter notebooks with the help of GPU support. MD simulations often generate very large trajectory files which need significant amount of storage. However, working on Colab solves this issue by mounting Google Drive for permanent file storage and then the input files (e.g., PDB, force fields) are uploaded on the drive along with the simulation outputs directly to drive thereby saving storage.

#### **3.6.1 MD SIMULATION ON GOOGLE COLAB**

##### **1. Setting up the Colab environment**

The setup uses OpenMM as the simulation engine and supports AMBER force field for proteins whereas GAFF2 force fields for small molecules or ligands respectively. It first installs dependencies through the optimized CondaColab setup which basically. This reduces the time taken for installation and improves the runtime stability. Once the CondaColab environment initiates the cell, the runtime kernel will restart automatically in order to apply the new environment before it goes forward with the simulation cell. This is followed by mounting the google drive on the system so all the files are read, written and stored there. In the mounted drive, the input files are uploaded.



**Fig 3.10-**Google Colab environment setup

## 2. System preparation

Once libraries and dependencies are installed and drive has the necessary input files of protein and ligand in PDB format the path to the folder containing the input files in drive is defined for colab to access the files. Here water is removed from protein file and since ligand was already prepared for docking in this step no hydrogens were added.

## 3. Generation of topology files

The topology files were created using using AMBER tools integrated within the platform. The ff19SB force field was then extended on protein, and for solvation purpose it was carried out using the model for water called TIP3P within a cubic box. The cubic box was 12 Å from the protein surface. For neutralization of the system ions like Na<sup>+</sup> /Cl<sup>-</sup> ions were used and ultimate concentration of salt of 0.15 M was chosen which mimics the physiological conditions. As for generating ligand topology the GAFF2 force field was employed and for preparing ligand parameters Antechamber and tleap modules of AMBER were chosen.

**Fig 3.11-** Path determination to access input files



> Parameters to generate the topology:

[5] Parameters to generate the protein topology:

Force\_field: ff19SB

Water\_type: TIP3P

Size Box (Angstroms):

Size\_box: 19

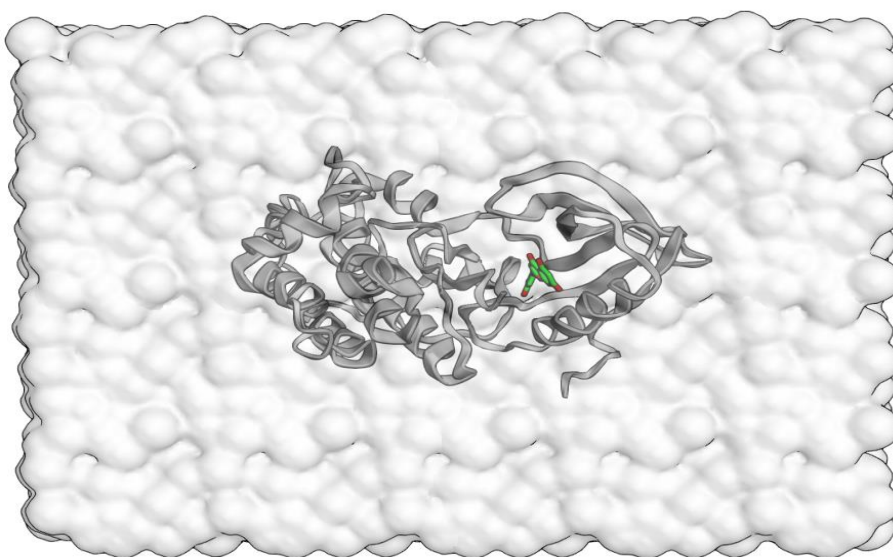
ATTENTION: Give the concentration in Molar units, AMBER tleap will neutralize your system automatically:

Ions: NaCl

Concentration: 0.15

Parameters to generate the ligand topology:

Ligand\_Force\_field: GAFF2



**Fig 3.12-** Topology file & Simulation box generation

#### 4. System equilibration

Before the production MD run the complex of protein-ligand needs to be stabilized within the solvated environment by applying the following parameters. For minimizing energy 20,000 A were executed using the algorithm called steepest descent to resolve the steric types of clashes and optimize geometry.

The equilibration run was performed for 5 nanoseconds (ns) using a 2 femtosecond (fs) integration timestep this confirms accurate temporal resolution of the atomic motion. Pressure along with temperature were maintained at 298K and 1 bar pressure which resemble the physiological conditions. To the heavy atoms in the complex, position restraint was applied with a force constant of 700 kJ/mol so that solvent molecules can equilibrate surrounding a rigid molecule. Trajectory frames were captured at every 1000 picoseconds and log file entries were recorded every 500 picoseconds to capture the temporal resolution and to ensure a stable equilibration run by monitoring the simulation parameters.

> **Parameters for MD Equilibration protocol:**

Jobname: "prot\_lig\_equil"

Minimization\_steps: 20000

Simulation time (in nanoseconds) and integration time (in femtoseconds):

Time: "5"

Integration\_timestep: 2

Temperature (in Kelvin) and Pressure (in bar)

Temperature: "298"

Pressure: "1"

Position restraints force constant (in kJ/mol):

Force\_constant:

Frequency to write the trajectory file (in picoseconds):

Write\_the\_trajectory: 1000

Frequency to write the log file (in picoseconds):

Write\_the\_log: 500

**Fig 3.13-** Equilibration protocol parameters

## 5. Production run

Post equilibration, the dynamic protein–ligand complex behaviour over an extended timescale is observed called as the production run. As a starting point, the equilibrated coordinates and velocities that were generated from the previous step is taken this is because after equilibration the system is considered to be in a thermodynamically relaxed state. The simulation in Colab uses a stride-based approach it is calculated as product of stride time and number of strides taking in consideration of the GPU run time limit. Here number of strides were kept as 5 and stride time was kept as 3 nanoseconds (ns) which makes a total of 15 ns. Integration Timestep kept as 2 femtoseconds (fs) and temperature was kept at 298 K with a pressure of 1 bar in an NPT ensemble to mimic physiological conditions. Here the trajectory frame capturing was changed to 100 picoseconds while the log output was kept the same value ie., captured every 500 ps.

Parameters for MD Production protocol:

Jobname: "prot\_lig\_prod"

Simulation time (in nanoseconds), number of strides (integers) and integration timestep (in femtoseconds):

Stride\_Time: "1"

Number\_of\_strides: "15"

Integration\_timestep: 2

Temperature (in Kelvin) and Pressure (in bar)

Temperature: "298"

Pressure: "1"

Frequency to write the trajectory file (in picoseconds):

Write\_the\_trajectory: 100

Frequency to write the log file (in picoseconds):

Write\_the\_log: 500

**Fig 3.14-** Production run parameters.

## 6. Concatenation and trajectory alignment

At the end of the production run, the individual strides are concatenated to generate a complete trajectory file to make multiple Colab sessions connected to each other and maintains consistency. Here no of strides were kept the same as 5 and duration of strides as 3 ns and the trajectory was saved every 100 ps. Water molecules were removed in this step on order to focus only on complex and to reduce file size for more efficient analysis. The output trajectory was saved in DCD format, and alignment was performed with a skip value of 1, ensuring that all frames were included. This followed by Trajectory Analysis in which the output trajectories were processed to calculate the following;

Root-mean-square based deviation (RMSD)

Root-mean-square based fluctuation (RMSF)

Radius of gyration

MM-PBSA method for estimating binding free energy

The image shows a web-based form for concatenating trajectory files. The form has the following fields and values:

- Google\_Drive\_Path: /content/drive/MyDrive/Test
- Equilibrated\_PDB: prot\_lig\_equil.pdb
- Jobname: prot\_lig\_prod
- Skip: 1
- Output\_format: dcd
- first\_stride: 1
- Number\_of\_strides: 5
- stride\_time: 3
- trajectory\_saved\_frequency: 100
- Remove\_waters: yes

**Fig 3.15-** Concatenation of trajectory files

## 3.6.2 MD SIMULATION ON DESMOND SCHRÖDINGER

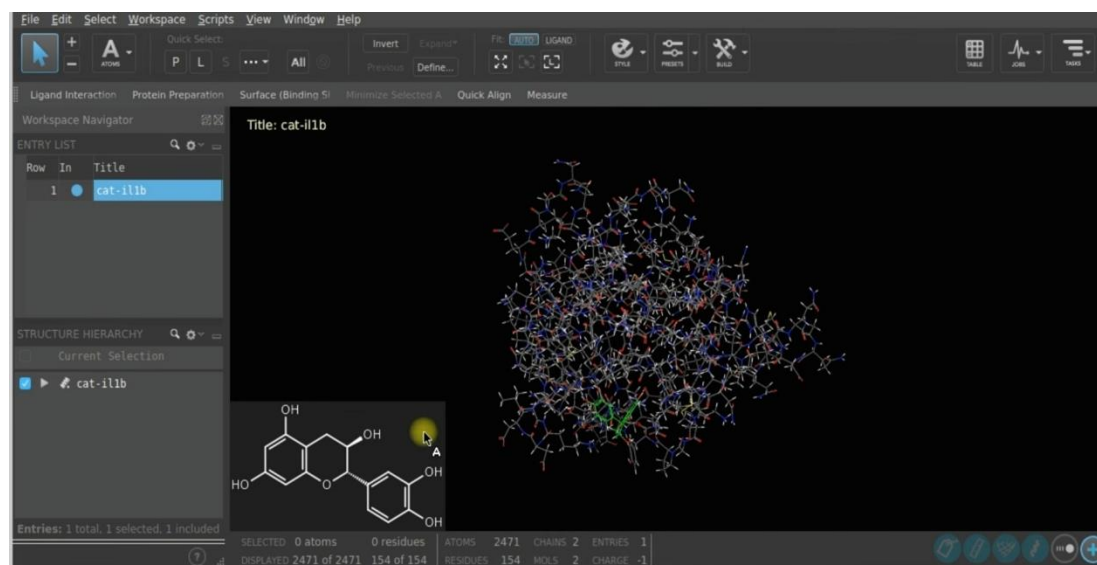
Desmond module from the Schrödinger suite was used to monitor the dynamic nature and stability of the protein-ligand complex. Desmond MD System is a simulation package developed by D. E. Shaw Research. This package is integrated within the Schrödinger Suite. It is known for its high speed and accuracy due to its efficient parallel algorithms and task-decomposition methods which enhances the computational result overall. For setting up simulations and analysing it Maestro was employed which is the graphical user interface (GUI) of Schrödinger. Maestro simplifies the preparation, execution, and analysis processes.

On Desmond a wide range of force fields are supported such as Optimized Potentials for Liquid Simulations (OPLS) family. In the OPLS family, OPLS3e is a highly parameterized version. Therefore, OPLS3e is being used in this study because of its better accuracy in generating physical and thermochemical properties of small molecules and biomolecules. To perform system solvation water model typically TIP3P was used in an orthorhombic box, and

counterions were used to neutralize the system and adjusted to approximate physiological salt concentrations.

### 1. Setting the system

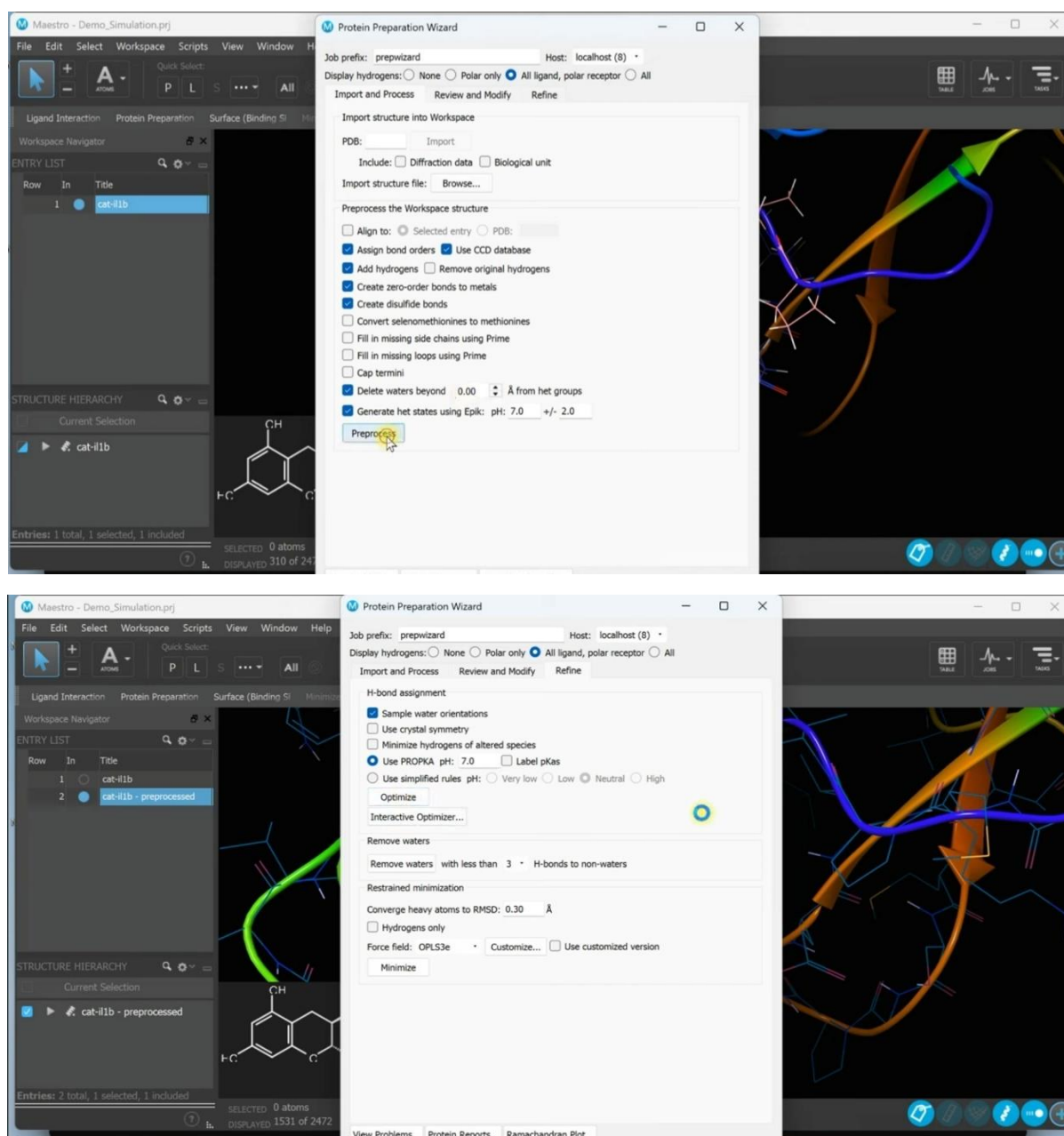
Once the Desmond Maestro window is open, the working directory needs to be changed by setting the path here where all the files generated during course of simulation will be stored and files will be read from. Then a new project needs to be initiated where protein- ligand complex simulation will happen. The PDB file of the protein and ligand complex which has been docked already is opened on the window by going to file -> Import structure.



**Fig 3.16-** Docked protein- ligand complex visualization on Desmond Maestro

### 2. Protein preparation

Next step is to open the protein preparation wizard in the in Maestro in order to assign the correct bond orders, adding the hydrogens, ionization states adjustment at pH 7.0, optimization of H-bonding network, removal of molecules of water beyond 0 Å away from the site of binding, creation of zero order bonds for the metals along with the disulphide bonds and then hitting on preprocess. In the navigator tab a pre-processed file will be seen.



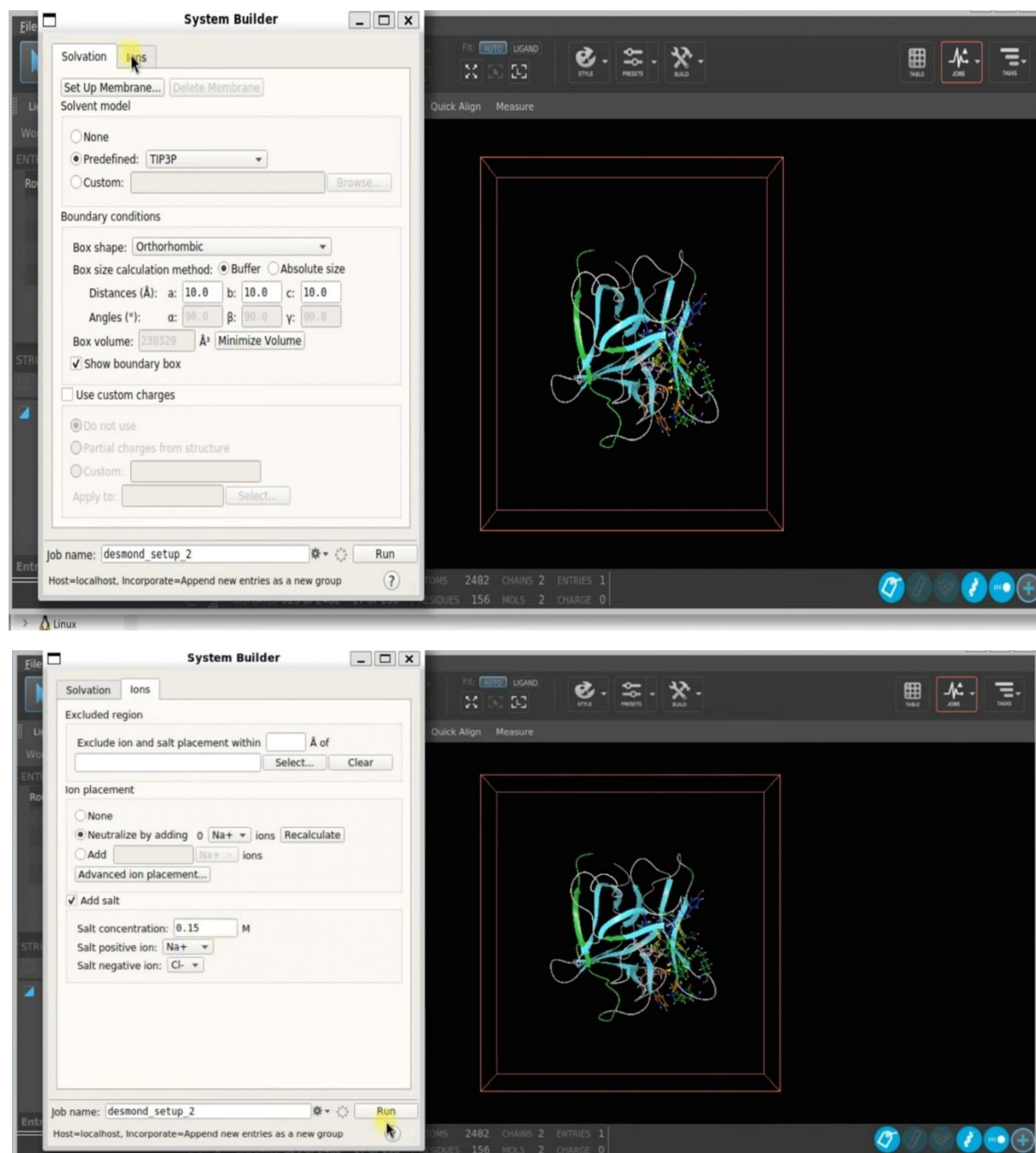
**Fig 3.17-** Protein preparation and refinement wizard

Next go to review and modify to check chain and heteroatoms for correctness and retained if relevant to the binding site followed by moving to refine section where the structure is optimized this will lead to generation of a hbond.opt file in the navigator window. In the refined section, in the restrain minimization parameter chose the force field as OPLS3e and hit on minimize to get a minimized protein-ligand complex. Restrained energy minimization basically removes any local strain and resolves steric clashes while preserving the overall geometry.

### 3. System building

The minimized protein-ligand complex is now ready for system building and solvation prior to the MD run. First in the solvation section select TIP3 as the predefine three-point water model solvent model, box shape is kept as orthorhombic which efficiently holds the molecular system thereby decreasing number of solvent molecules required, show boundary box is toggled on in

order to visualize the spatial limits of our simulation environment followed by volume minimization so that simulation box tightly fits around the solvated complex.



**Fig 3.18-** Solvation & Ions setting

Then in the ions section in the system builder, sodium ions are chosen to neutralize the system and recalculate it. Salt concentration is kept as 0.15 M and  $\text{Na}^+$  is chosen as positive ion and  $\text{Cl}^-$  is chosen as the negative ion to balance and salt the system. Once done a full system named file will show in navigation window.

#### 4. MD simulation run

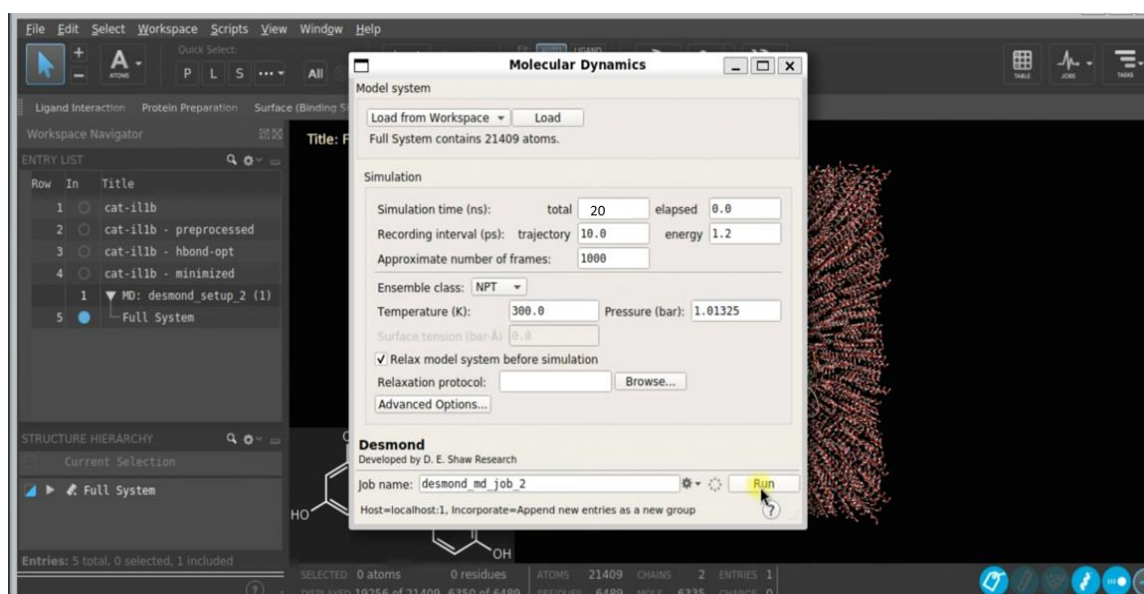
In the MD simulation panel, load the full system file, simulation time is set as 20 ns. Trajectory recording interval is kept at 100 ps to capture meaningful structural transitions and no of frames



at 1000 in order to get a comprehensive representation of molecular motions. Temperature is chosen 300 K with a pressure of 1 bar and simulation was performed under the NPT ensemble so that system can equilibrate pressure and volume fluctuations and at last the model system is relaxed before simulation in order to neutralize the strains. Once the simulation runs successfully a symbol T appears in front of file name which shows the trajectory files are now available for post-simulation analysis.

## 5. Post simulation analysis

After the 20 ns MD simulation is successfully completed in Desmond which is confirmed by the "T" symbol next to the full system file, post-simulation analyses were performed using the parameters like RMSD and RMSF to check structural stability and flexibility, radius of gyration for compactness evaluation and h-bond analysis to see the interaction stability.



**Fig 3.19-** MD simulation parameters setting

## **CHAPTER 4**

### **RESULT AND DISCUSSION**

#### **4.1 ADME AND DRUG LIKENESS ANALYSIS**

ADME studies stands for Absorption, distribution, metabolism and excretion which is used to analyse how a small molecule or drug which is in our case are phytochemicals being processed by the living organism.

Therefore, this research helps to establish the safety and toxicology profile of a compound.

The ADME analysis performed for the phytochemicals selected for this study after literature review and data mining shows the following result:

Majority of the compounds showed high Gastrointestinal absorption indicating good potential for oral bioavailability.

However, low GI absorption score was seen for phytocompounds like Cordifolioside A, Amritoside, Beta sisterol and octacosanol therefore these drugs need to be administered with another drug delivery system like nanoparticles in order to enhance their potential.

Other than Amritoside and Cordifolioside A, rest all of compounds showed bioavailability score of 0.55 which shows their moderate drug likeliness.

Lipophilicity is a determinant of membrane permeability and solubility. Here it is calculated as logP and the ideal range of logP should be in range of 1-3. Two compounds Amritoside and Cordifolioside A showed hydrophilic behaviour meaning poor membrane permeability instead with a logP value of -2.38 and -1.27 respectively.

Another compound Beta sisterol showed extremely high logP value of 7.24 which is not beneficial due to its poor solubility in aqueous environments which can lead to its accumulation in fatty tissues thereby affecting its pharmacokinetics.

Rest all of compounds showed logP value in their ideal range.

So, compounds like Amritoside and Cordifolioside are violating the Lipinski's rule of 5 due to being a high mass compound compared to others, lower values of lipophilicity, GI absorption and oral bioavailability score.



**Table 4.1** - SwissADME Analysis of Anti-cancer Phytochemicals from *Tinospora cordifolia*

Phytochemical	Molecular Formula	Molecular weight	GI Absorption	Bioavailability score	Lipophilicity
Berberine	C <sub>20</sub> H <sub>18</sub> NO <sub>4</sub>	336.36 g/mol	High	0.55	2.53
Columbin	C <sub>20</sub> H <sub>22</sub> O <sub>6</sub>	358.39 g/mol	High	0.55	2.12
Palmatine	C <sub>21</sub> H <sub>22</sub> NO <sub>4</sub> +	352.40 g/mol	High	0.55	2.64
Octacosanol	C <sub>28</sub> H <sub>58</sub> O	44.10 g/mol	Low	0.55	1.54
Cordifolioside A	C <sub>22</sub> H <sub>32</sub> O <sub>13</sub>	504.48 g/mol	Low	0.17	-1.27
Tinosporide	<u>C<sub>20</sub>H<sub>22</sub>O<sub>7</sub></u>	374.38 g/mol	High	0.55	1.61
Piperine	<u>C<sub>17</sub>H<sub>19</sub>NO<sub>3</sub></u>	285.34 g/mol	High	0.55	3.03
Tetrahydropalmatine	C <sub>21</sub> H <sub>25</sub> NO <sub>4</sub>	355.43 g/mol	High	0.55	3.08
Magnoflorine	C <sub>20</sub> H <sub>24</sub> NO <sub>4</sub> +	342.41 g/mol	High	0.55	0.65
Isocolumbin	<u>C<sub>20</sub>H<sub>22</sub>O<sub>6</sub></u>	358.4 g/mol	High	0.55	2.13
Tinosporin	C <sub>21</sub> H <sub>26</sub> O <sub>8</sub>	406.43 g/mol	High	0.55	1.50
Jatrorrhizine	C <sub>20</sub> H <sub>20</sub> NO <sub>4</sub> +	338.38 g/mol	High	0.55	2.31
Dehydrodiscreta mine	C <sub>19</sub> H <sub>18</sub> NO <sub>4</sub> +	324.35 g/mol	High	0.55	1.93
Sitagliptin	C <sub>16</sub> H <sub>15</sub> F <sub>6</sub> N <sub>5</sub> O	407.31 g/mol	High	0.55	2.51
Amritoside	<u>C<sub>26</sub>H<sub>26</sub>O<sub>18</sub></u>	626.47 g/mol	Low	0.17	-2.38
ECD (Epoxy Clerodane Diterpene)	C <sub>20</sub> H <sub>24</sub> O <sub>6</sub>	360.40 g/mol	High	0.55	1.94
Beta- sitosterol	C <sub>29</sub> H <sub>50</sub> O	414.71 g/mol	Low	0.55	7.24
Luteolin	<u>C<sub>15</sub>H<sub>10</sub>O<sub>6</sub></u>	286.24 g/mol	High	0.55	1.73

**Table 4.2-** Molsoft Analysis of Anti-cancer Phytochemicals from *Tinospora cordifolia*

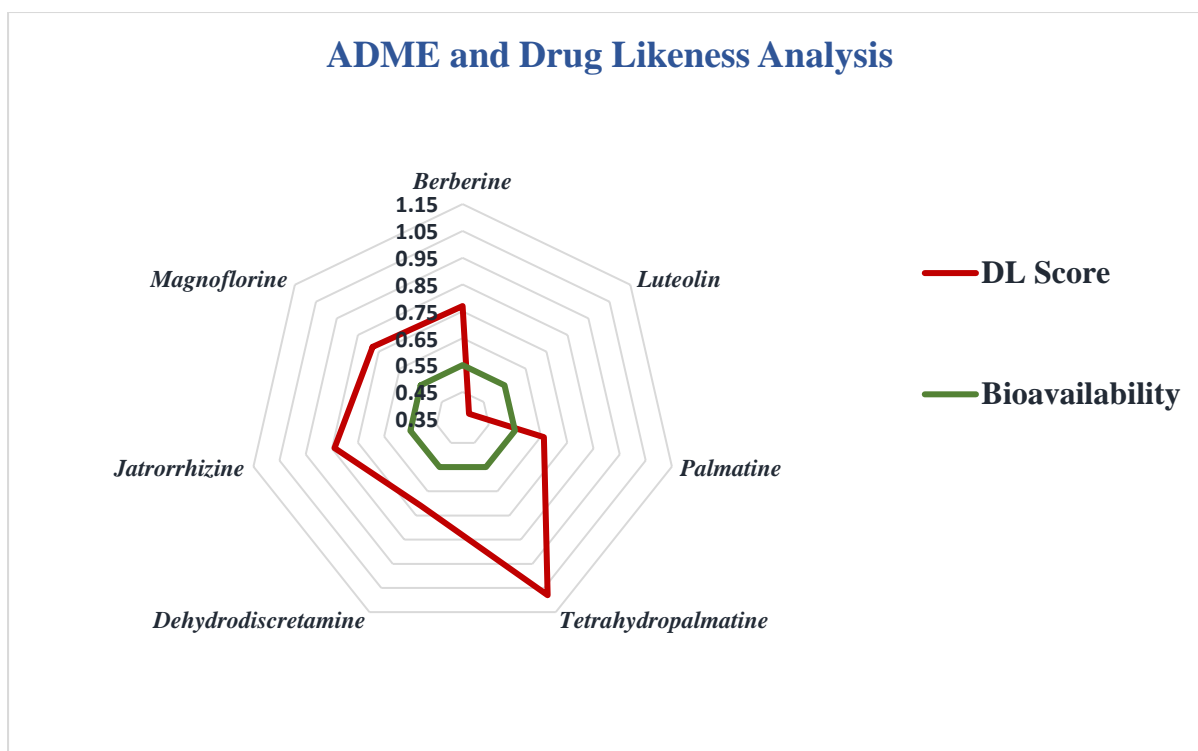
Phytochemical	Drug likeliness score (DL score)
Berberine	0.77
Columbin	-0.52
Palmatine	0.66
Octacosanol	-0.92
Cordifolioside A	0.53
Tinosporide	-0.75
Piperine	-0.16
Tetrahydropalmatine	1.08
Magnoflorine	0.78
Isocolumbin	-0.52
Tinosporin	0.27
Jatrorrhizine	0.84
Dehydrodiscretamine	0.71
Sitagliptin	0.52
Amritoside	0.35
ECD (Epoxy Clerodane Diterpene)	-0.28
Beta-sitosterol	0.78
Luteolin	0.50

Molsoft server for analysing drug likeness using machine learning models like SVM to train itself on known drug molecules and non-drug molecules obtained from database like ChEMBL etc and it uses the structural features of these compounds to predict the DL scores of the test/given compound. A negative or very low DL score suggests low drug likeness possibly due to size and structural complexity or solubility. While a score of  $> 0.5$  means higher similarity to drug like compounds so following this rule, from the 18 phytochemicals taken in this study, Tinosporin and Amritoside showed moderate drug likeness (0.27 & 0.35) while 6 compounds namely Columbin, Isocolumbin, Tinosporoside, ECD, piperine and Octacosanol showed a negative DL score very poor ability to behave as drug like- compounds.

Therefore, on the basis of this study 7 phytochemicals were selected due to their higher DL scores ( $\geq 0.5$ ) and better ADME analysis potential than rest for further in silico test using docking and simulation to check their therapeutic potential against LGSC targets:

**Table 4.3-** Best scoring Phytochemicals from SwissADME and Molsoft analysis

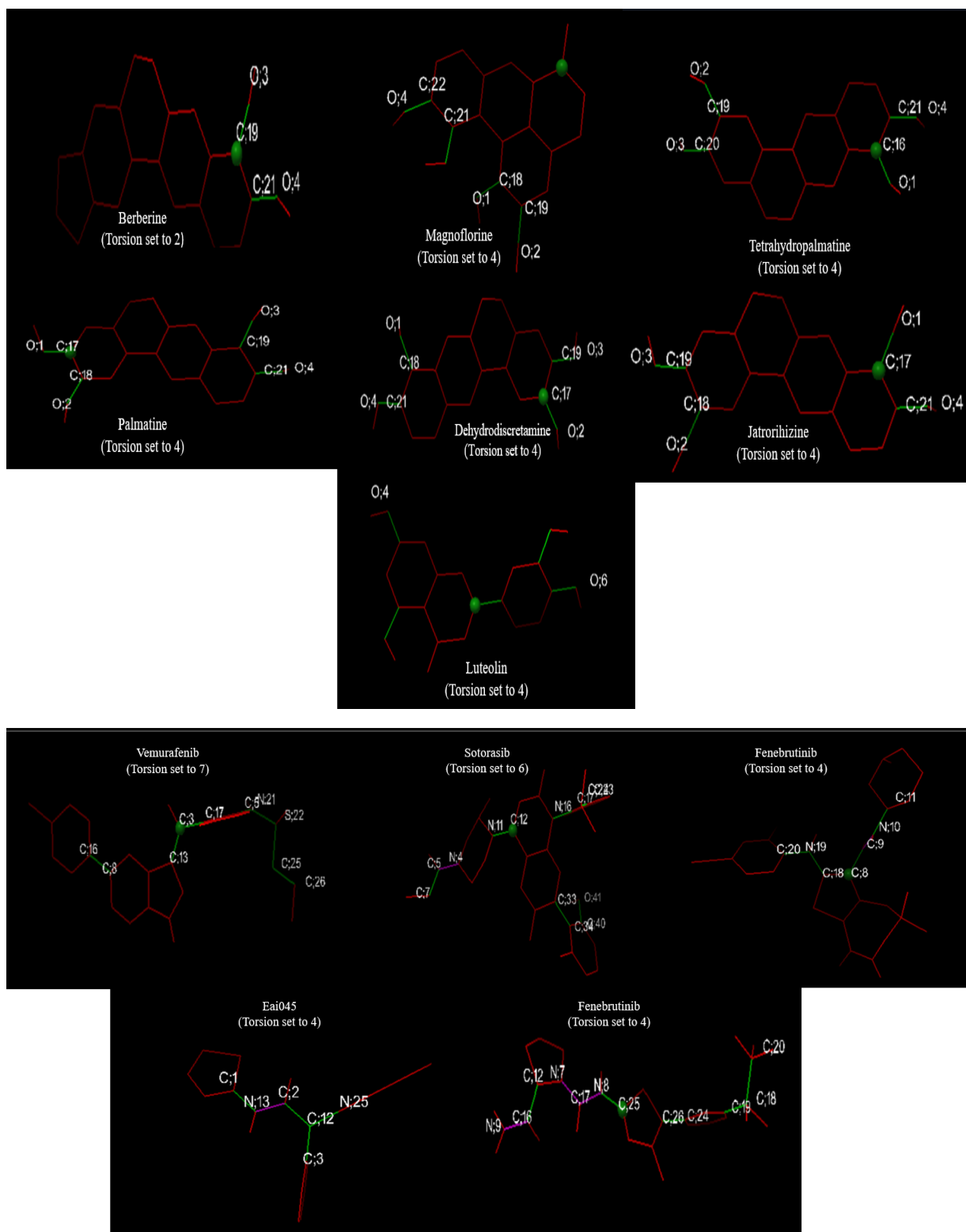
Phytochemical	GI Absorption	Bioavailability score	Lipophilicity	Drug likeliness score (DL score)
Berberine	High	0.55	2.53	0.77
Palmatine	High	0.55	2.64	0.66
Tetrahydropalmatine	High	0.55	3.08	1.08
Magnoflorine	High	0.55	0.65	0.78
Jatrorrhizine	High	0.55	2.31	0.84
Dehydrodiscretamine	High	0.55	1.93	0.71
Luteolin	High	0.55	1.73	0.50



**Fig 4.1-** Radar plot of selected phytochemicals

## 4.2 LIGAND PREPARATION

The selected phytochemicals along with co-crystallized known inhibitors of protein target were all subject to preparation using a standard protocol before decoking. The phytochemical library prepared from PubChem in structure data file format was changed to PDB format on open babel and then final preparation was done on ADT tools.



**Fig 4.2-** Ligand & control inhibitor preparation on ADT tool

The same protocol was followed with control inhibitors. Gasteiger partial charges were given to ligands and all non-polar hydrogens were combined. Rotatable bonds were detected along with root. A maximum of 32 torsions are allowed and on basis of that torsions are determined in ligand structure.

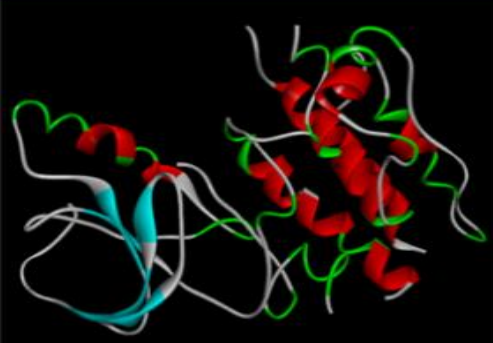
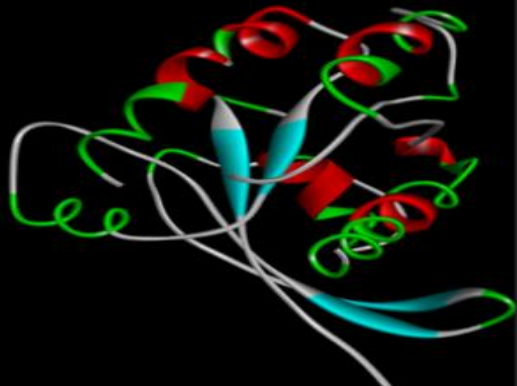
### 4.3 PROTEIN PREPARATION


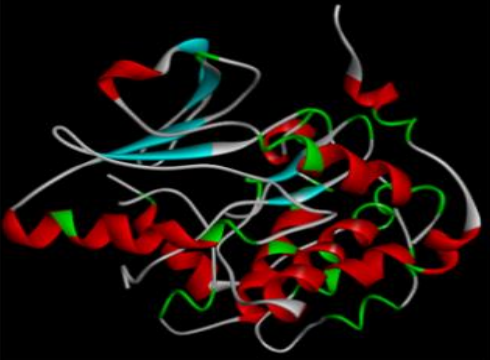
All the protein targets which are the key molecular driver of LGSC and associated drug resistance were downloaded from the RCSB PDB site and their structures were downloaded in the .pdf format. These structures were further cleaned on Discovery studio to remove water molecules, natural co-crystallized ligands and heteroatoms associated with the protein. Once cleaned their protein were subject to ADT tool- based preparation where any missing atoms were repaired in their structure and extra chain were deleted. Polar hydrogens are added along with Kolman charges. Those residues where charges were not evenly distributed were taken care of and at last the PDBQT format of protein is saved which is ready for further docking.

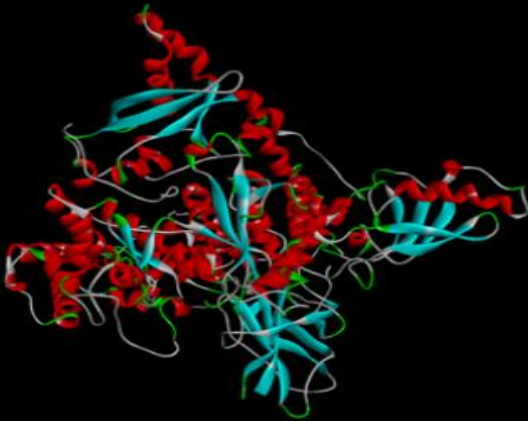
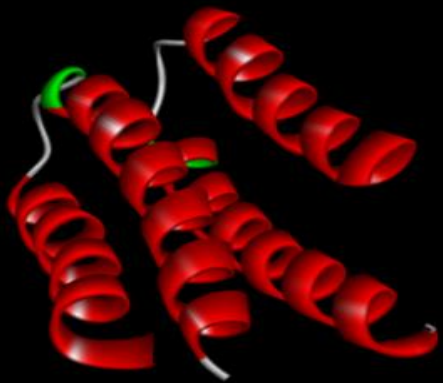
The binding pockets are also predicted for these proteins by loading their pdb structure file on CASTp 3.0 and further these predictions are validated using PrankWeb.

The binding site predicted for these target receptor proteins are-

**Table 4.4-** Predicted binding pockets in target proteins

Protein Target	Prepared structure	Chain having binding pocket	Binding pocket residues
BRAF		A	ILE463, GLY464, SER465, GLY466, SER467, VAL471, ALA481, LYS483, LEU485, GLU501, LEU505, LEU514, PHE516, ILE527, THR529, GLN530, TRP531, CYS532, GLY534, SER535, SER536, ASP576, LYS578, ASN580, ASN581, PHE583, GLY593, ASP594, PHE595, GLY596, GLY615, SER616.
KRAS		A	ASN116, LYS117, ASP119, CYS12, LEU120, GLY13, ALA146, LYS147, GLY15, LYS16, SER17, ALA18, PHE28, VAL29, ASP30, TYR32, PRO34, THR58

Protein Target	Prepared structure	Chain having binding pocket	Binding pocket residues
EGFR		A	LEU718, GLY719, SER720, GLY721, ALA722, PHE723, GLY724, VAL726, ALA743, ILE744, ILE745, LEU747, ILE759, GLU762, ALA763, MET766, CYS775, ARG776, LEU777, LEU788, MET790, LEU792, MET793, GLY796, CYS797, ASP800, ASP837, ARG841, ASN842, LEU844, THR854, ASP855, PHE856, LEU858, PRO877
MEK1		B	LEU101, ILE111, LEU115, LEU118, VAL127, PHE129, ILE141, MET143, GLU144, MET146, ASP147, GLY149, SER150, GLN153, HIS188, ARG189, ASP190, LYS192, SER194, ASN195, LEU197, CYS207, ASP208, PHE209, GLY210, VAL211, SER212, LEU215, ILE216, ARG227, SER228, TYR229, MET230, ARG234, SER248, LEU74, GLY75, ALA76, GLY77, ASN78, GLY79, GLY80, VAL82, ALA95

Protein Target	Prepared structure	Chain having binding pocket	Binding pocket residues
PI3KCA		A	SER27, ASN170, SER629, GLN630, ILE633, ARG662, PHE666, HIS670, LEU755, ASN756, MET811, GLN815, ARG818, PRO835, GLY837, CYS838, LEU839, and GLU849
HES1		A  B	ARG36, HIS40, ASN43, CYS44, GLN47, ILE48, TYR8  ALA10, GLY11, GLU14, ASN17, GLU18, LYS7

## 4.4 MOLECULAR DOCKING

It was performed on Pyrx software using AutoDock Vina to determine the energy of binding and interaction pattern between the receptor ligand. In this step All the seven phytochemicals were docked against the six protein targets from Low-grade serous carcinoma by taking one protein receptor at a time. Known reference inhibitors were also docked to serve as controls for comparative evaluation.

### 4.4.1 RESULT OF DOCKING WITH PHYTOCHEMICALS

The scores generated after docking (binding free energies,  $\Delta G$  in kcal per mol) of each phytochemical–protein combination are summarized below. Lower binding energy values indicate stronger predicted binding.

**Table 4.5-** Binding affinities of all Protein- ligand pairs

Phytochemicals	Binding energies ( $\Delta G$ in kcal/mol)					
	BRAF	KRAS	EGFR	MEK1	PI3KCA	HES1
Berberine	-8.4	-5.6	-8.8	-5.8	-8.7	-5.3
Dehydrodiscretamine	-8.7	-5.6	-8.5	-5.2	-8.1	-5.5
Magnoflorine	-8.8	-7.4	-8.0	-5	-8.5	-5.1
Palamtine	-8.4	-8.0	-8.2	-5	-8.3	-5
Tetrahydropalmatine	-8.2	-5.5	-8.3	-4.8	-8	-5.6
Jatrorihizine	-8.3	-5.5	-8.5	-5.1	-8.1	-5.6
Luteolin	-8.8	-5.6	-8.9	-5.3	-7.9	-5.6

Out of all the compounds from *T. cordifolia* that were tested against oncogenic proteins involved in implication of LGSC, Luteolin and Berberine came out to be the most potent multitargeting ligands. Luteolin showed the highest strength or affinity for binding with EGFR (-8.9 kcal per mol), close behind it is interactions with BRAF (-8.8 kcal/mol) and PI3KCA (-7.9 kcal per mol). Berberine on the other hand showcased high-affinity interactions with EGFR (-8.8 kcal/mol), PI3KCA (-8.7 kcal/mol), and BRAF (-8.4 kcal per mol), making it the second most strong candidate for further investigation.

Here, EGFR was found to be the most consistently targeted protein, as all phytochemicals showed high binding strengths (ranging from -8.0 to -8.9 kcal per mol) for it, emphasizing its relevance as a therapeutic target in LGSC. This is in accordance with previous reports that indicated that EGFR overexpression in ovarian cancer can lead to disease progression and resistance to chemotherapy.

KRAS and MEK1 which are main components of the MAPK signaling pathway, showed comparatively lower binding affinities across majority of the ligands. Palmatine, however, showed a relatively stronger interaction with KRAS (-8.0 kcal/mol) which suggest it might have some potential for modulating RAS-mediated signalling. On the other hand, MEK1 throughout showed the weakest emerging of interaction, with values ranging from -4.8 to -5.8 kcal/mol, which shows that these phytochemicals don't have sufficient direct inhibitory activity on MEK1.

PI3KCA which is an essential regulator of the PI3K/AKT/mTOR pathway, showed strong interactions with most compounds, especially Berberine (-8.7 kcal/mol), Magnoflorine (-8.5



kcal/mol), and Palmatine (-8.3 kcal/mol), which basically supports the hypothesis that *Tinospora cordifolia* phytoconstituents can effectively interfere with oncogenic PI3K signalling.

At last, the HES1 which is a factor involved in transcription is seen in the Notch signalling pathway and tumor stemness, showed low binding with all ligands out of which the best was with Tetrahydropalmatine, Jatrorrhizine, and Luteolin (all -5.6 kcal/mol).



**Fig 4.3-** Heatmap of Protein- ligand complexes using Binding energies

Out of the combinations, ligand–receptor pairs that showed binding energies equal to or greater than -8.5 kcal/mol were then taken further for next step that is simulations to further inspect the stability and dynamic behaviour of the complexes provided with near-physiological conditions. This pairs are;

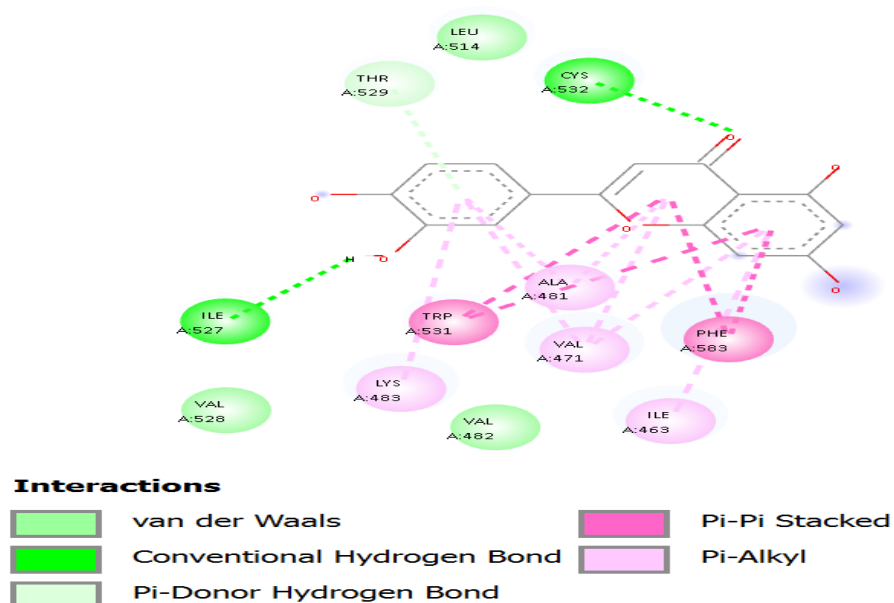
- BRAF with Magnoflorine (-8.8 kcal/mol)
- BRAF with Luteolin (-8.8 kcal/mol)
- BRAF with Dehydrodiscretamine (-8.7 kcal/mol)
- EGFR with Luteolin (-8.9 kcal/mol)
- EGFR with Berberine (-8.8 kcal/mol)
- PI3KCA with Berberine (-8.7 kcal/mol)

The 2D interaction diagram helps to show the types of non-covalent association (H-bonds, hydrophobic contacts, stacking of  $\pi$ -bonds, salt bridges, etc.) that are occurring between a ligand and the residues of amino acid within the binding cavity of the protein. The 2D interaction diagram of these selected protein- ligand complex are as follows-

#### 1. BRAF protein interaction with phytochemical Luteolin

The diagram shows Hydrogen bonds with CYS532, ILE527. Vander waals interaction was seen with VAL528, VAL482 and LEU514. Other types of bonds include Pi-Pi interaction TRP531, PHE583 and Pi alkyl bond with LYS483, VAL471, ILE463 and ALA481

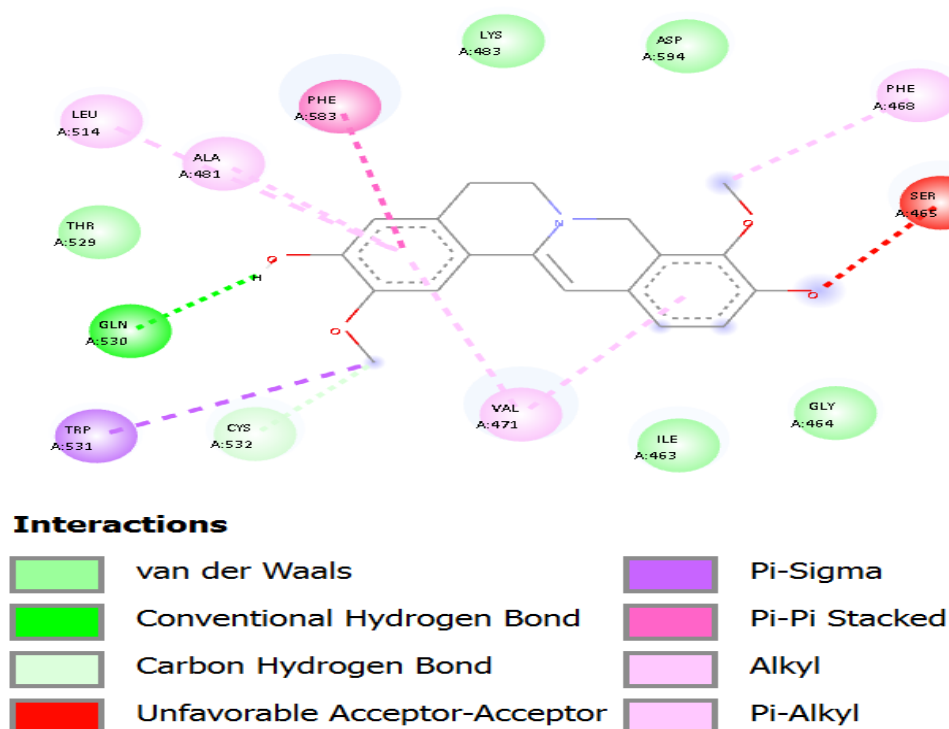




**Fig 4.4-** 2D interaction of BRAF with Luteolin

## 2. BRAF protein interaction with phytochemical Dehydrodiscretamine

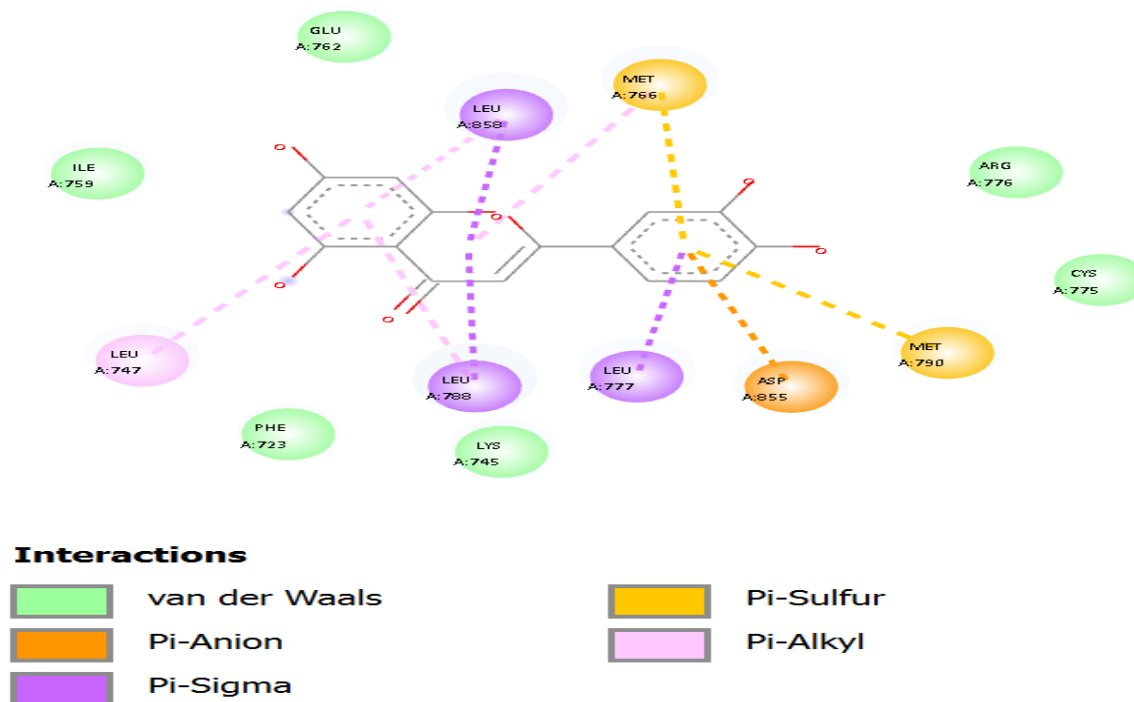
The diagram shows conventional hydrogen bonds with GLN530 whereas carbon H-bond with CYS 532. There is also Vander waals interaction was seen with THR529, ILE463, GLY464, LYS483, ASP594. Other types of bonds include Pi-Pi interaction PHE483 and Pi alkyl bond with PHE468, VAL471, ALA481, LEU514. There is also Pi-sigma bond observed with TRP531 and an unfavourable acceptor acceptor interaction with SER465.



**Fig 4.5-** 2D interaction of BRAF with Dehydrodiscretamine

### 3. EGFR protein interaction with phytochemical Luteolin

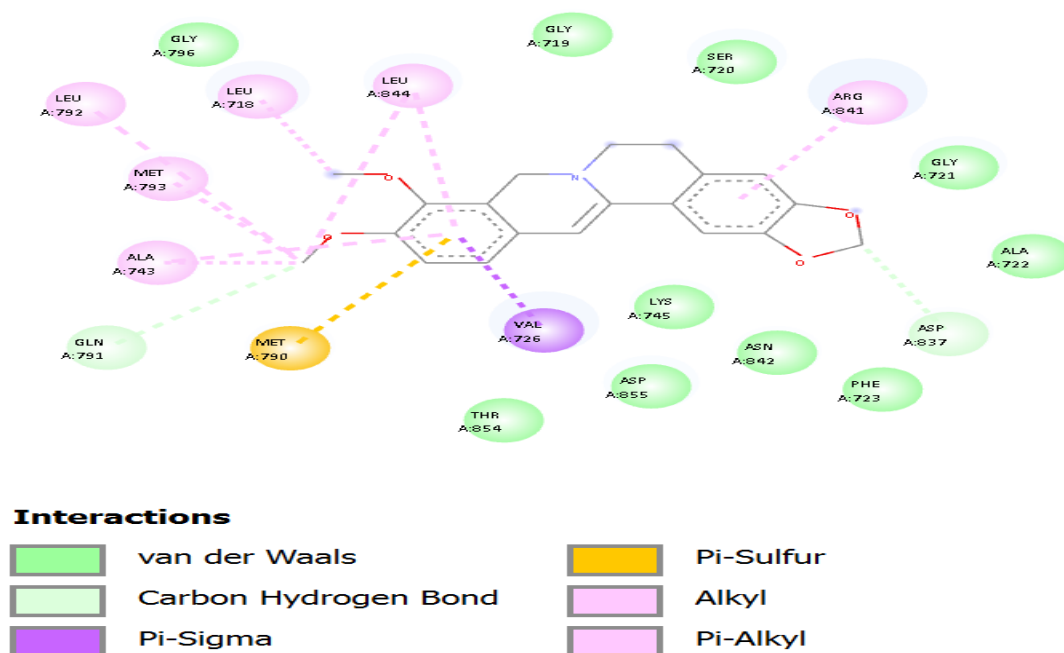
The diagram shows no hydrogen bonds but the formation of Vander Waals interaction with GLU762, ILE759, PHE723, LYS745, ARG776 and CYS775. Different types of Pi bonds were also seen like Pi-sigma bond with LEU858, LEU777 and LEU788. Pi-anion interaction was seen with ASP655 whereas Pi-sulphur bond could be seen with MET766 & MET790.



**Fig 4.6-** 2D interaction of EGFR with Luteolin

### 4. EGFR protein interaction with phytochemical Berberine

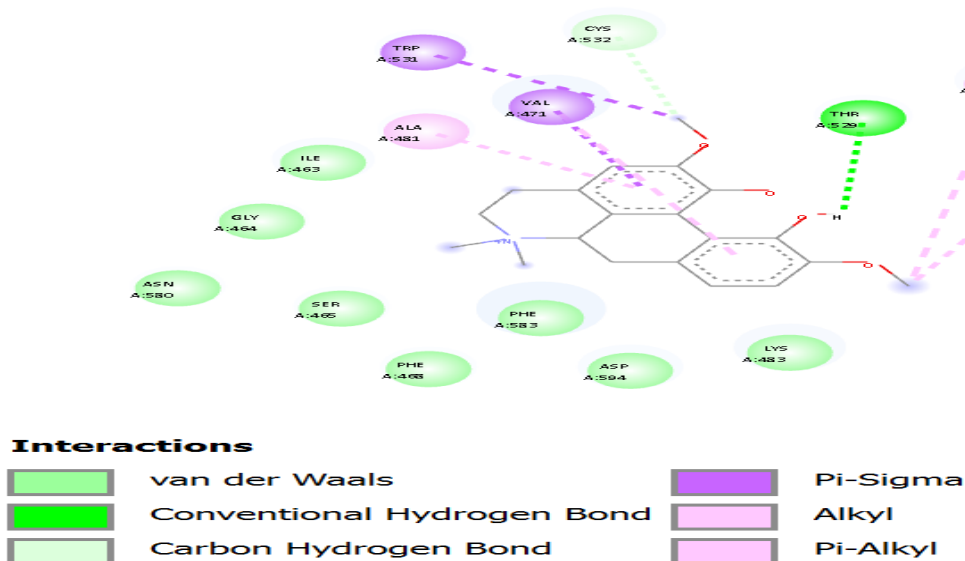
The diagram shows carbon hydrogen bonds with GLN791, ASP837, and Vander waals interaction was seen with GLY796, THR854, ASP855, LYS745, ASN842, PHE723, ALA722, GLY721. SER720, GLY719. Other types of bonds include  $\pi$ -sigma interaction with VAL726. and  $\pi$  alkyl bond with ALA743, MET793, LEU792 and Pi-sulfur bond with MET790



**Fig 4.7-** 2D interaction of EGFR with Berberine

#### 5. BRAF interaction with phytochemical Magnoflorine

The diagram shows carbon hydrogen bonds CYS532 and conventional h-bond with THR529 while Vander waals interaction was seen with multiple residues like ILE463, GLY564, ASN580, SER466, PHE468, PHE583, ASP594, LYS485. Other types of bonds include  $\pi$ -sigma association with VAL471. and  $\pi$ -alkyl bond with LEU514 & ILE527.



**Fig 4.8-** 2D interaction of BRAF with Magnoflorine

## 6. PI3KCA protein interaction with phytochemical Berberine

The diagram shows carbon hydrogen bonds with ASN756 and conventional h-bond with ARG818 while Vander waals interaction was seen with multiple residues like SER27, SER629, HIS670, ILE633, GLN815 and MET611. Other types of bonds include  $\pi$ -sigma interaction with PHE666 and  $\pi$ -alkyl bond with TYR26 and ARG662.

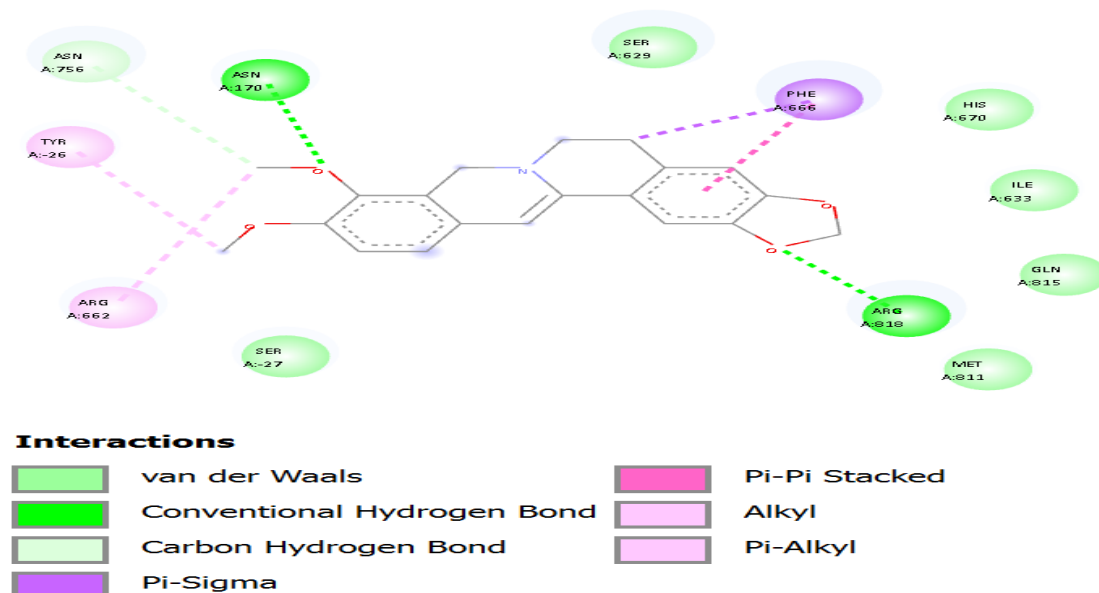


Fig 4.9- 2D interaction of PI3KCA with Berberine

### 4.4.2 RESULT OF DOCKING WITH CONTROL INHIBITORS

Control ligands known to bind the target proteins were included to validate the docking methodology. The binding energies of these ligands provide a benchmark for assessing phytochemical affinities, while RMSD values assess the accuracy of the docking poses.

Table 4.6- Control inhibitor docking results

Receptor Protein	Know inhibitor/ligand	Binding Energy (kcal/mol)	RMSD value
BRAF	Vemurafenib	-10.9	1.52
EGFR	Eai045	-10.7	1.34
PI3KCA	Alpelisib	-9.9	1.67

All RMSD values were below the acceptable threshold of 2.0 Å, confirming that the docking procedure was able to reliably reproduce the experimentally determined binding poses. This confirms the reliability of the docking workflow used in this study.

## 4.5 MOLECULAR DYNAMIC SIMULATION

At last, simulations were done for the complexes scoring the best based on their highest binding affinity scores in molecular docking. The simulations were run using the Desmond Schrodinger suite and through the Make It Rain Google Colab environment. On the former simulation was run for 50 ns and in Google colab the production run lasted for 20 ns due to the restraint on GPU limit. This mixed approach helped to observe and evaluate the complex stability, its flexibility and compactness, and interaction consistency in a given solvated system.

### 4.5.1 RESULT OF DYNAMIC SIMULATION USING DESMOND SCHRODINGER

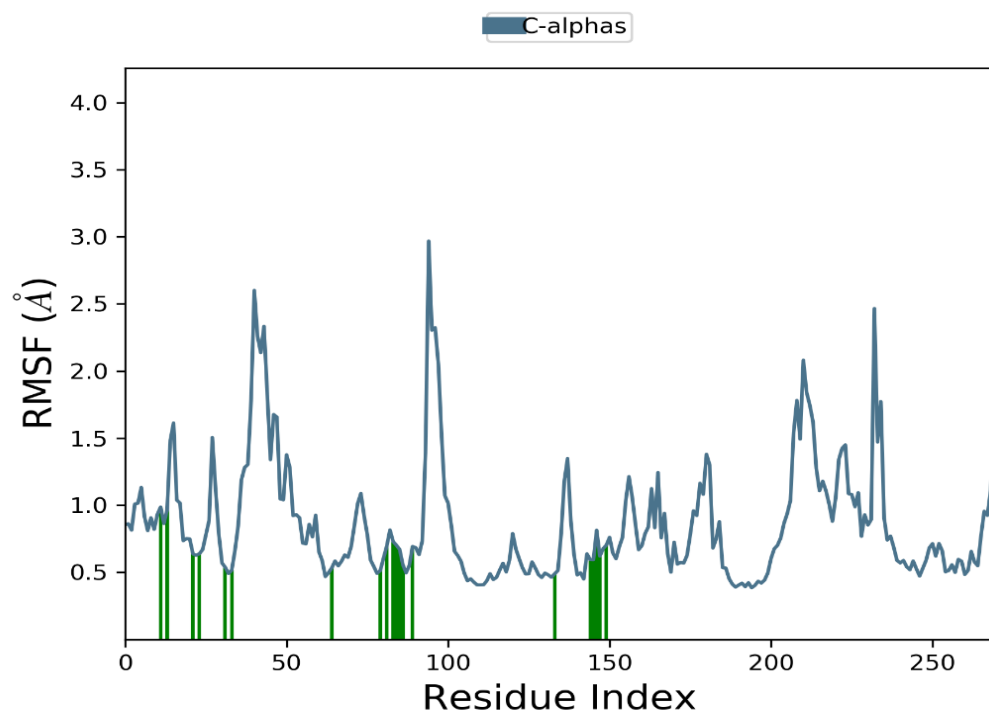
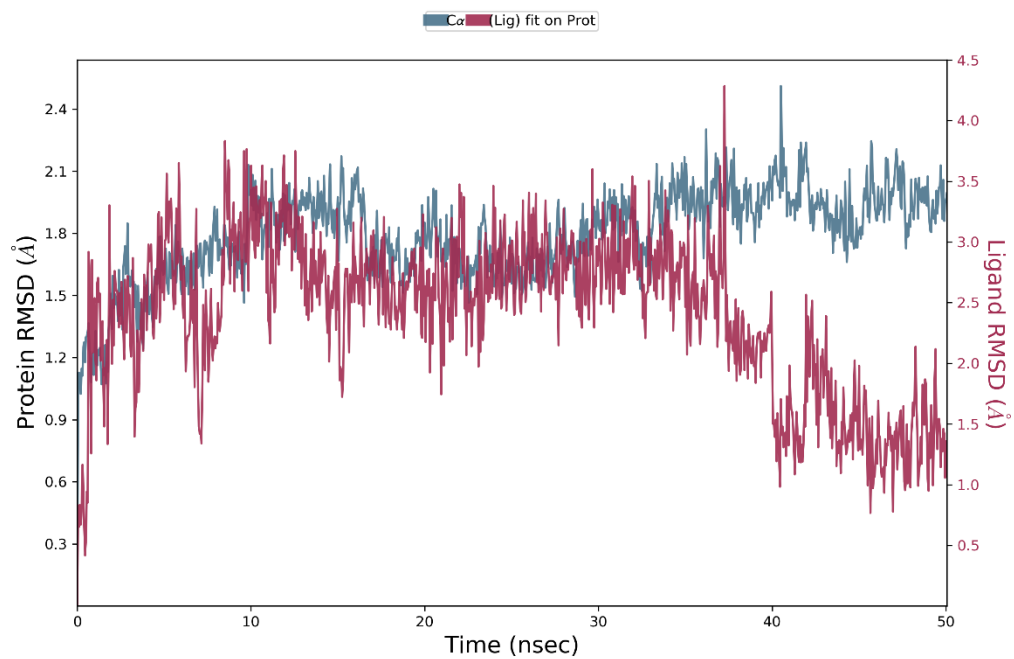
#### 1. BRAF with Dehydrodiscretamine

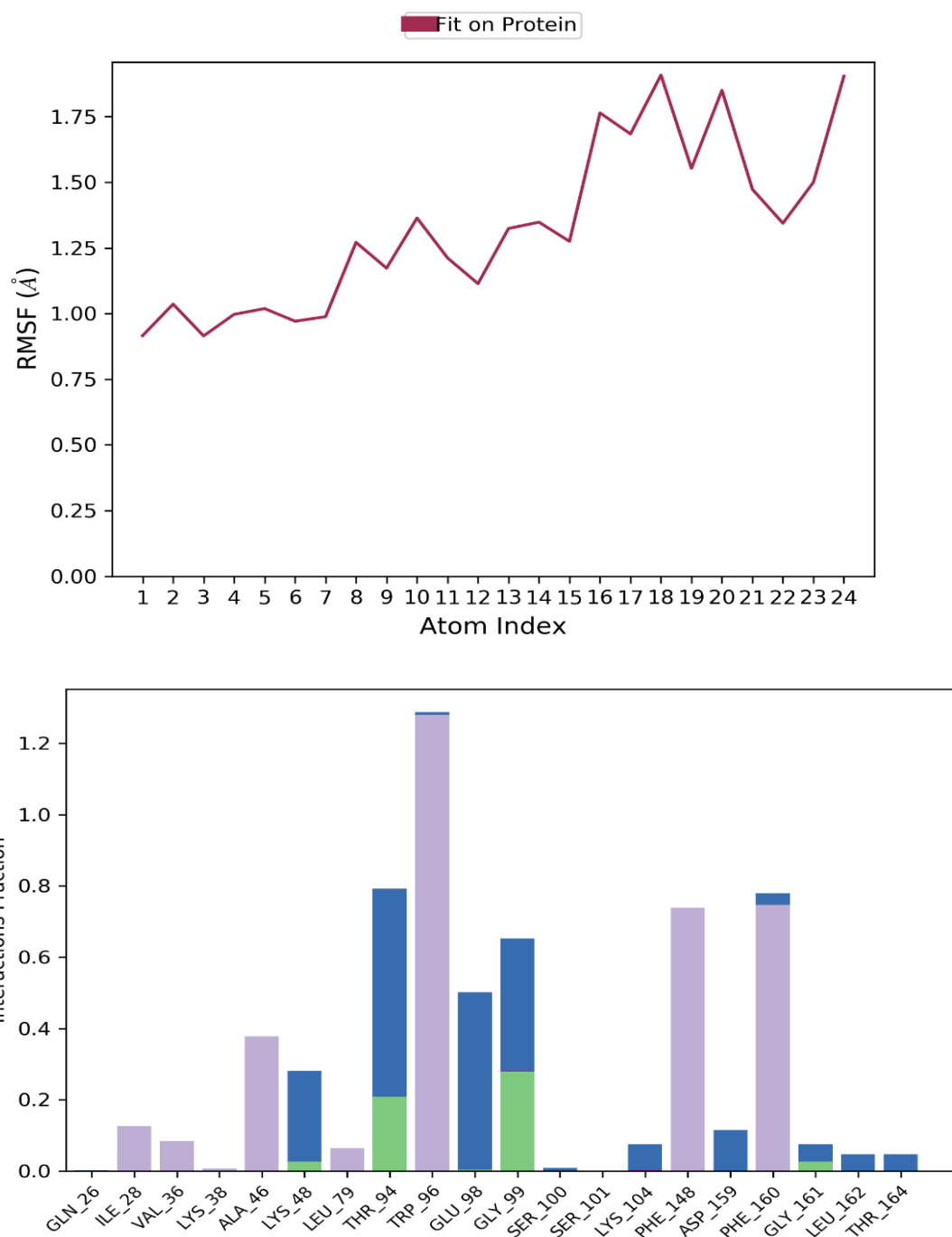
The structural stability of this complex was evaluated by analysing the RMSD of the backbone of the protein structure ( $C\alpha$  atom) and the ligand in regards to the protein's binding site over a 50 ns simulation run.

As it can be seen from the RMSD plot, the protein RMSD (blue line) first started with a short equilibration phase and it then stabilized after approximately 10 ns while fluctuating between 1.5 Å and 2.1 Å throughout the course of the run which shows that BRAF protein was able to maintained its overall structural integrity without going any major conformational changes.

The ligand RMSD represented by the maroon line was calculated after fitting on the protein backbone. The plot shows it initially increases in the early phase of the simulation, reaching up to ~3.5 Å. However, after ~15 ns, the ligand RMSD began to gradually decrease and stabilize and its value came down to below 2.0 Å toward the end of the trajectory. This behaviour suggests that initially the ligand is adjusting within the binding pocket, followed by a stable binding pose being maintained for most of the part of simulation.

The steady protein RMSD in association with the stabilization of ligand RMSD supports the hypothesis that Dehydrodiscretamine creates/generates a stable and persistent interaction with the BRAF active site.





**Fig 4.10-** MD simulation analysis of BRAF protein and Dehydrodiscretamine. (a) RMSD plot of complex, (b) BRAF RMSF plot, (c) Dehydrodiscretamine RMSF Plot, (d) Histogram of BRAF - Dehydrodiscretamine contacts

The RMSF of C $\alpha$  atoms of BRAF protein was calculated for 50ns to determine the flexibility associated with each amino acid residue and potential interaction sites. According to the RMSF analysis most of the residues were found to fluctuate in a moderate range of 0.5–1.5 Å, while higher elevated flexibility was observed in regions around residues 40–50, 95–100, and 215–225 which most likely corresponds to loops or terminal ends regions in the protein. Most importantly, residues within the binding site exhibited lower RMSF values, which suggests that

ligand binding offered local stabilization. This also supports the assumption that Dehydrodiscretamine binds stably within the BRAF active site and it involved in imparting balance and stability to structure of protein when the simulation was happening.

Additionally, the ligand RMSF plot to calculate the flexibility associated with each atom of ligand demonstrated that individual atoms of Dehydrodiscretamine maintained fluctuations mostly within the 1.0–1.8 Å range, with slightly higher flexibility observed toward the terminal atoms. This pattern suggests that the ligand maintained a comparatively stable orientation in between the binding pocket while allowing some peripheral flexibility.

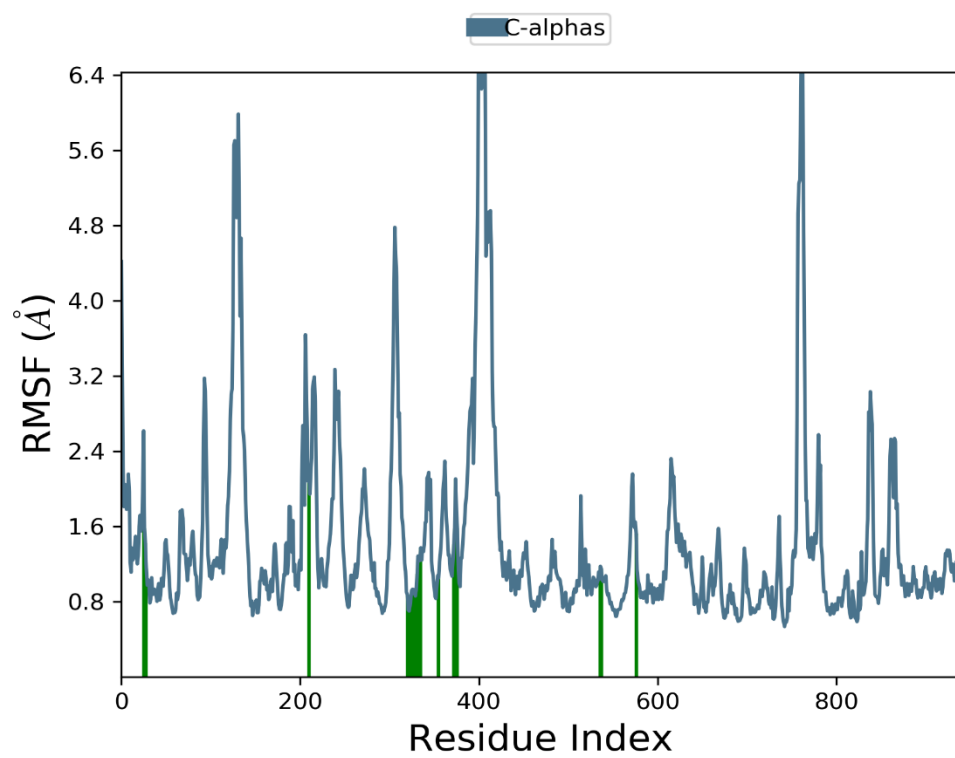
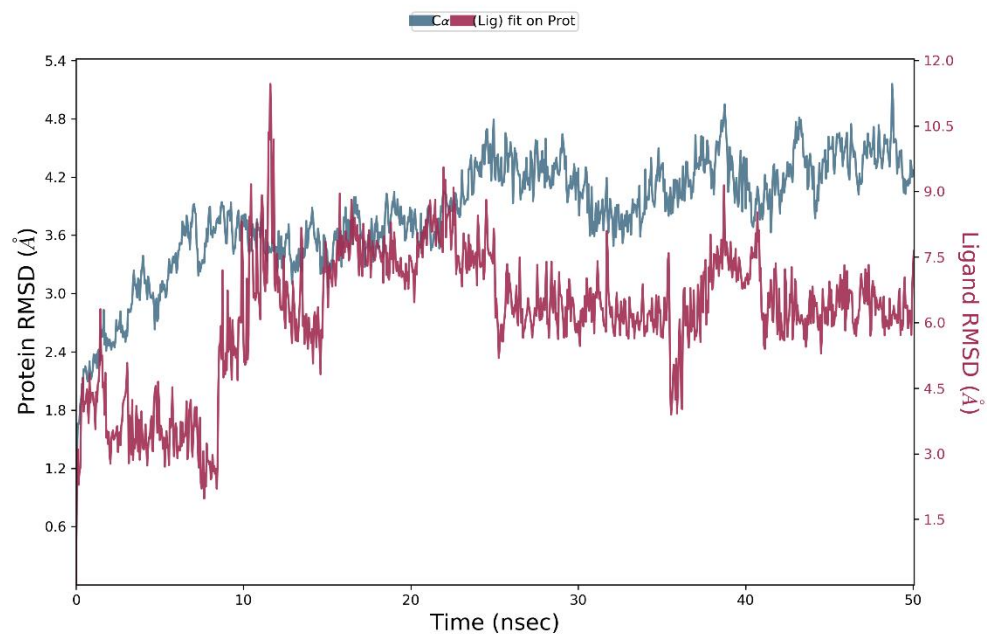
According to the histogram of protein-ligand contact, residues such as GLU-98, THR-94, and PHE-160 showed high interaction fractions which suggest they are important for stabilizing the complex. GLU-98 has the highest interaction frequency out of all so therefore it is constantly showing interaction throughout. Several residues like THR-94 and GLY-99 were involved in multiple types of interactions such as h-bonding, hydrophobic contacts, and water bridges. Therefore, the involvement of broad range of residues from GLN-26 to THR-164 suggests that dehydrosicretamine has a wide binding interface on BRAF.

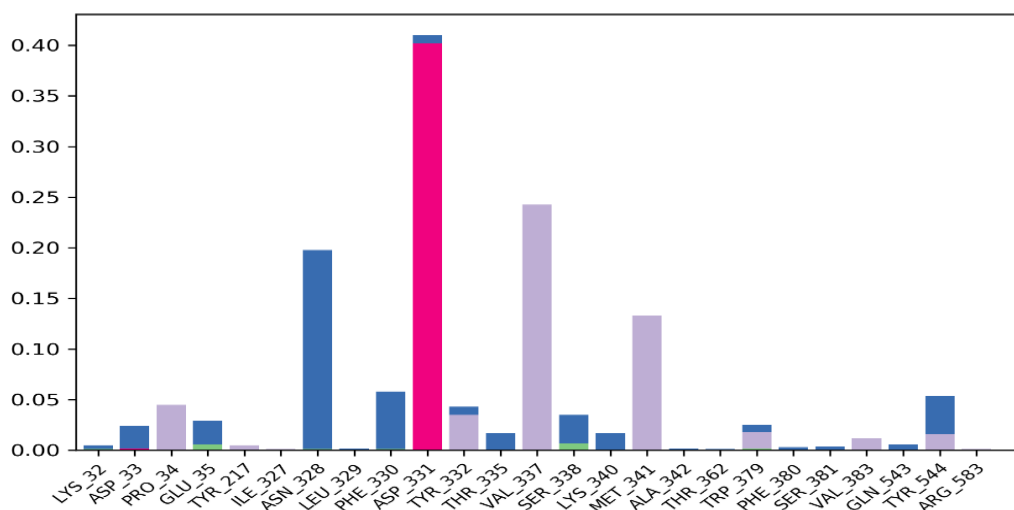
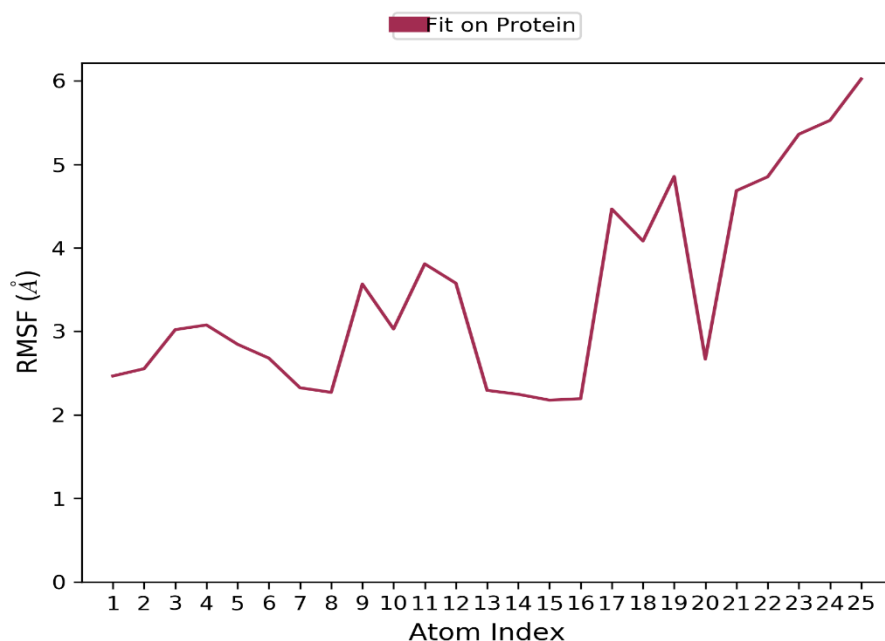
## 2. PIK3CA with Berberine

The RMSD plot calculated for PIK3CA protein C $\alpha$  atoms suggest that protein backbone (C $\alpha$  atoms) showed moderate conformational flexibility, The RMSD values first increases from ~1.5 Å to ~4.0–4.5 Å however it stabilizes after ~15 ns. An RMSD below 3 Å is generally considered very stable. Here, the protein RMSD is a bit higher (~4 Å) which suggests some moderate conformational flexibility. However, after ~15 ns, it plateaus, indicating that the system has equilibrated and is not unfolding or unstable. As for the ligand RMSD, calculated with respect to the protein, starts around 1.5 Å and fluctuates but it mostly remains between 3–7 Å, especially after 10 ns. In the beginning the ligand shows some movement, indicating conformational adjustment in the binding pocket. However, after 10–15 ns, the RMSD stabilizes around 5–6 Å, which is moderately high. This can help to assume that Berberine most likely does not completely dissociate from the protein but it still has some flexibility within the binding site or a shallow binding pocket therefore it means it is not rigidly bound, but still maintains the overall interaction, which might be sufficient for inhibitory activity depending on other parameters (like H-bonds, binding energy, etc).

According to the RMSF plot of the protein most of the residues are showing relatively low fluctuations below 2.0 Å meaning an overall structural stability. Some notable peaks were although observed at specific residue indices, with the highest fluctuations reaching up to ~6.4 Å which may be the loop regions or solvent-exposed areas as these regions are comparatively more flexible. Regions involved in binding with ligand were showing limited fluctuation which means the active site was conformationally stable throughout the run. So, berberine may maintain its interactions with proteins without getting displaced by local residue dynamics.







**Fig 4.11-** MD simulation analysis of PIK3CA and Berberine. (a) RMSD plot of PIK3CA and Berberine, (b) RMSF plot of PIK3CA, (c) RMSF plot of Berberine, (d) Histogram of PIK3CA – Berberine contact

The RMSF values of the ligand varied from about 2.4 Å to 6.0 Å, showing that some parts of the ligand were more flexible than others. In general, the atoms in the middle or core scaffold of the molecule were much more stable, compared to the atoms towards the terminal region that showed more movement. This helps in understanding that berberine stays in the binding region of the protein during the 50 ns however, it had some flexibility, specifically in its side groups or substituents which can eventually help the ligand to fit better into the binding site. Therefore, the ligand showed a stable interaction with the protein, with some natural flexibility present in its structure.

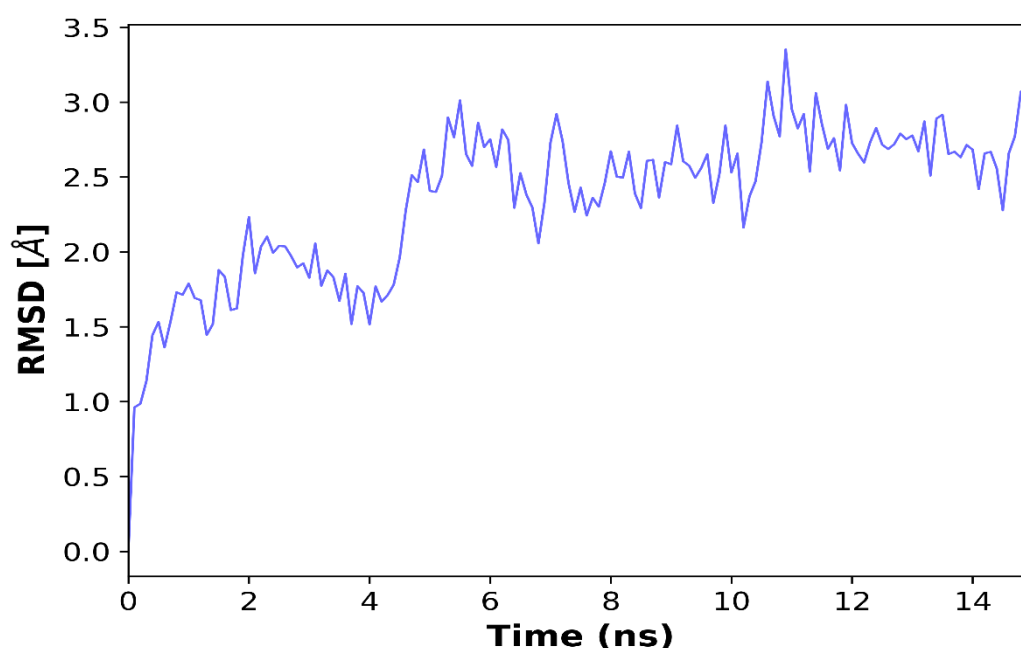
The histogram of protein- ligand contact shows that residue TYR-335 had the highest interaction fraction which means it is very important for holding berberine in binding pocket.

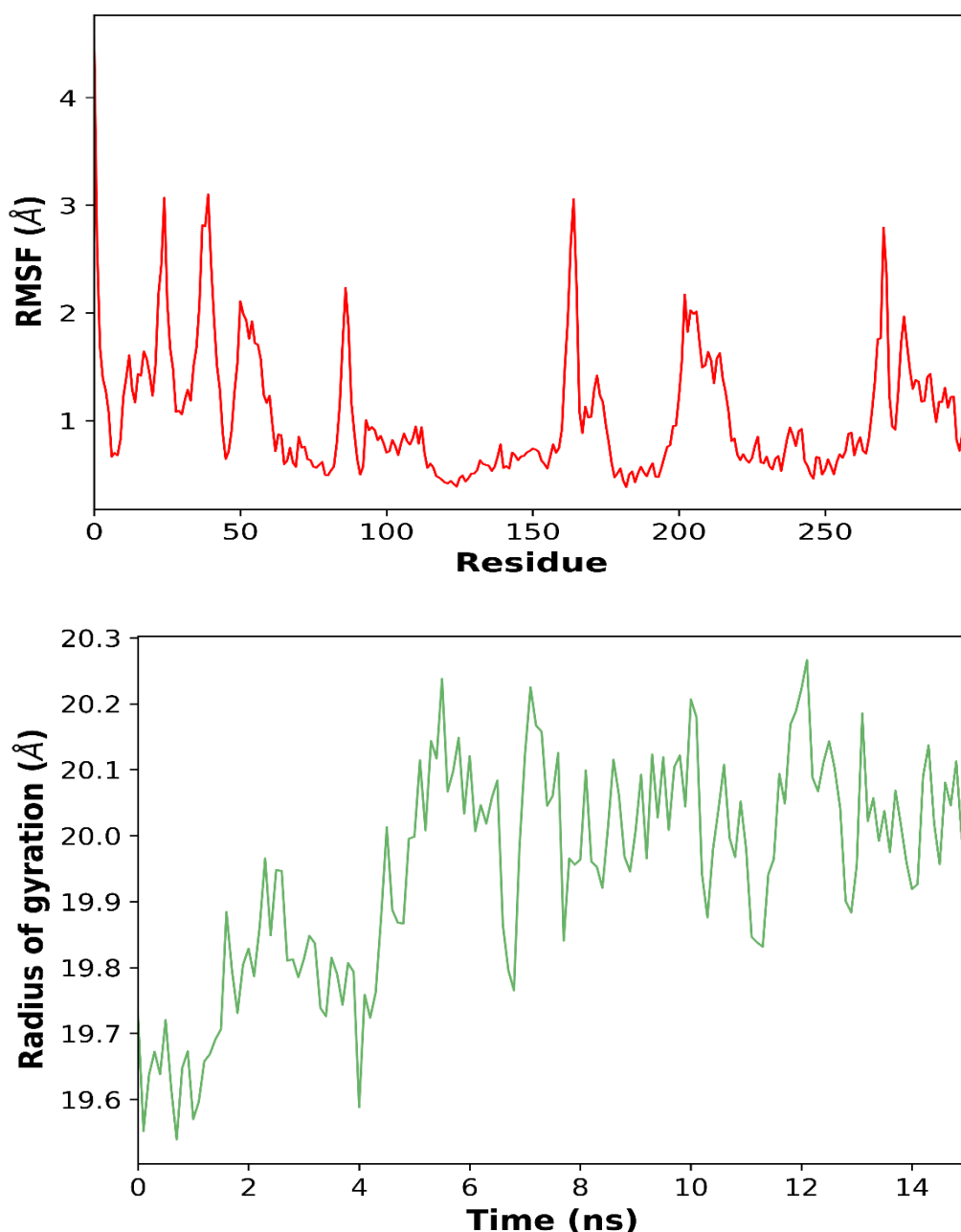
Other residues like ASN-328, LEU-329, SER-337, and LYS-340 also were showing contribution in the interaction with berberine which shows importance of these residues required for ligand stabilization. The types of bonds that were observed between the complex was hydrophobic contacts, hydrogen bonds and possibly water bridges or  $\pi$ -stacking. TYR-335 residue was seen to be involved in strong aromatic or  $\pi$ - $\pi$  stacking interactions with ligand. As these interactions are moderately distributed which supports that berberine makes contacts with the target across a defined region of the PI3KCA active site.

## 4.5.2 RESULT OF DYNAMIC SIMULATION USING GOOGLE COLAB

### 1. EGFR with luteolin

The RMSD of the protein backbone was calculated over a 15 ns trajectory. The values in the plot initially increased during the first ~2 ns, which shows the system equilibration phase and then the values gradually stabilized. After approximately 5 ns, the RMSD plateaued around an average value between 2.5 Å to 3.0 Å. These values suggest a particular degree of flexibility mainly in non-core regions and it remains generally in that range without showing a sharp or sustained drops/spikes which indicates stability but with normal dynamic flexibility.





**Fig 4.12-** MD simulation analysis of EGFR with luteolin. (a)RMSD of EGFR alpha carbon atoms, (b) RMSF of EGFR alpha-C atoms, (c) Radius of gyration (Rg) of EGRF

As for the RMSF plot of the protein most of the residues showed values lying in range of 0.5 Å and 2.0 Å, indicating limited flexibility and a generally stable backbone. But distinct peaks were seen at several regions like around residues 40, 60, 150, 210, and 260, Here the fluctuations went beyond 3.0 Å, with a maximum nearing 4.5 Å. These regions could most probably be loop regions or surface-unmasked segments of protein as they are flexible

However, amino acids in binding site of luteolin remained relatively stable, with fluctuations values staying less than 2.0 Å, suggesting that ligand binding contributes to local rigidity and conformational stabilization of the active site.

The radius of gyration was monitored to calculate how compact the protein is over time. And the average value of  $R_g$  was 20.0 Å. The  $R_g$  gradually increases during the first 5 ns, indicating slight expansion or relaxation of the structure but then it stabilizes so which means protein attains a more stable conformation during the latter part of the simulation.

**Table 4.7-** MMPBSA/ GBSA binding free energy of EGRR-Luteolin

MM/PBSA Results	
Energy Component	Average (kcal/mol)
van der Waals ( $\Delta E_{vdw}$ )	−39.29
Electrostatic ( $\Delta E_{ele}$ )	−23.50
Solvation Free Energy ( $\Delta G_{solv}$ )	+56.11
Binding Free Energy ( $\Delta G_{bind}$ )	−6.68
MM/GBSA Results	
Energy Component	Average (kcal/mol)
van der Waals ( $\Delta E_{vdw}$ )	−39.29
Electrostatic ( $\Delta E_{ele}$ )	−23.50
Interaction Energy ( $\Delta E_{interaction}$ )	−62.79
Solvation Free Energy ( $\Delta G_{solv}$ )	+28.40
Binding Free Energy ( $\Delta G_{bind}$ )	−34.39

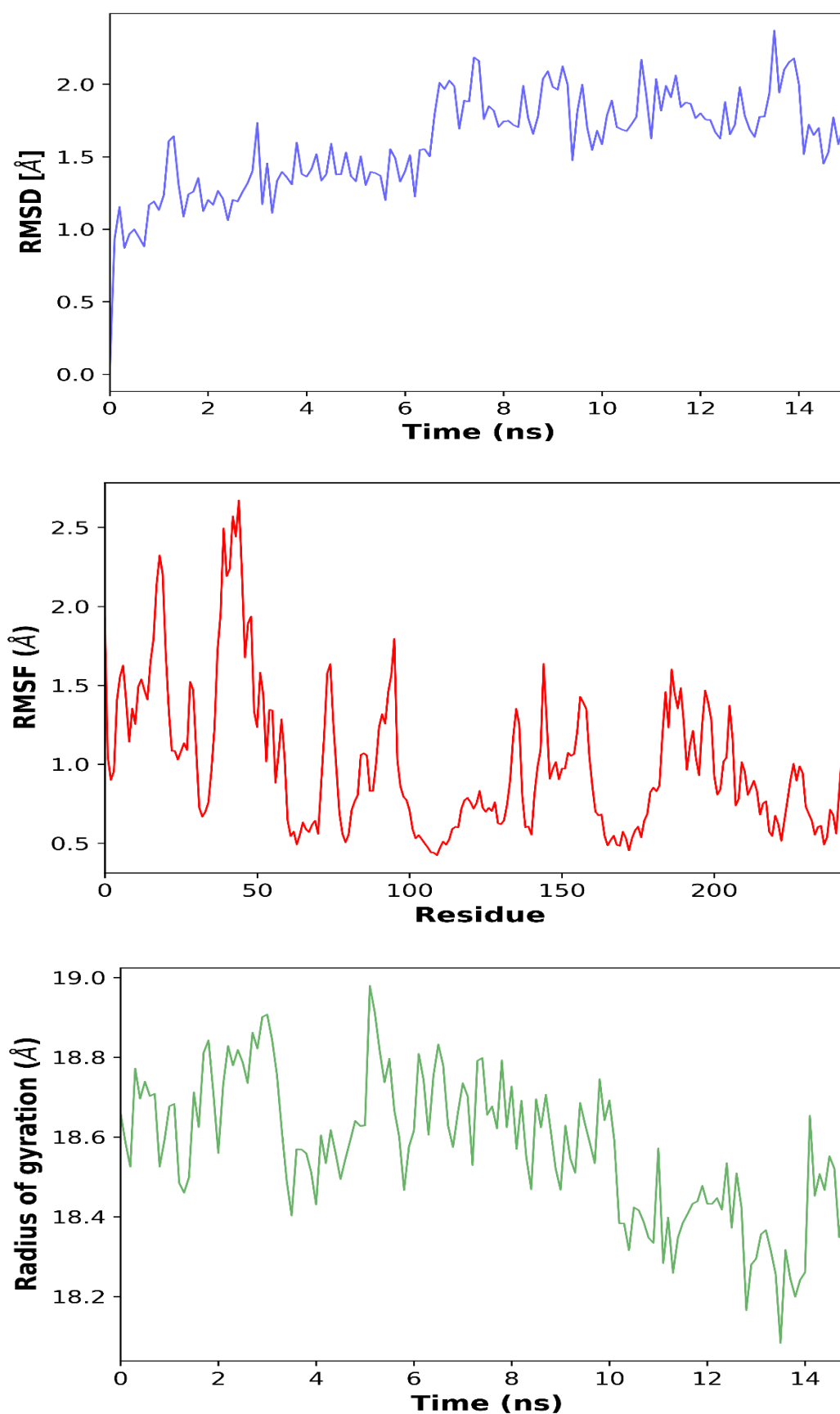
The MM/GBSA method shows strong binding affinity between the receptor and ligand ( $\Delta G \approx -34.4$  kcal/mol), whereas MM/PBSA gives a more moderate estimate ( $\Delta G \approx -6.7$  kcal/mol). The difference may be arising because of distinct treatment of the solvation model (GB vs. PB). Both methods are showing a favourable binding interaction between the ligand and receptor.

## 2. BRAF with luteolin

The RMSD of the C alpha atoms (backbone) of the BRAF protein in complex with luteolin was observed for a 15 ns run. In the start, value can be seen increasing from approximately 0.9 Å to around 1.5–2.0 Å and it is undergoing stabilization after about 6 ns which indicates that the protein is undergoing minor conformational adjustments before it reaches equilibration stage.

In range of 1.5 to 2.0 Å values remain stable for the rest of the run indicates that the overall backbone of BRAF stayed stable during ligand binding which means attachment of the luteolin does not trigger any induce major structural rearrangements in protein.

The initial changes in RMSD are acceptable for a globular protein and it shows the normal thermal motion.



**Fig 4.13-** MD simulation analysis of BRAF and Luteolin. (a) RMSD of BRAF C $\alpha$  with luteolin, (b) RMSF of BRAF C alpha atoms, (c) Rg plot for BRAF- luteolin

The RMSF analysis of the alpha carbon atoms in the BRAF protein-luteolin complex over a 15 ns simulation is showing that majority of residues have a moderate level of flexibility having fluctuations in range of 0.5 Å to 2.7 Å. Higher fluctuations can be seen for N- and C-terminal regions and loop segments around residues 40–60 as they are more dynamic compared to the core region (residues 100–200) which is showing stability important for protein's functionality. There binding of luteolin ligand is not a major destabilization of the protein.

According to the Radius of gyration plot, the Rg can be seen varying from 18.6–18.8 Å, showing slight expansion, but then it is gradually decreasing toward 18.2–18.4 Å in the latter part of the simulation so therefore the protein is overall attaining a compact and stable conformation as the time passes without losing its structural integrity.

**Table 4.8-** MMPBSA/ GBSA binding free energy of BRAF-Luteolin

MM/PBSA Results	
Energy Component	Average (kcal/mol)
van der Waals ( $\Delta E_{vdw}$ )	–33.99
Electrostatic ( $\Delta E_{ele}$ )	–3.05
Solvation Free Energy ( $\Delta G_{solv}$ )	+35.07
Binding Free Energy ( $\Delta G_{bind}$ )	–1.97
MM/GBSA Results	
Energy Component	Average (kcal/mol)
van der Waals ( $\Delta E_{vdw}$ )	–33.99
Electrostatic ( $\Delta E_{ele}$ )	–3.05
Interaction Energy ( $\Delta E_{interaction}$ )	–37.04
Solvation Free Energy ( $\Delta G_{solv}$ )	+8.20
Binding Free Energy ( $\Delta G_{bind}$ )	–28.84

The MM/GBSA total binding energy ( $\Delta G_{bind}$ ) is –28.84 kcal/mol showing a strong energetically favourable interaction which is mainly contributed by van der Waals interactions (–33.99 kcal/mol) while the solvation energy basically is opposing the binding slightly (+8.20 kcal/mol). The MM/PBSA method provide a less favourable  $\Delta G_{bind}$  of –1.97 kcal/mol which is showing a weak interaction but with greater influence from polar solvation terms. Overall result shows that luteolin is capable of binding to protein with appreciable affinity.

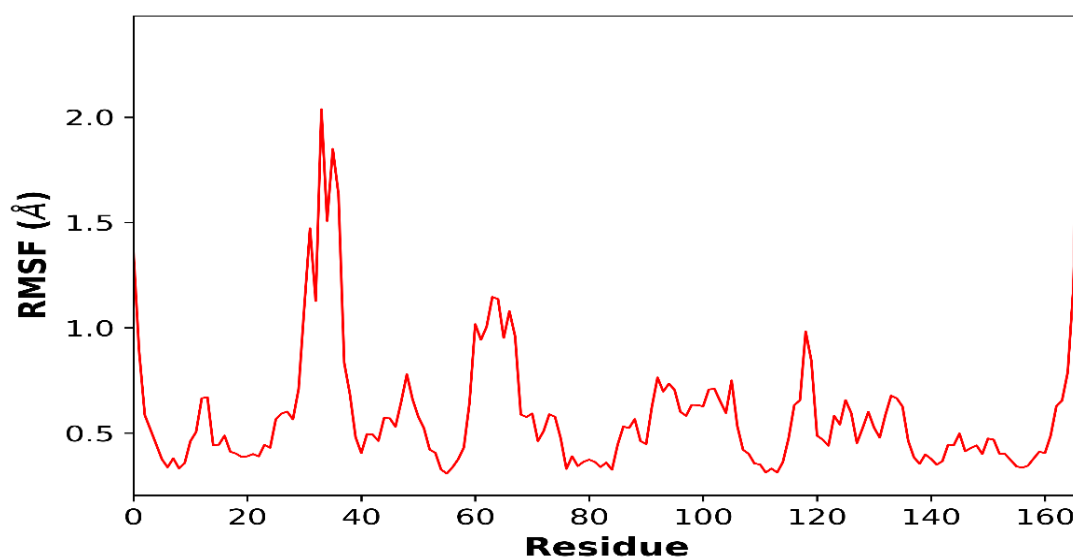
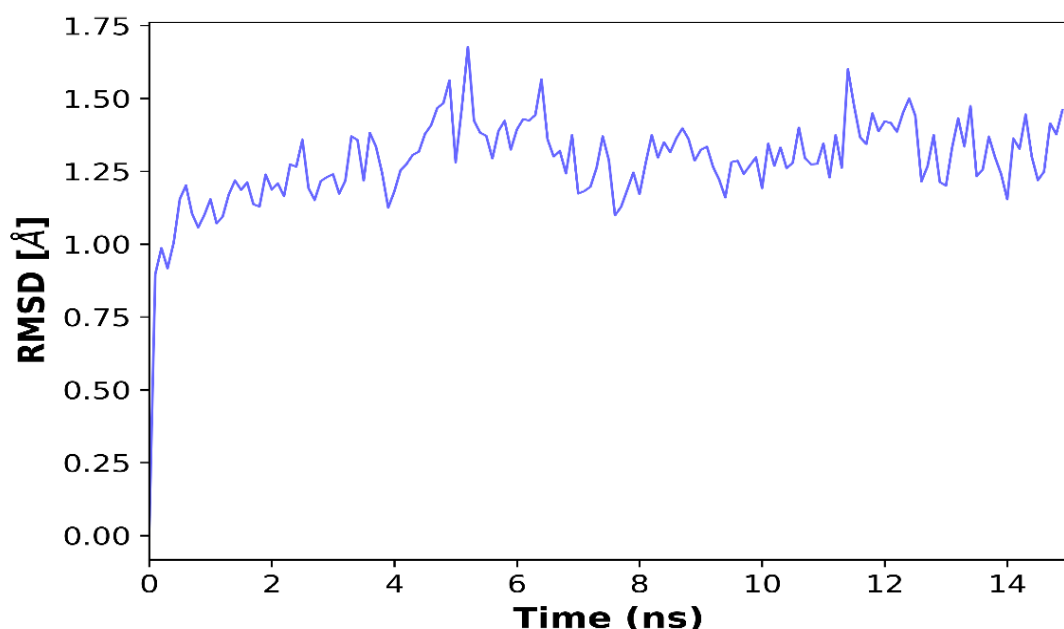
### 3. BRAF with Magnoflorine

The RMSD plot of the BRAF–magnoflorine complex shows an initial increase happening within the first 2 ns, reaching around 1.2 Å however, this initial rise is followed by moderate level of fluctuations in between range of 1.2 and 1.5 Å throughout the 15 ns simulation.

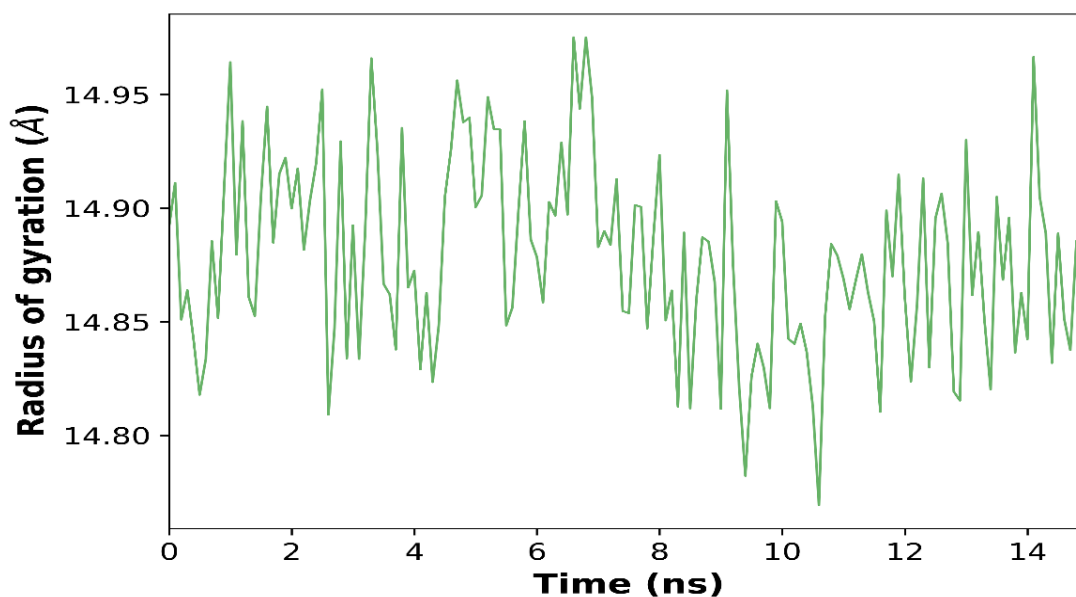
Therefore, the complex is keeping the overall structural stability after equilibration, with no major conformational shifts, suggesting that Magnoflorine shows stable binding to BRAF.

For RMSF plot, most of amino acids in BRAF protein have lower fluctuations that is below 1.0 Å showing a stable and rigid backbone throughout 15ns run. Some peaks were noted around residues 30 to 40 where the fluctuations were to go beyond 2.0 Å. Some minor variations were also observed around residues 60, 100, and 120 but still they stayed within an acceptable range. Overall, the plot suggests that binding of ligand magnoflorine is not inducing a major conformational change in the protein confirming its structural stability.

The radius of gyration for this complex is suggesting that Rg values are staying consistent with mild fluctuation around an average of approximately 14.88 Å for the course of the run of 15 ns. As these variations are very minor it is suggested that protein is keeping a stable and compact conformation when the ligands bind to it with no unfolding or structural expansion found.







**Fig 4.14-** MD simulation analysis of BRAF- Magnoflorine. (a) RMSD plot for BRAF C $\alpha$  atoms, (b) RMSF plot for BRAF C $\alpha$  atoms, (c) Radius of gyration plot for BRAF-Magnoflorine

**Table 4.9-** MMPBSA/ GBSA binding free energy of BRAF-Magnoflorine

MM/PBSA Results	
Energy Component	Average (kcal/mol)
van der Waals ( $\Delta E_{vdw}$ )	-32.38
Electrostatic ( $\Delta E_{ele}$ )	-1.93
Interaction Energy ( $\Delta E_{interaction}$ )	-34.31
Solvation Free Energy ( $\Delta G_{solv}$ )	+34.16
MM/GBSA Results	
Energy Component	Average (kcal/mol)
van der Waals ( $\Delta E_{vdw}$ )	-32.38
Electrostatic ( $\Delta E_{ele}$ )	-1.93
Interaction Energy ( $\Delta E_{interaction}$ )	-34.31
Solvation Free Energy ( $\Delta G_{solv}$ )	+8.26
<b>Binding Free Energy (<math>\Delta G_{bind}</math>)</b>	<b>-26.04</b>

The MM/GBSA analysis shows a strong binding affinity with a  $\Delta G$  of -26.04 kcal/mol which is mostly due to van der Waals and electrostatic interactions. Whereas in case of MM/PBSA a much weaker binding with a  $\Delta G$  of -0.14 kcal/mol is observed, due to higher solvation penalties which shows the result of solvation models on binding energy calculations.

## **CHAPTER 5**

### **CONCLUSION AND FUTURE SCOPE**

OC is a key reason of female relate mortality across the globe. This disease progresses asymptotically making its detection at early stages difficult and often the disease gets detected when it has already progressed to third or 4th stage. Initially thought to develop from ovaries, it is now that other than ovaries it can originate from fallopian tubes and structures surrounding ovaries like peritoneum or endometrium. There are multiple subtypes of OC showing high tumor heterogeneity across them. These subtypes vary in terms of their pathology, prognosis. Majorly classified in to epithelial and non- epithelial OC. Out of these classes, EOC is the most predominant form of OC (90% of total cases). EOC further has many subtypes including serous, endometriosis, mucinous and CCC. However serous EOC is the most prevalent subtype. Serous EOC although has two classification HGSC and low-grade serous carcinoma. While the former is a more common subtype of serous EOC it has been studied very extensively and has well established treatment protocols. This study however, chose to focus on LGSC which is rare compared to others and represents a unique challenge because even though it is less aggressive but significantly more chemo-resistant, and current treatments have limited efficacy. Moreover, LGSC has distinct molecular drivers like KRAS, BRAF, MEK1/2, and others which is different from HGSC having a dominating TP53 profile. LGSC shows a lower level of sensitivity towards chemotherapy-based treatment options including platinum-based options when compared to HGSC. This specific subtype shows resistance in primary, neoadjuvant and adjuvant chemotherapy treatment as well as when the disease reoccurs. A major reason behind that is LGSC cells grow slowly compared to HGSC. And chemotherapy-based drugs mostly target the rapidly dividing cells limiting their effectiveness. LGSCs are associated with chemosensitivity due to defective DNA repair. LGSCs mainly have mutations in their MAPK pathway especially in KRAS, BRAF, and MEK1/2 which supports the cell survival and proliferation through signalling pathways which don not directly trigger apoptosis, making LGSC cells less vulnerable to the apoptotic mechanisms which are targeted by conventional chemotherapy. LGSC shows inherent resistance and they have lower response rates (~4–6%) to standard chemotherapy protocols. By focusing on LGSC, this study aimed to contribute to this gap by identifying phytochemicals that could modulate LGSC-specific pathways and potentially overcome its inherent resistance. The targets chosen in this study were BRAF, KRAS, MEK1 which are central molecular drivers of LGSC promoting the increase in growth of tumor and survival. EGFR according to studies is said to be overexpressed in some cases of LGSC and in upstream activation of MAPK and PI3K/AKT pathways making it an important target for modulation of growth signals in case of chemoresistant tumor. PI3KCA also participates in the PI3K/AKT/mTOR pathway responsible for metabolism and apoptotic resistance and HES1 transcription factor which is involved cell stemness, and resistance has been found to be overexpressed also. Therefore, this study aimed to target both oncogenic drivers and targets involved in drug resistance to LGSC. For this study phytochemicals obtained from *Tinospora cordifolia* has been chosen to target the key target protein and enzymes involved in LGSC. *T. cordifolia* phytochemicals have been reported to be used for their therapeutic action against different cancer like colon cancer, oral cancer etc. Using extensive literature study and data mining a total of 18 phytochemicals were shortlisted

from phytochemicals with potential anti carcinogenic ability. A computational approach was chosen to investigate the cause. Incorporating ADME screening, molecular docking and MD simulation. The 18 phytochemicals shortlisted from lit. Review were first subjected to ADME and drug likeness screening first to rule out all those candidates not viable to be used as drug compounds. All those phytochemicals having a DL score greater than equal to 0.5 and good ADME profile were selected for further computational analysis. These phytochemicals were Berberine, Magnoflorine, Tetrahydroplamatine, Palmatine, Luteolin, Dehydrodiscretamine, Jatrorihizine. These seven phytocompounds were tested against the 6 LGSC specific target using PyrX based virtual screening. AutoDock vina based molecular docking result showed Luteolin and Berberine came out as the most effective multitargeting compounds. They showed strong binding with key cancer-related proteins like EGFR, BRAF, and PI3KCA showing their potential to interfere with multiple cancer pathways. Among all targets, EGFR was consistently being targeted supporting its role in LGSC progression. PI3KCA also showed good interaction with several compounds which means these phytochemicals may help block the PI3K/AKT/mTOR pathway. In contrast, KRAS and MEK1 had weaker interactions with most ligands, showing limited direct inhibition. HES1 also showed only mild interactions, suggesting a minor role in direct targeting. Based on the docking results, ligand–protein pairs with binding energies equal to or greater than -8.5 kcal/mol were selected for further molecular simulations to study their durability and conduct under near-physiological conditions. BRAF against Magnoflorine/ Luteolin, Dehydrodiscretamine, EGFR against berberine/ luteolin and PI3KCA against berberine. known control inhibitors were used to validate the docking protocol. All poses had acceptable RMSD values, confirming that the docking method used was reliable and accurate.

The selected combinations were subjected to MD simulation using two different software Desmond Schrodinger suite and Google colab. On Desmond Schrodinger the pair were subjected to a simulation run of 50 ns however due to computational Constraints on google colab, only an equilibration run of 5ns followed by md production run of 15 ns.

BRAF–Dehydrodiscretamine complex was structurally stable over 50 ns, with minimal backbone deviations. Binding site residues such as GLU-98, THR-94, and PHE-160 maintained stable interactions, indicating a strong and persistent binding interface.

PI3KCA–Berberine the complex showed moderate stability, with protein RMSD plateauing after initial fluctuations. Persistent hydrophobic, hydrogen bonding, and  $\pi$ -stacking interactions with residues TYR-335, ASN-328, and LYS-340 were observed.

EGFR–Luteolin complex demonstrated overall structural stability with moderate backbone fluctuations and stable binding site dynamics. MM/GBSA and MM/PBSA free energy analyses indicated favourable receptor–ligand interactions.

BRAF–Magnoflorine structural stability was maintained throughout the 15 ns simulation, with low residue fluctuations and consistent compactness. MM/GBSA energies reflected strong ligand affinity through van der Waals and electrostatic interactions.

Luteolin, Magnoflorine, and Dehydrodiscretamine are found to be the best-performing phytochemicals from *Tinospora cordifolia* for this study. Luteolin showcased a strong interaction or binding with BRAF and EGFR, while Berberine effectively targeted EGFR. Dehydrodiscretamine also showed stable interaction with BRAF. These compounds showed

good stability in MD simulations, suggesting their potential as multitarget inhibitors for overcoming chemoresistance in LGSC.

This study lays the foundation for exploring *Tinospora cordifolia* phytochemicals as potential therapeutics in low-grade serous ovarian cancer. Future work should include in vitro validation study of top compounds, detailed mechanistic studies on pathways like MAPK pathway and those involved in drug resistance, and exploration of combination therapy with existing drugs. Additionally, formulation strategies like nanoparticles can be developed to increase the bioavailability of promising ligands making the way for translational cancer therapeutics.

## REFERENCES

1. Ahmad, W., Kumar Jaiswal, K., & Amjad, M. (2020). Euphorbia herita leaf extract as a reducing agent in a facile green synthesis of iron oxide nanoparticles and antimicrobial activity evaluation. *Inorganic and Nano-Metal Chemistry*, 51(9), 1147–1154. <https://doi.org/10.1080/24701556.2020.1815062>
2. Ahmed, N., Abubaker, K., & Findlay, J. K. (2014). Ovarian cancer stem cells: Molecular concepts and relevance as therapeutic targets. *Molecular Aspects of Medicine*, 39, 110–125. <https://doi.org/10.1016/J.MAM.2013.06.002>
3. Ahmed, S., Marotte, H., Kwan, K., Ruth, J. H., Campbell, P. L., Rabquer, B. J., Pakozdi, A., & Koch, A. E. (2008). Epigallocatechin-3-gallate inhibits IL-6 synthesis and suppresses transsignaling by enhancing soluble gp130 production. *Proceedings of the National Academy of Sciences of the United States of America*, 105(38), 14692–14697. [https://doi.org/10.1073/PNAS.0802675105/SUPPL\\_FILE/0802675105SI.PDF](https://doi.org/10.1073/PNAS.0802675105/SUPPL_FILE/0802675105SI.PDF)
4. Alajmi, M. F., Mothana, R. A., Al-Rehaily, A. J., & Khaled, J. M. (2018). Antimycobacterial Activity and Safety Profile Assessment of *Alpinia galanga* and *Tinospora cordifolia*. *Evidence-Based Complementary and Alternative Medicine : ECAM*, 2018, 2934583. <https://doi.org/10.1155/2018/2934583>
5. Alatise, K. L., Gardner, S., & Alexander-Bryant, A. (2022). Mechanisms of Drug Resistance in Ovarian Cancer and Associated Gene Targets. In *Cancers* (Vol. 14, Issue 24). MDPI. <https://doi.org/10.3390/cancers14246246>
6. Arjaans, M., Munnink, T. H. O., Oosting, S. F., Van Scheltinga, A. G. T. T., Gietema, J. A., Garbacik, E. T., Timmer-Bosscha, H., Lub-De Hooge, M. N., Schröder, C. P., & De Vries, E. G. E. (2013). Bevacizumab-induced normalization of blood vessels in tumors hampers antibody uptake. *Cancer Research*, 73(11), 3347–3355. <https://doi.org/10.1158/0008-5472.CAN-12-3518>,
7. Arnold, C. N., Goel, A., & Boland, C. R. (2003). Role of hMLH1 promoter hypermethylation in drug resistance to 5-fluorouracil in colorectal cancer cell lines. *International Journal of Cancer*, 106(1), 66–73. <https://doi.org/10.1002/ijc.11176>
8. Arora, T., Mullangi, S., Vadakekut, E. S., & Lekkala, M. R. (2024). *Epithelial Ovarian Cancer*. <https://www.ncbi.nlm.nih.gov/books/NBK567760/>
9. Arpita R. Pawar, A. T. C. J. R. K. P. S. N. B. C. (2024). *Tinospora Cordifolia – As An Anticancer Agent: Recent And Advance Study*. *International Journal of Pharmaceutical Sciences*, 2(1). <https://doi.org/10.5281/ZENODO.10578070>
10. Bardram, L., Funch-Jensen, P., Jensen, P., Kehlet, H., & Crawford, M. E. (1995). Recovery after laparoscopic colonic surgery with epidural analgesia, and early oral nutrition and mobilisation. *The Lancet*, 345(8952), 763–764. [https://doi.org/10.1016/S0140-6736\(95\)90643-6](https://doi.org/10.1016/S0140-6736(95)90643-6),
11. Bast, R. C., Hennessy, B., & Mills, G. B. (2009). The biology of ovarian cancer: new opportunities for translation. *Nature Reviews Cancer* 2009 9:6, 9(6), 415–428. <https://doi.org/10.1038/nrc2644>
12. Bergamini, A., Candiani, M., Taccagni, G., Rabaiotti, E., Viganò, R., Marzi, P. De, Ferrari, D., & Mangili, G. (2016). Different Patterns of Disease Spread between Advanced-Stage Type I and II Epithelial Ovarian Cancer. *Gynecologic and Obstetric Investigation*, 81(1), 10–14. <https://doi.org/10.1159/000381261>
13. Budiana, I. N. G., Angelina, M., & Pemayun, T. G. A. (2019). Ovarian cancer: Pathogenesis and current recommendations for prophylactic surgery. *Journal of the Turkish German Gynecological Association*, 20(1), 47. <https://doi.org/10.4274/JTGGA.GALENOS.2018.2018.0119>

14. Campos-Vega, R., & Dave Oomah, B. (2013). Chemistry and Classification of Phytochemicals. *Handbook of Plant Food Phytochemicals: Sources, Stability and Extraction*, 5–48.  
<https://doi.org/10.1002/9781118464717.CH2;PAGEGROUP:STRING:PUBLICATION>
15. Chailyan, A., Marcatili, P., & Tramontano, A. (2011). The association of heavy and light chain variable domains in antibodies: implications for antigen specificity. *The Febs Journal*, 278(16), 2858. <https://doi.org/10.1111/J.1742-4658.2011.08207.X>
16. Chaudhary, A., Das, R., Mehta, K., & Mehta, D. K. (2024). Indian herb *Tinospora cordifolia* and *Tinospora* species: Phytochemical and therapeutic application. *Heliyon*, 10(10), e31229. <https://doi.org/10.1016/J.HELİYON.2024.E31229>
17. Choma, I. M., & Nikolaichuk, H. (2022). TLC bioprofiling—A tool for quality evaluation of medicinal plants. *Evidence-Based Validation of Herbal Medicine: Translational Research on Botanicals*, 407–422. <https://doi.org/10.1016/B978-0-323-85542-6.00014-7>
18. Colombo, N., Sessa, C., Du Bois, A., Ledermann, J., McCluggage, W. G., McNeish, I., Morice, P., Pignata, S., Ray-Coquard, I., Vergote, I., Baert, T., Belaroussi, I., Dashora, A., Olbrecht, S., Planchamp, F., & Querleu, D. (2019). ESMO–ESGO consensus conference recommendations on ovarian cancer: pathology and molecular biology, early and advanced stages, borderline tumours and recurrent disease. *Annals of Oncology*, 30(5), 672–705. <https://doi.org/10.1093/ANNONC/MDZ062>
19. Colombo, P. E., Fabbro, M., Theillet, C., Bibeau, F., Rouanet, P., & Ray-Coquard, I. (2014). Sensitivity and resistance to treatment in the primary management of epithelial ovarian cancer. *Critical Reviews in Oncology/Hematology*, 89(2), 207–216.  
<https://doi.org/10.1016/j.critrevonc.2013.08.017>
20. Cook, S. A., & Tinker, A. V. (2019). PARP Inhibitors and the Evolving Landscape of Ovarian Cancer Management: A Review. *Bio Drugs : Clinical Immunotherapeutics, Biopharmaceuticals and Gene Therapy*, 33(3), 255–273.  
<https://doi.org/10.1007/S40259-019-00347-4>
21. Cornelison, R., Llaneza, D. C., & Landen, C. N. (2017). Emerging Therapeutics to Overcome Chemoresistance in Epithelial Ovarian Cancer: A Mini-Review. *International Journal of Molecular Sciences*, 18(10). <https://doi.org/10.3390/IJMS18102171>
22. Dabur, R., & Mittal, A. (2016). Detection and qualitative analysis of fatty acid amides in the urine of alcoholics using HPLC-QTOF-MS. *Alcohol*, 52, 71–78.  
<https://doi.org/10.1016/J.ALCOHOL.2016.03.004>
23. Deeb, K. K., Trump, D. L., & Johnson, C. S. (2007). Vitamin D signalling pathways in cancer: Potential for anticancer therapeutics. *Nature Reviews Cancer*, 7(9), 684–700.  
<https://doi.org/10.1038/NRC2196>,
24. Deepa, B., Babaji, H. V., Hosmani, J. V., Alamir, A. W. H., Mushtaq, S., Raj, A. T., & Patil, S. (2019). Effect of *Tinospora cordifolia*-Derived Phytocomponents on Cancer: A Systematic Review. *Applied Sciences* 2019, Vol. 9, Page 5147, 9(23), 5147.  
<https://doi.org/10.3390/APP9235147>
25. Du, P., Wang, Y., Chen, L., Gan, Y., & Wu, Q. (2016). High ERCC1 expression is associated with platinum-resistance, but not survival in patients with epithelial ovarian cancer. *Oncology Letters*, 12(2), 857–862. <https://doi.org/10.3892/OL.2016.4732>,
26. *Efficacy of Tinospora cordifolia (Willd.) extracts on blood lipid profile in streptozotocin diabetic rats. Is it beneficial to the heart? | Request PDF.* (n.d.). Retrieved May 27, 2025, from  
[https://www.researchgate.net/publication/271218114\\_Efficacy\\_of\\_Tinospora\\_cordifolia\\_Willd\\_extracts\\_on\\_blood\\_lipid\\_profile\\_in\\_streptozotocin\\_diabetic\\_rats\\_Is\\_it\\_beneficial\\_to\\_the\\_heart](https://www.researchgate.net/publication/271218114_Efficacy_of_Tinospora_cordifolia_Willd_extracts_on_blood_lipid_profile_in_streptozotocin_diabetic_rats_Is_it_beneficial_to_the_heart)

27. *Epithelial carcinoma of the ovary, fallopian tube, and peritoneum: Histopathology - UpToDate*. (n.d.). Retrieved May 10, 2025, from [https://www.uptodate.com/contents/epithelial-carcinoma-of-the-ovary-fallopian-tube-and-peritoneum-histopathology?search=Epithelial%20carcinoma%20of%20the%20ovary,%20fallopian%20tube,%20and%20peritoneum:%20histopathology&source=search\\_result&selectedTitle=1%7E150&usage\\_type=default&display\\_rank=1](https://www.uptodate.com/contents/epithelial-carcinoma-of-the-ovary-fallopian-tube-and-peritoneum-histopathology?search=Epithelial%20carcinoma%20of%20the%20ovary,%20fallopian%20tube,%20and%20peritoneum:%20histopathology&source=search_result&selectedTitle=1%7E150&usage_type=default&display_rank=1)
28. Erber, R., Eichelsbacher, U., Powajbo, V., Korn, T., Djonov, V., Lin, J., Hammes, H. P., Grobholz, R., Ullrich, A., & Vajkoczy, P. (2006). EphB4 controls blood vascular morphogenesis during postnatal angiogenesis. *EMBO Journal*, 25(3), 628–641. <https://doi.org/10.1038/SJ.EMBOJ.7600949>,
29. Erickson, B. K., Conner, M. G., & Landen, C. N. (2013). The role of the fallopian tube in the origin of ovarian cancer. *American Journal of Obstetrics and Gynecology*, 209(5), 409–414. <https://doi.org/10.1016/J.AJOG.2013.04.019>,
30. Eze, M. N., Odoh, H. E., & Apeh, M. C. (2023). ASSESSMENT OF PHYTOCHEMICALS AND ANTIOXIDANT POTENTIAL OF THE STEM BARK OF ALBIZIA CHEVALIERI. *The Bioscientist Journal*, 11(1), 43–56. [https://bioscientistjournal.com/index.php/The\\_Bioscientist/article/view/137](https://bioscientistjournal.com/index.php/The_Bioscientist/article/view/137)
31. Feng, Q., Li, X., Sun, W., Sun, M., Li, Z., Sheng, H., Xie, F., Zhang, S., & Shan, C. (2020). Targeting G6PD reverses paclitaxel resistance in ovarian cancer by suppressing GSTP1. *Biochemical Pharmacology*, 178. <https://doi.org/10.1016/j.bcp.2020.114092>
32. Ferlini, C., Cicchillitti, L., Raspaglio, G., Bartollino, S., Cimitan, S., Bertucci, C., Mozzetti, S., Gallo, D., Persico, M., Fattorusso, C., Campiani, G., & Scambia, G. (2009). Paclitaxel directly binds to Bcl-2 and functionally mimics activity of Nur77. *Cancer Research*, 69(17), 6906–6914. <https://doi.org/10.1158/0008-5472.CAN-09-0540>,
33. Flaum, N., Crosbie, E. J., Edmondson, R. J., Smith, M. J., & Evans, D. G. (2020). Epithelial ovarian cancer risk: A review of the current genetic landscape. *Clinical Genetics*, 97(1), 54–63. <https://doi.org/10.1111/CGE.13566>,
34. Franco, M., Roswall, P., Cortez, E., Hanahan, D., & Pietras, K. (2011). Pericytes promote endothelial cell survival through induction of autocrine VEGF-A signaling and Bcl-w expression. *Blood*, 118(10), 2906–2917. <https://doi.org/10.1182/BLOOD-2011-01-331694>,
35. Friedrich, M., Friedrich, D., Kraft, C., & Rogmans, C. (2021). Multimodal treatment of primary advanced ovarian cancer. *Anticancer Research*, 41(7), 3253–3260. <https://doi.org/10.21873/ANTICANRES.15111>,
36. Gaona-Luviano, P., Adriana, L., Medina-Gaona, & Magaña-Pérez, K. (2020). Epidemiology of ovarian cancer. In *Chinese Clinical Oncology* (Vol. 9, Issue 4). AME Publishing Company. <https://doi.org/10.21037/cco-20-34>
37. Gatti, L., & Zunino, F. (2005). Overview of Tumor Cell Chemoresistance Mechanisms. *Methods in Molecular Medicine*, 111, 127–148. <https://doi.org/10.1385/1-59259-889-7:127>
38. Gulcubuk, A., Altunatmaz, K., Sonmez, K., Haktanir-Yatkin, D., Uzun, H., Gurel, A., & Aydin, S. (2006a). Effects of curcumin on tumour necrosis factor- $\alpha$  and interleukin-6 in the late phase of experimental acute pancreatitis. *Journal of Veterinary Medicine Series A: Physiology Pathology Clinical Medicine*, 53(1), 49–54. <https://doi.org/10.1111/J.1439-0442.2006.00786.X>;WGROU:STRING:PUBLICATION
39. Gulcubuk, A., Altunatmaz, K., Sonmez, K., Haktanir-Yatkin, D., Uzun, H., Gurel, A., & Aydin, S. (2006b). Effects of curcumin on tumour necrosis factor- $\alpha$  and interleukin-6 in the late phase of experimental acute pancreatitis. *Journal of Veterinary Medicine Series A: Physiology Pathology Clinical Medicine*, 53(1), 49–54.

- <https://doi.org/10.1111/J.1439-0442.2006.00786.X>;WGROU:STRING:PUBLICATION
40. Guo, H., & Rubinstein, J. L. (2018a). Cryo-EM of ATP synthases. *Current Opinion in Structural Biology*, 52, 71–79. <https://doi.org/10.1016/J.SBI.2018.08.005>
  41. Guo, H., & Rubinstein, J. L. (2018b). Cryo-EM of ATP synthases. *Current Opinion in Structural Biology*, 52, 71–79. <https://doi.org/10.1016/J.SBI.2018.08.005>
  42. Gupta, C., & Prakash, D. (2014). Phytonutrients as therapeutic agents. *Journal of Complementary and Integrative Medicine*, 11(3), 151–169. <https://doi.org/10.1515/JCIM-2013-0021/MACHINEREADABLECITATION/RIS>
  43. Hadjzadeh, M. -al-R., Tavakol Afshari, J., & Ghorbani, A. (2005). P.144 The effects of aqueous extract of garlic (allium sativum L.) On laryngeal cancer cells (hep-2) and 1929 cells in vitro. *Oral Oncology Supplement*, 1(1), 190. [https://doi.org/10.1016/S1744-7895\(05\)80507-3](https://doi.org/10.1016/S1744-7895(05)80507-3)
  44. Holohan, C., Van Schaeybroeck, S., Longley, D. B., & Johnston, P. G. (2013). Cancer drug resistance: an evolving paradigm. *Nature Reviews. Cancer*, 13(10), 714–726. <https://doi.org/10.1038/NRC3599>
  45. Huang, Y., Sheikh, M. S., Fornace, A. J., & Holbrook, N. J. (1999). Serine protease inhibitor TPCK prevents Taxol-induced cell death and blocks c-Raf-1 and Bcl-2 phosphorylation in human breast carcinoma cells. *Oncogene*, 18(23), 3431–3439. <https://doi.org/10.1038/sj.onc.1202685>
  46. Jayson, G. C., Kohn, E. C., Kitchener, H. C., & Ledermann, J. A. (2014a). Ovarian cancer. *The Lancet*, 384(9951), 1376–1388. [https://doi.org/10.1016/S0140-6736\(13\)62146-7](https://doi.org/10.1016/S0140-6736(13)62146-7)
  47. Jayson, G. C., Kohn, E. C., Kitchener, H. C., & Ledermann, J. A. (2014b). Ovarian cancer. *The Lancet*, 384(9951), 1376–1388. [https://doi.org/10.1016/S0140-6736\(13\)62146-7](https://doi.org/10.1016/S0140-6736(13)62146-7)
  48. Jones, S., Wang, T. L., Kurman, R. J., Nakayama, K., Velculescu, V. E., Vogelstein, B., Kinzler, K. W., Papadopoulos, N., & Shih, I. M. (2012). Low-grade serous carcinomas of the ovary contain very few point mutations. *Journal of Pathology*, 226(3), 413–420. <https://doi.org/10.1002/PATH.3967>,
  49. Kastan, M. B., & Bartek, J. (2004). Cell-cycle checkpoints and cancer. *Nature*, 432(7015), 316–323. <https://doi.org/10.1038/NATURE03097>,
  50. Kattupalli, S., Vesta, V., Vangara, S., & Spandana, U. (2019). *THE MULTI-ACTIVITY HERBACEOUS VINE-TINOSPORA CORDIFOLIA*. 12. <https://doi.org/10.22159/ajpcr.2019.v12i3.29949>
  51. Kimyon Comert, G., Turkmen, O., Karalok, A., Basaran, D., Kilic, C., Koc, S., Kayikcioglu, F., & Boran, N. (2018). Management of catheter-related complications during intraperitoneal chemotherapy for ovarian cancer: Two case reports and review of the literature. *Marmara Medical Journal*, 31(2), 88–93. <https://doi.org/10.5472/MARUMJ.430817>
  52. KLANGJAREONCHAI, T., PUTADECHAKUM, S., & ROONGPISUTHIPONG, C. (2015). Review of Anti-Hyperglycemic Effect of Tinospora crispa. *Walailak Journal of Science and Technology (WJST)*, 12(5), 403–406. <https://wjst.wu.ac.th/index.php/wjst/article/view/551>
  53. Koche, D., Shirsat, R., J, M. K.-H., & 2016, undefined. (n.d.). An overview of major classes of phytochemicals: their types and role in disease prevention. *Researchgate.NetD Koche, R Shirsat, M KawaleHislopi J, 2016•researchgate.Net*. Retrieved May 12, 2025, from [https://www.researchgate.net/profile/Dipak-Koche/publication/327304552\\_AN\\_OVERVIEW\\_OF\\_MAJOR\\_CLASSES\\_OF\\_PHYTOCHEMICALS\\_THEIR\\_TYPES\\_AND\\_ROLE\\_IN\\_DISEASE\\_PREVENTION/link](https://www.researchgate.net/profile/Dipak-Koche/publication/327304552_AN_OVERVIEW_OF_MAJOR_CLASSES_OF_PHYTOCHEMICALS_THEIR_TYPES_AND_ROLE_IN_DISEASE_PREVENTION/link)



- s/5b8766b392851c1e123b329d/AN-OVERVIEW-OF-MAJOR-CLASSES-OF-PHYTOCHEMICALS-THEIR-TYPES-AND-ROLE-IN-DISEASE-PREVENTION.pdf
54. Koshiyama, M., Matsumura, N., & Konishi, I. (2014). Recent concepts of ovarian carcinogenesis: Type i and type II. *BioMed Research International*, 2014. <https://doi.org/10.1155/2014/934261>,
  55. Kossaï, M., Leary, A., Scoazec, J. Y., & Genestie, C. (2018). Ovarian Cancer: A Heterogeneous Disease. *Pathobiology*, 85(1–2), 41–49. <https://doi.org/10.1159/000479006>
  56. Kumar, S., Prahalathan, P., & Raja, B. (2011). Antihypertensive and antioxidant potential of vanillic acid, a phenolic compound in L-NAME-induced hypertensive rats: A dose-dependence study. *Redox Report*, 16(5), 208–215. <https://doi.org/10.1179/1351000211Y.0000000009;PAGE:STRING:ARTICLE/CHAPTER>
  57. Kurman, R. J., & Shih, I. M. (2010). The origin and pathogenesis of epithelial ovarian cancer: A proposed unifying theory. *American Journal of Surgical Pathology*, 34(3), 433–443. <https://doi.org/10.1097/PAS.0B013E3181CF3D79>,
  58. Kuroki, L., & Guntupalli, S. R. (2020). Treatment of epithelial ovarian cancer. *The BMJ*, 371. <https://doi.org/10.1136/BMJ.M3773>,
  59. Lalwani, N., Prasad, S. R., Vikram, R., Shanbhogue, A. K., Huettnner, P. C., & Fasih, N. (2011). Histologic, Molecular, and Cytogenetic Features of Ovarian Cancers: Implications for Diagnosis and Treatment. <https://doi.org/10.1148/Rg.313105066>, 31(3), 625–646. <https://doi.org/10.1148/RG.313105066>
  60. Lee, D. H., Rhee, J. G., & Lee, Y. J. (2009). Reactive oxygen species up-regulate p53 and puma; A possible mechanism for apoptosis during combined treatment with trail and wogonin. *British Journal of Pharmacology*, 157(7), 1189–1202. <https://doi.org/10.1111/J.1476-5381.2009.00245.X;WEBSITE:WEBSITE:BPSPUBS;WGROU:STRING:PUBLICATION>
  61. Lin, D. I., Killian, J. K., Venstrom, J. M., Ramkissoon, S. H., Ross, J. S., & Elvin, J. A. (2021). Recurrent urothelial carcinoma-like FGFR3 genomic alterations in malignant Brenner tumors of the ovary. *Modern Pathology: An Official Journal of the United States and Canadian Academy of Pathology, Inc*, 34(5), 983–993. <https://doi.org/10.1038/S41379-020-00699-1>
  62. MacQueen, A. J. (2015). Catching a (Double-Strand) Break: The Rad51 and Dmc1 Strand Exchange Proteins Can Co-occupy Both Ends of a Meiotic DNA Double-Strand Break. *PLoS Genetics*, 11(12). <https://doi.org/10.1371/JOURNAL.PGEN.1005741>,
  63. Maloney, S. M., Hoover, C. A., Morejon-Lasso, L. V., & Prosperi, J. R. (2020). Mechanisms of taxane resistance. *Cancers*, 12(11), 1–57. <https://doi.org/10.3390/CANCERS12113323>,
  64. Mangala, L. S., Zuzel, V., Schmandt, R., Leshane, E. S., Halder, J. B., Armaiz-Pena, G. N., Spannuth, W. A., Tanaka, T., Shahzad, M. M. K., Lin, Y. G., Nick, A. M., Danes, C. G., Lee, J. W., Jennings, N. B., Vivas-Mejia, P. E., Wolf, J. K., Coleman, R. L., Siddik, Z. H., Lopez-Berestein, G., ... Sood, A. K. (2009). Therapeutic targeting of ATP7B in ovarian carcinoma. *Clinical Cancer Research*, 15(11), 3770–3780. <https://doi.org/10.1158/1078-0432.CCR-08-2306>,
  65. McCluggage, W. G. (2008). My approach to and thoughts on the typing of ovarian carcinomas. *Journal of Clinical Pathology*, 61(2), 152–163. <https://doi.org/10.1136/JCP.2007.049478>,
  66. *Micropropagation of Tinospora cordifolia (Willd.) Miers ex Hook. F & Thoms — a multipurpose medicinal plant on JSTOR*. (n.d.). Retrieved May 10, 2025, from <https://www.jstor.org/stable/24096816>

67. Mirza, M. R., Monk, B. J., Herrstedt, J., Oza, A. M., Mahner, S., Redondo, A., Fabbro, M., Ledermann, J. A., Lorusso, D., Vergote, I., Ben-Baruch, N. E., Marth, C., Mądry, R., Christensen, R. D., Berek, J. S., Dørum, A., Tinker, A. V., du Bois, A., González-Martín, A., ... Matulonis, U. A. (2016). Niraparib Maintenance Therapy in Platinum-Sensitive, Recurrent Ovarian Cancer. *New England Journal of Medicine*, 375(22), 2154–2164. <https://doi.org/10.1056/NEJMOA1611310>,
68. Mishra, R., & Kaur, G. (2013). Aqueous Ethanolic Extract of *Tinospora cordifolia* as a Potential Candidate for Differentiation Based Therapy of Glioblastomas. *PLOS ONE*, 8(10), e78764. <https://doi.org/10.1371/JOURNAL.PONE.0078764>
69. Momenimovahed, Z., Tiznobaik, A., Taheri, S., & Salehiniya, H. (2019). Ovarian cancer in the world: Epidemiology and risk factors. *International Journal of Women's Health*, 11, 287–299. <https://doi.org/10.2147/IJWH.S197604>,
70. Motohara, T., & Katabuchi, H. (2019). Ovarian Cancer Stemness: Biological and Clinical Implications for Metastasis and Chemotherapy Resistance. *Cancers 2019*, Vol. 11, Page 907, 11(7), 907. <https://doi.org/10.3390/CANCERS11070907>
71. Muggia, F. (2021). Weekly Carboplatin and Paclitaxel for Ovarian Cancer: The “Finer Points.” *The Oncologist*, 26(1), 1–3. <https://doi.org/10.1002/ONCO.13572>
72. Nair, J., Huang, T. T., Murai, J., Haynes, B., Steeg, P. S., Pommier, Y., & Lee, J. M. (2020). Resistance to the CHK1 inhibitor prexasertib involves functionally distinct CHK1 activities in BRCA wild-type ovarian cancer. *Oncogene*, 39(33), 5520–5535. <https://doi.org/10.1038/S41388-020-1383-4>,
73. Nikolaou, M., Pavlopoulou, A., Georgakilas, A. G., & Kyrodimos, E. (2018). The challenge of drug resistance in cancer treatment: a current overview. *Clinical & Experimental Metastasis 2018 35:4*, 35(4), 309–318. <https://doi.org/10.1007/S10585-018-9903-0>
74. Ortiz, M., Wabel, E., Mitchell, K., & Horibata, S. (2022). Mechanisms of chemotherapy resistance in ovarian cancer. *Cancer Drug Resistance*, 5(2), 304. <https://doi.org/10.20517/CDR.2021.147>
75. *Ovarian Cancer — Cancer Stat Facts*. (n.d.). Retrieved May 10, 2025, from <https://seer.cancer.gov/statfacts/html/ovary.html>
76. Park, S. Y., Jeong, K. J., Lee, J., Yoon, D. S., Choi, W. S., Kim, Y. K., Han, J. W., Kim, Y. M., Kim, B. K., & Lee, H. Y. (2007). Hypoxia enhances LPA-induced HIF-1 $\alpha$  and VEGF expression: Their inhibition by resveratrol. *Cancer Letters*, 258(1), 63–69. <https://doi.org/10.1016/J.CANLET.2007.08.011>
77. Parkes, E. E., & Kennedy, R. D. (2016). Clinical Application of Poly (ADP-Ribose) Polymerase Inhibitors in High-Grade Serous Ovarian Cancer. *The Oncologist*, 21(5), 586–593. <https://doi.org/10.1634/theoncologist.2015-0438>
78. Patel, R. P., Kuhn, S., Yin, D., Hotz, J., Maher, F. A., Robey, R. W., Gottesman, M. M., & Horibata, S. (2021). Cross-resistance of cisplatin selected cells to anti-microtubule agents: Role of general survival mechanisms. *Translational Oncology*, 14(1). <https://doi.org/10.1016/j.tranon.2020.100917>
79. Patil, S., Ashi, H., Hosmani, J., Almalki, A. Y., Alhazmi, Y. A., Mushtaq, S., Parveen, S., Baeshen, H. A., Varadarajan, S., Raj, A. T., Patil, V. R., & Vyas, N. (2021). *Tinospora cordifolia* (Thunb.) Miers (Giloy) inhibits oral cancer cells in a dose-dependent manner by inducing apoptosis and attenuating epithelial-mesenchymal transition. *Saudi Journal of Biological Sciences*, 28(8), 4553. <https://doi.org/10.1016/J.SJBS.2021.04.056>
80. Pawase, P. A., Goswami, C., Shams, R., Pandey, V. K., Tripathi, A., Rustagi, S., & G, D. (2024). A conceptual review on classification, extraction, bioactive potential and role of phytochemicals in human health. *Future Foods*, 9. <https://doi.org/10.1016/j.fufo.2024.100313>

81. Persson, U., Willis, M., Ödegaard, K., & Apelqvist, J. (2000). The cost-effectiveness of treating diabetic lower extremity ulcers with becaplermin (regranex): A core model with an application using swedish cost data. *Value in Health*, 3(SUPPL. 1), 39–46. <https://doi.org/10.1046/j.1524-4733.2000.36027.x>
82. Pinto, M. P., Sotomayor, P., Carrasco-Avino, G., Corvalan, A. H., & Owen, G. I. (2016). Escaping antiangiogenic therapy: Strategies employed by cancer cells. *International Journal of Molecular Sciences*, 17(9). <https://doi.org/10.3390/IJMS17091489>,
83. Rais, J., Jafri, A., Siddiqui, S., Tripathi, M., & Arshad, M. (2017a). Phytochemicals in the treatment of ovarian cancer. *Frontiers in Bioscience - Elite*, 9(1), 67–75. <https://doi.org/10.2741/E786>,
84. Rais, J., Jafri, A., Siddiqui, S., Tripathi, M., & Arshad, M. (2017b). Phytochemicals in the treatment of ovarian cancer. *Frontiers in Bioscience - Elite*, 9(1), 67–75. <https://doi.org/10.2741/E786>,
85. Ranjith, M. S., Ranjitsingh, A. J. A., Shankar, S. G., Vijayalaksmi, G. S., Deepa, K., & Sidhu, H. S. (2008). Enhanced Phagocytosis and Antibody Production by *Tinospora cordifolia* - A new dimension in Immunomodulation. *African Journal of Biotechnology*, 7(2), 81–085. <https://www.ajol.info/index.php/ajb/article/view/58327>
86. Rao, P. R., Kumar, V. K., Viswanath, R. K., & Subbaraju, G. V. (2005). Cardioprotective Activity of Alcoholic Extract of *Tinospora cordifolia* in Ischemia-Reperfusion Induced Myocardial Infarction in Rats. *Biological and Pharmaceutical Bulletin*, 28(12), 2319–2322. <https://doi.org/10.1248/BPB.28.2319>
87. Rodríguez, I. M., & Prat, J. (2002). Mucinous tumors of the ovary: A clinicopathologic analysis of 75 borderline tumors (of intestinal type) and carcinomas. *American Journal of Surgical Pathology*, 26(2), 139–152. <https://doi.org/10.1097/00000478-200202000-00001>,
88. Rushworth, S. A., & Micheau, O. (2009). Molecular crosstalk between trail and natural antioxidants in the treatment of cancer. *British Journal of Pharmacology*, 157(7), 1186–1188. <https://doi.org/10.1111/J.1476-5381.2009.00266.X>;WEBSITE:WEBSITE:BPSPUBS;WGROU:STRING:PUBLICATION
89. Saha, S., & Ghosh, S. (2012). *Tinospora cordifolia*: One plant, many roles. *Ancient Science of Life*, 31(4), 151. <https://doi.org/10.4103/0257-7941.107344>
90. Sambasivan, S. (2022). Epithelial ovarian cancer: Review article. In *Cancer Treatment and Research Communications* (Vol. 33). Elsevier Ltd. <https://doi.org/10.1016/j.ctarc.2022.100629>
91. Santiago-O’Farrill, J. M., Weroha, S. J., Hou, X., Oberg, A. L., Heinzen, E. P., Maurer, M. J., Pang, L., Rask, P., Amaravadi, R. K., Becker, S. E., Romero, I., Rubio, M. J., Matias-Guiu, X., Santacana, M., Llombart-Cussac, A., Poveda, A., Lu, Z., & Bast, R. C. (2020). Poly (adenosine diphosphate ribose) polymerase inhibitors induce autophagy-mediated drug resistance in ovarian cancer cells, xenografts, and patient-derived xenograft models. *Cancer*, 126(4), 894–907. <https://doi.org/10.1002/CNCR.32600>,
92. Seo, J. H., Jeong, K. J., Oh, W. J., Sul, H. J., Sohn, J. S., Kim, Y. K., Cho, D. Y., Kang, J. K., Park, C. G., & Lee, H. Y. (2010). Lysophosphatidic acid induces STAT3 phosphorylation and ovarian cancer cell motility: Their inhibition by curcumin. *Cancer Letters*, 288(1), 50–56. <https://doi.org/10.1016/J.CANLET.2009.06.023>
93. *Sex cord-stromal tumors of the ovary: Epidemiology, clinical features, and diagnosis in adults - UpToDate*. (n.d.). Retrieved May 10, 2025, from <https://www.uptodate.com/contents/sex-cord-stromal-tumors-of-the-ovary-epidemiology-clinical-features-and-diagnosis-in-adults>
94. Shaik, B., Zafar, T., Balasubramanian, K., & Gupta, S. P. (2020). An Overview of Ovarian Cancer: Molecular Processes Involved and Development of Target-based

- 96

110. Vaghasia, H., Patel, R., Prajapati, J., Shah, K., Saraf, M., & Rawal, R. M. (2025). Cytotoxic and immunomodulatory properties of *Tinospora cordifolia*, *Boerhaavia diffusa*, *Berberis aristata*, and *Ocimum basilicum* extracts against HPV-positive cervical cancer cell line. *BMC Complementary Medicine and Therapies*, 25(1), 1–18. <https://doi.org/10.1186/S12906-025-04817-X/FIGURES/10>
111. Vahedi, S., Chufan, E. E., & Ambudkar, S. V. (2017). Global alteration of the drug-binding pocket of human P-glycoprotein (ABCB1) by substitution of fifteen conserved residues reveals a negative correlation between substrate size and transport efficiency. *Biochemical Pharmacology*, 143, 53–64. <https://doi.org/10.1016/J.BCP.2017.07.014>,
112. Vaidyanathan, A., Sawers, L., Gannon, A. L., Chakravarty, P., Scott, A. L., Bray, S. E., Ferguson, M. J., & Smith, G. (2016). ABCB1 (MDR1) induction defines a common resistance mechanism in paclitaxel- and olaparib-resistant ovarian cancer cells. *British Journal of Cancer*, 115(4), 431–441. <https://doi.org/10.1038/BJC.2016.203>,
113. Van Der Burg, M. E. L., Onstenk, W., Boere, I. A., Look, M., Ottevanger, P. B., De Gooyer, D., Kerkhofs, L. G. M., Valster, F. A. A., Ruit, J. B., Van Reisen, A. G. P. M., Goey, S. H., Van Der Torren, A. M. E., Ten Bokkel Huinink, D., Kok, T. C., Verweij, J., & Van Doorn, H. C. (2014a). Long-term results of a randomised phase III trial of weekly versus three-weekly paclitaxel/platinum induction therapy followed by standard or extended three-weekly paclitaxel/platinum in European patients with advanced epithelial ovarian cancer. *European Journal of Cancer*, 50(15), 2592–2601. <https://doi.org/10.1016/j.ejca.2014.07.015>
114. Van Der Burg, M. E. L., Onstenk, W., Boere, I. A., Look, M., Ottevanger, P. B., De Gooyer, D., Kerkhofs, L. G. M., Valster, F. A. A., Ruit, J. B., Van Reisen, A. G. P. M., Goey, S. H., Van Der Torren, A. M. E., Ten Bokkel Huinink, D., Kok, T. C., Verweij, J., & Van Doorn, H. C. (2014b). Long-term results of a randomised phase III trial of weekly versus three-weekly paclitaxel/platinum induction therapy followed by standard or extended three-weekly paclitaxel/platinum in European patients with advanced epithelial ovarian cancer. *European Journal of Cancer*, 50(15), 2592–2601. <https://doi.org/10.1016/j.ejca.2014.07.015>
115. Varqa, A. N. (2014a). Natural history of ovarian cancer. *Ecancermedicalscience*, 8, 465. <https://doi.org/10.3332/ECANCER.2014.465>
116. Varqa, A. N. (2014b). Natural history of ovarian cancer. *Ecancermedicalscience*, 8, 465. <https://doi.org/10.3332/ECANCER.2014.465>
117. Varqa, A. N. (2014c). Natural history of ovarian cancer. *Ecancermedicalscience*, 8, 465. <https://doi.org/10.3332/ECANCER.2014.465>
118. Vergote, I., Tropé, C. G., Amant, F., Kristensen, G. B., Ehlen, T., Johnson, N., Verheijen, R. H. M., van der Burg, M. E. L., Lacave, A. J., Panici, P. B., Kenter, G. G., Casado, A., Mendiola, C., Coens, C., Verleye, L., Stuart, G. C. E., Pecorelli, S., & Reed, N. S. (2010). Neoadjuvant Chemotherapy or Primary Surgery in Stage IIIC or IV Ovarian Cancer. *New England Journal of Medicine*, 363(10), 943–953. [https://doi.org/10.1056/NEJMOA0908806/SUPPL\\_FILE/NEJMOA0908806\\_DISCLOSURES.PDF](https://doi.org/10.1056/NEJMOA0908806/SUPPL_FILE/NEJMOA0908806_DISCLOSURES.PDF)
119. Vescarelli, E., Gerini, G., Megiorni, F., Anastasiadou, E., Pontecorvi, P., Solito, L., De Vitis, C., Camero, S., Marchetti, C., Mancini, R., Benedetti Panici, P., Dominici, C., Romano, F., Angeloni, A., Marchese, C., & Ceccarelli, S. (2020). MiR-200c sensitizes Olaparib-resistant ovarian cancer cells by targeting Neuropilin 1. *Journal of Experimental and Clinical Cancer Research*, 39(1). <https://doi.org/10.1186/S13046-019-1490-7>,
120. Visvanathan, K., Gross, A. L., Kurman, R. J., Vang, R., & Shih, I. M. (2010). Precursor lesions of high-grade serous ovarian carcinoma: Morphological and molecular characteristics. *Journal of Oncology*, 2010. <https://doi.org/10.1155/2010/126295>,

121. Wang, H., Liu, J., Zhang, Z., Peng, J., Wang, Z., Yang, L., Wang, X., Hu, S., & Hong, L. (2024).  $\beta$ -Sitosterol targets ASS1 for Nrf2 ubiquitin-dependent degradation, inducing ROS-mediated apoptosis via the PTEN/PI3K/AKT signaling pathway in ovarian cancer. *Free Radical Biology and Medicine*, 214, 137–157. <https://doi.org/10.1016/J.FREERADBIOMED.2024.02.004>,
122. Wang, H., Wang, Z., Zhang, Z., Liu, J., & Hong, L. (2023).  $\beta$ -Sitosterol as a Promising Anticancer Agent for Chemoprevention and Chemotherapy: Mechanisms of Action and Future Prospects. *Advances in Nutrition*, 14(5), 1085–1110. <https://doi.org/10.1016/J.ADVNUT.2023.05.013>,
123. Wang, Z., Chen, W., Zuo, L., Xu, M., Wu, Y., Huang, J., Zhang, X., Li, Y., Wang, J., Chen, J., Wang, H., & Sun, H. (2022). The Fibrillin-1/VEGFR2/STAT2 signaling axis promotes chemoresistance via modulating glycolysis and angiogenesis in ovarian cancer organoids and cells. *Cancer Communications*, 42(3), 245–265. <https://doi.org/10.1002/CAC2.12274>,
124. Watson, Z. L., Yamamoto, T. M., McMellen, A., Kim, H., Hughes, C. J., Wheeler, L. J., Post, M. D., Behbakht, K., & Bitler, B. G. (2019). Histone methyltransferases EHMT1 and EHMT2 (GLP/G9A) maintain PARP inhibitor resistance in high-grade serous ovarian carcinoma. *Clinical Epigenetics*, 11(1). <https://doi.org/10.1186/S13148-019-0758-2>,
125. Whitaker, R. H., & Placzek, W. J. (2019). Regulating the bcl2 family to improve sensitivity to microtubule targeting agents. *Cells*, 8(4). <https://doi.org/10.3390/CELLS8040346>,
126. Wiegand, K. C., Shah, S. P., Al-Agha, O. M., Zhao, Y., Tse, K., Zeng, T., Senz, J., McConechy, M. K., Anglesio, M. S., Kalloger, S. E., Yang, W., Heravi-Moussavi, A., Giuliany, R., Chow, C., Fee, J., Zayed, A., Prentice, L., Melnyk, N., Turashvili, G., ... Huntsman, D. G. (2010a). ARID1A Mutations in Endometriosis-Associated Ovarian Carcinomas. *New England Journal of Medicine*, 363(16), 1532–1543. <https://doi.org/10.1056/NEJMOA1008433>,
127. Wiegand, K. C., Shah, S. P., Al-Agha, O. M., Zhao, Y., Tse, K., Zeng, T., Senz, J., McConechy, M. K., Anglesio, M. S., Kalloger, S. E., Yang, W., Heravi-Moussavi, A., Giuliany, R., Chow, C., Fee, J., Zayed, A., Prentice, L., Melnyk, N., Turashvili, G., ... Huntsman, D. G. (2010b). ARID1A Mutations in Endometriosis-Associated Ovarian Carcinomas. *New England Journal of Medicine*, 363(16), 1532–1543. <https://doi.org/10.1056/NEJMOA1008433>,
128. Wilson, M. K., Pujade-Lauraine, E., Aoki, D., Mirza, M. R., Lorusso, D., Oza, A. M., du Bois, A., Vergote, I., Reuss, A., Bacon, M., Friedlander, M., Gallardo-Rincon, D., Joly, F., Chang, S. J., Ferrero, A. M., Edmondson, R. J., Wimberger, P., Maenpaa, J., Gaffney, D., ... Ochiai, K. (2017). Fifth Ovarian Cancer Consensus Conference of the Gynecologic Cancer InterGroup: recurrent disease. *Annals of Oncology*, 28(4), 727–732. <https://doi.org/10.1093/ANNONC/MDW663>
129. Wong, T. L., Strandberg, K. R., Croley, C. R., Fraser, S. E., Nagulapalli Venkata, K. C., Fimognari, C., Sethi, G., & Bishayee, A. (2021). Pomegranate bioactive constituents target multiple oncogenic and oncosuppressive signaling for cancer prevention and intervention. *Seminars in Cancer Biology*, 73, 265–293. <https://doi.org/10.1016/J.SEMCANCER.2021.01.006>
130. Xu, W., Rush, J., Rickett, K., & Coward, J. I. G. (2016). Mucinous ovarian cancer: A therapeutic review. *Critical Reviews in Oncology/Hematology*, 102, 26–36. <https://doi.org/10.1016/j.critrevonc.2016.03.015>
131. Yamamoto, T. M., McMellen, A., Watson, Z. L., Aguilera, J., Ferguson, R., Nurmammedov, E., Thakar, T., Moldovan, G. L., Kim, H., Cittelly, D. M., Joglar, A. M., Brennecke, E. P., Wilson, H., Behbakht, K., Sikora, M. J., & Bitler, B. G. (2019).

- Activation of Wnt signaling promotes olaparib resistant ovarian cancer. *Molecular Carcinogenesis*, 58(10), 1770–1782. <https://doi.org/10.1002/MC.23064>,
132. Zhang, L., Conejo-Garcia, J. R., Katsaros, D., Gimotty, P. A., Massobrio, M., Regnani, G., Makrigiannakis, A., Gray, H., Schlienger, K., Liebman, M. N., Rubin, S. C., & Coukos, G. (2003). Intratumoral T Cells, Recurrence, and Survival in Epithelial Ovarian Cancer. *New England Journal of Medicine*, 348(3), 203–213. <https://doi.org/10.1056/NEJMOA020177>,

# Pratyaksha\_Thesis.docx



Delhi Technological University

## Document Details

### Submission ID

trn:oid:::27535:98037944

### Submission Date

May 28, 2025, 12:29 AM GMT+5:30

### Download Date

May 28, 2025, 12:32 AM GMT+5:30

### File Name

Pratyaksha\_Thesis.docx

### File Size

15.9 MB

112 Pages

28,041 Words

168,683 Characters







# 6% Overall Similarity

The combined total of all matches, including overlapping sources, for each database.




## Filtered from the Report

- Bibliography
- Cited Text

## Match Groups

-  **153** Not Cited or Quoted 6%  
Matches with neither in-text citation nor quotation marks
-  **0** Missing Quotations 0%  
Matches that are still very similar to source material
-  **1** Missing Citation 0%  
Matches that have quotation marks, but no in-text citation
-  **0** Cited and Quoted 0%  
Matches with in-text citation present, but no quotation marks

## Top Sources

- 4%  Internet sources
- 3%  Publications
- 5%  Submitted works (Student Papers)

## Integrity Flags

### 0 Integrity Flags for Review

No suspicious text manipulations found.

Our system's algorithms look deeply at a document for any inconsistencies that would set it apart from a normal submission. If we notice something strange, we flag it for you to review.

A Flag is not necessarily an indicator of a problem. However, we'd recommend you focus your attention there for further review.

## \*% detected as AI

AI detection includes the possibility of false positives. Although some text in this submission is likely AI generated, scores below the 20% threshold are not surfaced because they have a higher likelihood of false positives.

**Caution: Review required.**

It is essential to understand the limitations of AI detection before making decisions about a student's work. We encourage you to learn more about Turnitin's AI detection capabilities before using the tool.

### Disclaimer

Our AI writing assessment is designed to help educators identify text that might be prepared by a generative AI tool. Our AI writing assessment may not always be accurate (it may misidentify writing that is likely AI generated as AI generated and AI paraphrased or likely AI generated and AI paraphrased writing as only AI generated) so it should not be used as the sole basis for adverse actions against a student. It takes further scrutiny and human judgment in conjunction with an organization's application of its specific academic policies to determine whether any academic misconduct has occurred.

## Frequently Asked Questions

### How should I interpret Turnitin's AI writing percentage and false positives?

The percentage shown in the AI writing report is the amount of qualifying text within the submission that Turnitin's AI writing detection model determines was either likely AI-generated text from a large-language model or likely AI-generated text that was likely revised using an AI-paraphrase tool or word spinner.

False positives (incorrectly flagging human-written text as AI-generated) are a possibility in AI models.

AI detection scores under 20%, which we do not surface in new reports, have a higher likelihood of false positives. To reduce the likelihood of misinterpretation, no score or highlights are attributed and are indicated with an asterisk in the report (\*%).

The AI writing percentage should not be the sole basis to determine whether misconduct has occurred. The reviewer/instructor should use the percentage as a means to start a formative conversation with their student and/or use it to examine the submitted assignment in accordance with their school's policies.

### What does 'qualifying text' mean?

Our model only processes qualifying text in the form of long-form writing. Long-form writing means individual sentences contained in paragraphs that make up a longer piece of written work, such as an essay, a dissertation, or an article, etc. Qualifying text that has been determined to be likely AI-generated will be highlighted in cyan in the submission, and likely AI-generated and then likely AI-paraphrased will be highlighted purple.

Non-qualifying text, such as bullet points, annotated bibliographies, etc., will not be processed and can create disparity between the submission highlights and the percentage shown.

